UNIVERSIDADE FEDERAL DE SANTA CATARINA

CENTRO TECNOLÓGICO

PROGRAMA DE PÓS-GRADUAÇÃO EM CIÊNCIA E ENGENHARIA DE MATERIAIS

Tainá Pigosso

N-DOPED ZINC OXIDE NANOPARTICLES OBTAINED BY SOLUTION COMBUSTION SYNTHESIS FOR THE PHOTOCATALYTIC REMOVAL OF TETRACYCLINE HYDROCHLORIDE

Florianópolis

2022

Tainá Pigosso

N-DOPED ZINC OXIDE NANOPARTICLES OBTAINED BY SOLUTION COMBUSTION SYNTHESIS FOR THE PHOTOCATALYTIC REMOVAL OF TETRACYCLINE HYDROCHLORIDE

Dissertação submetida ao Programa de Pós-Graduação em Ciência e Engenharia de Materiais da Universidade Federal de Santa Catarina para a obtenção do grau de Mestre em Ciência e Engenharia de Materiais.

Orientador: Prof. Cristiano Binder, Dr.
Coorientador: Leandro Lima Evangelista, Dr.

Florianópolis
2022

Ficha de identificação da obra elaborada pelo autor, através do Programa de Geração Automática da Biblioteca Universitária da UFSC.

Tainá Pigosso

N-doped zinc oxide nanoparticles obtained by solution combustion synthesis for the photocatalytic removal of tetracycline hydrochloride

O presente trabalho em nível de mestrado foi avaliado e aprovado pela banca examinadora composta pelos seguintes membros:

Alexsandra Valério, Dra.
Membro Externo/TNS Nano

Prof. Dachamir Hotza, Dr.
Membro Interno/PPGMAT UFSC

Certificamos que esta é a **versão original e final** do trabalho de conclusão que foi julgado adequado para obtenção do título de Mestre em Ciência e Engenharia de Materiais

_____
Prof. João Batista Rodrigues Neto, Dr.
Coordenação do Programa de Pós-Graduação

_____
Prof. Cristiano Binder, Dr.
Orientador

_____
Leandro Lima Evangelista, Dr.
Coorientador

Florianópolis, 2022.

Este trabalho é dedicado aos meus pais, Vera e Dirceu.

E aos meus avós Orildes e Hermes, Luiz e Emília.

AGRADECIMENTOS

Este trabalho é um quebra-cabeça com uma quantidade significativa de peças. Entre embaralhá-las, retirá-las, colocá-las e encaixá-las, as peças que compõem as páginas a seguir montam este quebra-cabeça, em partes. Isto porque talvez existam peças duplicadas, peças que faltam e tantas outras que ainda permanecem embaralhadas. Entre contar a história deste quebra-cabeça e a vontade de continuar a montá-lo, eu não estive sozinha e as pessoas que agradeço a seguir são, sem sombra de dúvidas, peças essenciais.

Aos meus pais, Vera e Dirceu Pigosso e a minha família, por serem minha fonte de inspiração e amor. Por serem o meu porto seguro onde quer que eu esteja.

Ao meu orientador, Prof. Dr. Cristiano Binder, pela confiança e apoio ao longo de todo o trabalho. Pela sua visão gestora e por oferecer os melhores recursos para execução desta pesquisa. Por me impulsionar a aprender e evoluir como pessoa e como profissional.

Ao meu co-orientador, Dr. Leandro Lima Evangelista, por toda sua dedicação, inteligência e sabedoria. Pelas ricas trocas de conhecimento, ensinamentos e por não medir esforços pelo tema.

Ao Prof. Dr. Sérgio Yesid Goméz González, pelos excelentes insights ao longo da execução deste trabalho, pelo suporte nas atividades e pela parceria desenvolvida.

Ao meu bolsista de Iniciação Científica, Byron Andrade Amorim de Melo, pela dedicação no desenvolvimento e execução do trabalho. E pela contribuição mútua no crescimento pessoal e profissional.

Às amizades da *Sala two* do Laboratório de Materiais (LabMat) por transformarem este caminho em um percurso mais leve. Por compartilharem de elevada competência técnica-científica e de um instinto humano que permite bons momentos e boas risadas.

Aos demais professores e colegas que compõem o LabMat, pelo elevado profissionalismo, prestatividade e trocas de experiência e conhecimento.

Às minhas amizades mais próximas, por me apoiar, incentivar, entender e estar ao meu lado ao longo desta trajetória.

Ao Frederico Pereira Júnior, pelo apoio técnico na execução deste trabalho e por idealizar e construir a FredBox – essencial aos meus experimentos.

Ao LabMat, por ser um modelo em pesquisa, desenvolvimento e integração universidade-indústria.

Ao Laboratório de Filmes Finos e Superfícies (LFFS), em nome da prof.ª Cristiani Campos Plá Cid e ao Andrés Pardo, por abrirem as portas para execução de ensaios, pelas

atividades em parceria e por proporcionarem excelentes momentos de troca e ensinamentos.

Ao LINDEN-metro e ao Laboratório de Controle de Processos (LCP), por serem fundamentais na minha pesquisa.

A todos os demais laboratórios que contribuíram de maneira pertinente a este trabalho.

À UFSC e ao PPGMAT, pela excelência e suporte. A CAPES e ao CNPq pelo financiamento da pesquisa.

A todas as pessoas que encontro ao longo deste caminho e que contribuem direta ou indiretamente na minha vida, o meu muito obrigado!

"É necessário sair da ilha para ver a ilha. Não nos vemos se não saímos de nós."

José Saramago

RESUMO

Contaminantes emergentes (ECs) são substâncias naturais ou sintéticas e microrganismos que apresentam potenciais problemas à saúde humana e ao equilíbrio ambiental. Compostos farmacêuticos e genes de resistência a antibióticos são ECs típicos encontrados em diferentes matrizes do ambiente. A tecnologia de fotocatálise é uma abordagem assertiva e viável para degradar e inativar esses poluentes químicos de risco biológico por meio de um método verde e seguro. Como material fotocatalisador, o óxido de zinco (ZnO) é um candidato robusto com uma atividade fotocatalítica atraente e notável em comparação a materiais tradicionais. Apesar disso, suas aplicações fotocatalíticas em condições ambientes são limitadas à baixa absorção de luz visível. Estratégias como a dopagem são direcionadas para modificar e adaptar a estrutura do ZnO, de modo a melhorar a resposta da fotocatálise em luz visível e criar arquiteturas que potencializem as suas propriedades de superfície. Esta pesquisa visa, então, desenvolver uma abordagem de uma etapa para sintetizar e dopar óxido de zinco pelo método de combustão em solução, onde nitrato de zinco hexahidratado e sacarose atuam como oxidante e combustível, respectivamente. E a ureia, como fonte combustível e dopante de nitrogênio. Cinco amostras foram preparadas em diferentes razões molares de ureia-sacarose, nas frações de 0%, 25%, 50%, 75% e 100% de ureia. As reações ocorreram em um forno Mufla pré-aquecido a 500 ºC durante 10 minutos, adicionados a uma etapa de calcinação de 20 minutos. A influência da razão molar ureia-sacarose nas propriedades físico-químicas e na atividade fotocatalítica sob luz visível do ZnO dopado com nitrogênio foram investigadas. As amostras foram caracterizadas por difração de raios – X (DRX), microscopia eletrônica de varredura (MEV), espalhamento dinâmico de luz (DLS), adsorção-dessorção de nitrogênio (BET/BJH), espectroscopia de fotoelétrons de raios – X (XPS), análise elementar (CHN(S)) e espectroscopia UV/visível. A remoção fotocatalítica do poluente hidrocloridrato de tetraciclina (TC – HCl) foi simulada em luz visível com o uso de uma lâmpada fluorescente (15 W, $\lambda > 420$ nm) para avaliar o desempenho dos fotocatalisadores N – ZnO. Os resultados deste trabalho revelam a viabilidade da produção de óxido de zinco nanométrico funcionalizado com nitrogênio através do método de combustão em solução. Na razão molar ureia-sacarose, supõe-se que a sacarose controla os parâmetros de tamanho, enquanto a ureia atua como fonte dopante e altera a cinética da reação em teores mais elevados. Os materiais possuem a estrutura cristalina wurtzita do ZnO sem a presença de fases adicionais após o fenômeno de dopagem. Os fotocatalisadores à base de ZnO têm tamanhos de partículas que variam de 78 a 820 nm por DLS e áreas de superfície de até 26 m^2/g. O band gap é reduzido de 3.11 eV para até 1.65 eV, atribuído ao efeito do nitrogênio e das vacâncias de oxigênio desenvolvidas na reação de combustão. Na razão molar de 50% ureia-sacarose, maximiza-se a remoção fotocatalítica do poluente TC – HCl para cerca de 75% , em 60 minutos de irradiação de luz, o que representa uma melhoria de eficiência de 40% e uma taxa de remoção 1.86 vezes mais rápida do que o ZnO não-dopado. A estrutura mesoporosa do material em sinergia com a propriedade fotocatalítica também é estudada e demonstra uma degradação fotocatalítica próxima a 100% da TC – HCl, após 120 minutos, propondo um novo material adsorvente-fotocatalítico.

Palavras-chaves: óxido de zinco N-dopado; síntese por combustão de solução; fotocatálise; luz visível.

RESUMO EXPANDIDO

Introdução

O ser humano de maneira inerente a sua condição modifica o ambiente. As ações antrópicas evoluíram e alcançaram uma tendência acelerada de crescimento econômico e de urbanização. Consequência destas múltiplas transformações, há o reconhecido peso de ações negativas que pode ser exemplificado no surgimento de uma nova geração de poluentes, conhecidos como contaminantes emergentes. Processos de oxidação avançada, os quais incluem a fotocatálise, tem ganhado especial interesse pela eficiência em energia, simplicidade e capacidade de degradar substâncias de alto potencial tóxico, através de um processo limpo e seguro. Dentre os materiais fotocatalíticos, o óxido de zinco (ZnO) possui notável e comprovada ação de degradação fotocatalítica, competitiva a outros materiais tradicionais. Dado o exposto, os avanços nas pesquisas direcionam-se para a obtenção em escala nanométrica e funcionalizada do ZnO, de modo a modificar a sua estrutura eletrônica e a química de defeitos de superfície, em benefício a sua propriedade de fotocatálise sob condições ambientes. Então, destaca-se a importância do conhecimento em técnicas de síntese e processamento deste material, conectados com as propriedades a serem alcançadas. Uma nova perspectiva para este cenário reside na rota por síntese de combustão de solução, a qual permite a obtenção de óxido de zinco de maneira versátil, econômica, eficiente e com potencial aplicação em áreas de remediação ambiental e energia.

Objetivos

O objetivo principal deste trabalho concentra-se em desenvolver nanopartículas de óxido de zinco (ZnO) funcionalizadas através de processo de dopagem com nitrogênio e aplicá-las em processos de fotocatálise de contaminantes emergentes sob luz visível. De maneira específica, objetiva-se: (I) avaliar o potencial da rota simultânea de síntese e dopagem pelo método de combustão de solução para a produção das nanopartículas N-dopadas de óxido de zinco; (II) determinar a influência do teor de ureia como fonte de nitrogênio nas propriedades físico-químicas dos materiais; (III) quantificar a performance fotocatálica dos materiais de ZnO N-dopados em luz visível e correlacionar com as propriedades físico-químicas destes materiais; e (IV) elucidar o fenômeno que ocorre durante o período de escuro, prévio a irradiação de luz nos ensaios de fotocatálise.

Metodologia

A síntese base por combustão de solução do ZnO não-dopado compreende a mistura de 3.569 g (12 mmol) de nitrato de zinco hexahidratado, como fonte oxidante, e 1.2 g (3.5 mmol) de sacarose, como combustível, que são misturados a 3 ml de água destilada até a completa dissolução dos sólidos. A solução resultante é levada a um forno Mufla pré-aquecido a 500 ºC, onde a reação de combustão ocorre de maneira rápida. Após cerca de 10 minutos, tem-se uma estrutura porosa, a qual é quebrada para expor o carbono residual e removê-lo na forma de CO_2, mantendo-se o material a 500 ºC por 20 minutos. O material resultante é um pó de aspecto fino e branco, característico de óxido de zinco. Com base neste protocolo, a metodologia de dopagem adotada reside na capacidade intrínseca da síntese por combustão de solução (SCS) em modificar as propriedades finais do material, através da influência dos percursores combustíveis utilizados. Nesta etapa, o método SCS transforma-se em uma estratégia de dopagem in situ do óxido de zinco, através da modificação da razão molar ureia-sacarose, onde a ureia atua como combustível e fonte de nitrogênio dopante. O método de uma etapa de síntese e dopagem compreende uma escala de cinco porcentagens molares de ureia (0% (ZnO U0), 25% (ZnO U25), 50% (ZnO U50), 75% (ZnO U75) e 100% (ZnO U100)), calculadas com base na quantidade molar de

sacarose. A influência da ureia como fonte dopante nos materiais a base de ZnO foi avaliada quanto a estrutura cristalina, parâmetros de rede e tamanho de cristalito por difração de raios – X (DRX), morfologia e tamanho de partícula por microscopia eletrônica de varredura (MEV) e espalhamento dinâmico da luz (DLS), propriedades texturais (área de superfície, tamanho e volume de poros) por ensaios de adsorção-dessorção de nitrogênio (N_2), composição química e estados de oxidação na superfície por espectroscopia de fotoelétrons excitados por raios – X (XPS) e análise elementar (CHN(S)), absorção de luz e estrutura eletrônica do band gap por espectroscopia UV/visível. O desempenho dos materiais ZnO N-dopados como fotocatalisadores em luz visível foi testado em ensaios de bancada para degradação do composto fármaco hidrocloridrato de tetraciclina (TC – HCl), como modelo de contaminante emergente, sob irradiação de uma lâmpada fluorescente (15W, $\lambda > 420$ nm) por 60 minutos.

Resultados e discussões

A síntese e dopagem simultânea de materiais de óxido de zinco pelo método de combustão de solução resulta em um rendimento de, aproximadamente, uma grama de material para cada formulação estudada, em até 30 minutos. As caracterizações por DRX asseguram a formação de óxido de zinco na estrutura hexagonal da wurtzita e após a funcionalização por nitrogênio, nenhuma impureza ou fase adicional é observada. Na estrutura cristalina, o efeito do aumento do teor de ureia na razão molar ureia-sacarose possui dois efeitos: (I) os parâmetros de rede "*a*" e "*c*" diminuem de 3.2531(2) – 3.2460(0) Å e 5.214(0) – 5.2026(9) Å, respectivamente, dada as condições mais vigorosas da reação de combustão que levam a contração da célula unitária; e (II), o tamanho de cristalito dos materiais aumenta de 36 nm para 86 nm, devido ao efeito de coalescimento induzido pelo aumento da temperatura das reações. Com base nas micrografias de MEV, alcançou-se óxido de zinco nanoparticulado de morfologia predominantemente esférica. Entretanto, para altas concentrações de ureia (ZnO U100), a morfologia tende a ser alterada para formatos piramidais na escala submicrométrica. Por DLS, o diâmetro hidrodinâmico das partículas foi mensurado na faixa de 78 a 820 nm, corroborando os resultados de tamanho de cristalito e o crescimento exponencial dos materiais ZnO N-dopados. Em sequência, as propriedades texturais foram designadas em termos da área de superfície, em um máximo de 25.93 m²/g para ZnO U50 e um mínimo de 4.47 m²/g, na ZnO U100. Os resultados de tamanho e volume de poros indicam a natureza mesoporosa das amostras e seguem a tendência da área de superfície, com perfil mais compacto nos materiais com maior teor de nitrogênio. Análises de composição química e estados de oxidação por XPS, revelaram conteúdos de até 0.64 at.% de nitrogênio e a mudança do ambiente em torno da estrutura do ZnO após o fenômeno de dopagem. A síntese e dopagem simultânea por combustão de solução intensifica o número de vacâncias de oxigênio (V_O), induz a formação de ligações N – Zn, com o nitrogênio de forma substitucional e de ligações como N – H e N – O, dada a adsorção de nitrogênio na superfície do ZnO, pela decomposição da ureia. Em linha com estes resultados, a absorbância das amostras de ZnO 0% a 100% ureia foi descolada para maiores comprimentos de onda ($\lambda > 400$ nm), que correspondem a região do espectro visível. A maior absorbância desencadeia a diminuição do band gap de valores de 3.11 eV para até 1.65 eV, pela formação de estados intermediários na estrutura eletrônica do ZnO. Os resultados até aqui descritos representam as características físico-químicas dos materiais de ZnO dopados com nitrogênio pela rota de síntese de combustão de solução. O desempenho fotocatalítico na degradação do composto hidrocloridrato de tetraciclina (TC – HCl) revelou-se não-linear com o aumento do teor de ureia de 0% a 100% no ZnO. Para o ZnO não-dopado (ZnO U0), a eficiência fotocatálica é de 53.62% a uma taxa de 12.17x10⁻³ min⁻¹. Para a condição de N – ZnO U50, há um ganho de eficiência próximo a

40%, que representa uma degradação de 75% da TC – HCl, após 60 minutos e uma reação 1.86 vezes mais rápida que a ZnO U0. No entanto, o contínuo aumento de ureia representa um decréscimo de até 64% na eficiência da amostra ZnO U100 com uma degradação de TC – HCl de apenas 19.17%, por exemplo, devido a menor área de superfície e número de sítios ativos disponíveis. Por fim, ensaios adicionais, demonstraram a sinergia entre a capacidade de adsorção pela estrutura mesoporosa e a atividade fotocatalítica para impulsionar a remoção do hidrocloridrato de tetraciclina. Como modelo, a combinação dos dois fenômenos pela amostra ZnO U50 desencadeou uma degradação de 97.76% de TC – HCl, após 120 minutos.

Considerações finais

Questões acerca de contaminantes emergentes que ameaçam a segurança em nível de saúde pública e ecossistemas do ambiente são desafios crescentes na busca pelo desenvolvimento de materiais, técnicas e processos para superá-las. O óxido de zinco é um material fotocatalisador e a sua crescente aplicabilidade em fenômenos de fotocatálise reside, em sua maioria, nos avanços desenvolvidos e alcançados pela nanotecnologia e pela Ciência e Engenharia de Materiais. Neste estudo, provou-se que o método de combustão de solução é apto para simultaneamente sintetizar e funcionalizar nanopartículas de óxido de zinco através da dopagem com nitrogênio. Os resultados alcançados demonstraram a forte dependência das propriedades físico-químicas e, consequentemente, do desempenho fotocatalítico com a relação molar ureia-sacarose. Altos teores de ureia promovem o crescimento exponencial do tamanho de cristalito e do tamanho de partícula, diminuem a área de superfície e o volume de poros, além de reduzir excessivamente o band gap dos materiais. Em contrapartida, relações balanceadas entre sacarose e ureia, promovem os melhores resultados em termos de propriedade do material e desempenho fotocatalítico. Tal consideração reforça o ponto-chave do conhecimento relacionado ao processamento do material na aplicação desejada. Para finalizar, o desenvolvimento deste trabalho abre as portas para a continuação do tema que abrange pontos, tais como:

- Avaliar o potencial da síntese e dopagem de uma etapa por combustão de solução sem a etapa de calcinação para remoção do carbono residual;
- Investigar o efeito da reação de combustão de solução sob atmosfera controlada no nível de dopagem do material semicondutor e suas respectivas características;
- Avaliar experimentalmente o mecanismo fotocatalítico e a geração de espécies reativas de oxigênio (ROS) durante a remoção do poluente modelo.

ABSTRACT

Emerging contaminants (ECs) are natural or synthetic substances and microorganisms that pose potential issues to human health and environmental equilibrium. Pharmaceutical compounds and antibiotic-resistance genes are typical ECs found in different natural matrices. Photocatalysis technology is an assertive and feasible approach to degrading and inactivating chemical and biohazard pollutants through a green and safe method. As a photocatalyst material, zinc oxide (ZnO) is a robust candidate with an attractive and remarkable photocatalytic activity compared to traditional materials. Despite it, its photocatalysis applications under room conditions are limited to low visible light absorption. Strategies such as doping are assigned for modifying and tailoring the ZnO structure to enhance the photocatalytic response in visible light and create architectures that potentialize its surface properties. Therefore, this research aims to develop a one-step approach to synthesize and dope zinc oxide nanoparticles by the solution combustion method with zinc nitrate hexahydrate and sucrose as the oxidizer and the fuel, respectively. While urea acts as a fuel and nitrogen source. Five samples were prepared to vary the urea-to-sucrose molar ratio in fractions of 0%, 25%, 50%, 75%, and 100% of urea. The reactions took place in a pre-heated Muffle furnace at 500 ºC for 10 minutes, added to a calcination step of 20 minutes. The influence of the urea-to-sucrose molar ratio on the physicochemical properties and photocatalytic activity under visible light of the nitrogen-doped ZnO was investigated. The samples were characterized through X-ray diffraction (XRD), scanning electron microscopy (SEM), dynamic light scattering (DLS), nitrogen adsorption-desorption (BET/BJH), X-ray photoelectron spectroscopy (XPS), elementary analysis (CHN(S)), and UV/visible spectroscopy. Photocatalytic removal of the pollutant tetracycline hydrochloride (TC – HCl) was performed under a fluorescent lamp (15 W, $\lambda > 420$ nm) to evaluate the performance of the N – ZnO photocatalysts under visible light. The results in this work reveal the feasibility of producing zinc oxide at the nanoscale modified with nitrogen doping through the solution combustion method in a great yield at a short time scale. In the urea-to-sucrose molar ratio, sucrose is supposed to control the size parameters, while the urea acts as the dopant source and changes the kinetics of the reaction at higher contents. The materials have on the whole the wurtzite crystal structure of the ZnO without any other phase due to the nitrogen doping. The ZnO-based photocatalysts have particle sizes ranging from 78 to 820 nm by DLS and surface areas up to 26 m^2/g. The band gap is narrowed from 3.11 eV to 1.65 eV, assigned to the nitrogen doping and oxygen vacancies developed in the combustion reaction. A balanced content of the fuel reactants, namely the 50% urea-to-sucrose molar ratio, maximizes the photocatalytic abatement of the TC – HCl to around 75% for 60 minutes of irradiation, which means an efficiency improvement of 40% and a removal rate 1.86 faster than the ZnO undoped. The mesoporous structure of the material in synergy with the photocatalytic property was also investigated and shows a photocatalytic abatement of almost 100% of TC – HCl, after 120 minutes, proposing a novel adsorption-photocatalytic material.

Keywords: N-doped zinc oxide; solution combustion synthesis; photocatalysis; visible light active.

LIST OF FIGURES

LIST OF TABLES

SUMMARY

1. INTRODUCTION

Society is meeting a time of immense challenges to sustainable development. Global health threats, more frequent and intense natural disasters, natural resource depletion, and adverse impacts of environmental degradation, including land degradation, freshwater scarcity, and loss of biodiversity, add to and exacerbate the list of challenges that humanity face. The 2030 Agenda from United Nations Organization for sustainable development recognizes the need to decisively threat posed by environmental degradation through the environmentally sound management and safe use of chemicals, the reduction and recycling of waste, and more efficient use of water and energy (Nations, 2015).

Emerging contaminants have been addressed as one of the main concerns for water quality around the world. The absence of laws on the surveillance in drinkwater and the low removal along the traditional treatments for these chemicals poses potential environmental and health risks. Besides, their isolated or combined adverse effects for recent or prolonged use are still not well-known or quantified (Polianciuc *et al.*, 2020; Wilkinson, Boxall e Kolpin, 2019). In Brazil, recent data from a deep study about emerging contaminants revealed the detection of 87 pharmaceutical drugs and personal care products, 58 pesticides, 8 hormones, 2 illicit drugs, caffeine, and bisphenol-A in distinct matrices, i.e., wastewater, groundwater, seawater, rainwater, surface water, drinking water, and hospital effluent in the last decade (2011 – 2021) (Marson *et al.*, 2022). However, this is a time for immense opportunity and significant progress to fight against many of these issues.

Advanced oxidation processes (AOPs) as an efficient and reliable alternative to degrade emerging contaminants in aqueous matrices. Heterogeneous photocatalysis has been widely explored as an AOP, in which the photocatalyst material is activated by a light source and creates redox reactions with the pollutants (Dewil *et al.*, 2017; Malato *et al.*, 2009). In terms of photocatalytic materials, zinc oxide as a multifunctional material has its own merits and demerits over the other ones (Hernández-Alonso *et al.*, 2009). Appropriate strategies have been developed to turn the ZnO able to capture sunlight or visible light radiation to directly activate the photocatalytic system and overcome its only UV-absorption ability and the barely 6% of UV light that solar light offers out of its whole spectrum (Kumar e Koteswara Rao, 2015; Majumder *et al.*, 2020).

In this era, where the words "sustainability", "green", "environmental benefits", "energy saving", and "renewable" are the most pronounced ones, it is aware of the fact that the benefit starts already from the preparation of materials, where the Materials Science

and Engineering become active (Deganello e Tyagi, 2018; Sheldon, 2017). In this perspective, environmental and energy issues do not concern only the applications of materials, but also the synthesis and processing of the materials themselves. "Efficiency" is another word that is strongly associated with the other ones. Efficiency is highly required for successful synthesis and materials processing. Efficiency is high for a maximum yield with minimum energy, time, and waste. From another point of view, efficiency is high if the scientist knows well the process and its maximum potentialities and possibilities to positively aid the environment, society, and economy, as well mentioned by F. Deganello and A.K. Tyagib (Deganello e Tyagi, 2018).

Nanoarchitectonics strategies to construct functional materials from fundamental units can be a useful way for the science of photocatalytic materials with promoted efficiencies. In this approach, functional materials systems are produced from the nanoscale through combinations and selections of various unit processes, such as atoms and molecules manipulations (Ariga *et al.*, 2016). Compared to macro and micro materials, nanoarchitecture has a dominant behavior of atoms on the surface of the particles over those insides of them, which ultimately alters the catalytic activity of the material since photocatalysis is a surface-driven reaction (Ariga *et al.*, 2015).

Zinc oxide (ZnO) as a semiconductor metal oxide is an eminent candidate for photocatalysis. The nanoarchitecture would provide an extra degree of freedom in the development of novel ZnO-based photocatalysts by the rational design of the availability of the adsorption sites and tuning the extension of excitation wavelength (Mbenga *et al.*, 2022). However, the synthesis of ZnO nanostructures on a large scale through physical and chemical techniques could be limited to the difficulty of controlling the surface properties of the bulky materials. Additionally, non-environmentally friendly chemicals and high-temperature procedures for the oxide make its processing not suitable and attractive (Gonzalez-Cortes e Zhang, 2022).

Therefore, this work provides a new perspective on the concept to obtain simultaneously zinc oxide (ZnO) materials at the nanoscale and nitrogen-doped to perform visible light photocatalysis. It describes a one-step synthesis and doping by solution combustion method by tailoring the urea-to-sucrose molar ratio in a mixture with zinc nitrate hexahydrate to achieve ZnO and N-doped ZnO. The technique is a relatively new manufacturing and green route from an energy-efficient point of view that adopts low-costly starting materials and saves energy and time, by producing about one gram of material in a matter of minutes. ZnO nitrogen-doped with around 120 nm, a great surface

area of up to 26 m^2/g, mesoporosity, and a good optical band gap of 2.89 eV has a first-rate performance of up to 75% photocatalytic degradation efficiency of the tetracycline hydrochloride (TC – HCl), as one of the most concerning emerging contaminants, under 60 minutes of visible light. The developed physiochemical features on the ZnO-based materials through solution combustion also enable synergy between the adsorption-photocatalysis phenomenon that outperforms an almost complete TC – HCl degradation.

Furthermore, the Appendix of this work brings a brief context and work restrictions of the other processing route developed in this research to functionalize the zinc oxide for photocatalysis applications. This route relies on the plasma-assisted doping of the materials and has been built as a new possibility to explore the solid knowledge of plasma technology that the Materials Laboratory has on it. In summary, this Master's thesis has addressed new approaches and strategies that possess high potential and versatility on materials for environmental and energy purposes.

2. OBJECTIVES

2.1. MAIN OBJECTIVE

The main goal of this work is to develop zinc oxide (ZnO) nanoparticles functionalized through nitrogen doping and apply them in the photocatalysis processes of emerging contaminants under visible light irradiation.

2.2. SPECIFICS OBJECTIVES

- To evaluate the potential of the one-step approach of synthesis and doping by solution combustion method to produce the N-doped zinc oxide nanoparticles;
- To determine the influence of the urea-to-sucrose molar ratio on the physicochemical properties of the ZnO-based materials;
- To quantify the performance of the N – ZnO materials as photocatalysts under visible light;
- To correlate the properties of the ZnO functionalized nanoparticles with their photocatalytic performance;
- To elucidate the phenomenon that happens in the dark step before the light irradiation on the photocatalysis essays.

3. LITERATURE REVIEW

3.1. ENVIRONMENTAL BACKGROUND

Water is our planet's most crucial natural resource, essential for all living organisms. Earth's freshwater corresponds to only 2.5% of the entire water that covers the Earth's surface. And, a rare amount of only 0.002% might be considered humanly accessible. The rarity of this resource is further intensified through the increasing demand related to the natural changes assigned by the development of consumption linked to human needs and activities (Alrumman, El-kott e Keshk, 2016). With rapid development, industries and technologies have grown and expanded much of the world. Behalf of it, Earth's freshwater is more and more polluted with different chemicals and contaminants that exhibit potent cumulative harmful effects (Baaloudj *et al.*, 2021; Boyd, 2019).

The United States Geological Survey defines emerging contaminants as *"chemical of synthetic or natural origin, or any pathogenic microorganism that is not monitored in the environment, normally present in low to traces quantities, but with the potential to cause an adverse or lethal problem on ecological and human health systems*" (Gomes *et al.*, 2022). Pharmaceuticals are one of the major contaminant groups of emerging concern, such as antibiotics drugs. Most of these substances are poorly absorbed, with 40 to 90% being eliminated and reaching the environment in their active form (Polianciuc *et al.*, 2020). The global usage of antibiotics as therapeutic and prophylactic medicines, nutrient supplements in humans, livestock, and agricultural health management has resulted in the widespread occurrence of these highly stable compounds in natural aquatic habitats, as mixtures at various concentrations from a few ng/L up to a high μg/L (Figure 1) (Baaloudj *et al.*, 2021; Starling, Amorim e Leão, 2019).

Studies from the Society of Environmental Toxicology and Chemistry collected water samples from different rivers all over the world. 65% of them contained traces of at least one of the 14 main organic molecules, which belongs to commonly used antibiotics. They are prone to bioaccumulate and persist in the aquatic media, which induces risks associated with genotoxicity and endocrine disruption (Valério *et al.*, 2020; Wilkinson, Boxall e Kolpin, 2019). Apart from it, the immoderate use of antibiotics is the key driving force behind the occurrence and dissemination of antibiotic resistance (Xue *et al.*, 2021). Antibiotic-resistant bacteria (ARBs) and antibiotic-resistance genes (ARGs) should be considered emerging contaminants since infectious diseases treatable with antibiotics can

become untreatable and fatal by the year 2050 (Dadgostar, 2019). It is projected that these resistances will be responsible for approximately 10 million deaths worldwide in the upcoming 30 years, which has been identified as one of the largest threats to global health in the 21st century (Ghazali, Shaikh e Ahammad, 2022). The presence of ARBs and ARGs in the aquatic environment happens since the hazardous contaminants exert selective pressure on resistant strains and promote antimicrobial resistance, resulting in an aqueous habitat as a source for ARGs (Xue *et al.*, 2021).

Figure 1 – Sources of antibiotics and their effects on the environment, as emerging contaminants.
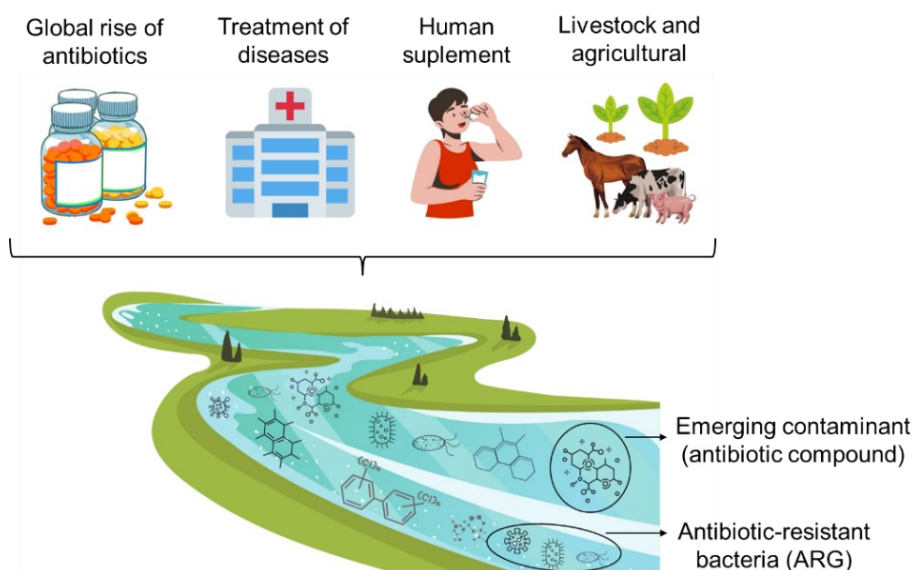
Source: Author (2022), based on (Jufer, Reilly e Mojica, 2019).

Tetracyclines (TCs) are the second main group of antibiotics produced and consumed worldwide. Besides their use in humans, tetracyclines are applied in agricultural practices as antibiotics to suppress the growth of bacteria, in both plants and animals (Borghi e Palma, 2014). The broad-spectrum family of tetracycline is stable and difficult to oxidize in the environment, which makes it a very persistent compound with a half-life of up to 180 days. The tetracyclines are not just present in the aquatic environment but also in soils and air (Ahmad, Zhu e Sun, 2021). Tetracycline's basic structural element is a tetracyclic ring system with various hydroxyl, methyl, keto, and di-methyl-amino functional groups, as drawn in Figure 2.

The environmental fate of the antibiotics like tetracycline has emerged as a research topic in the previous and present decades to address the issue of the serious threat caused by them. The removal of emerging pollutants in decontamination systems, both by physical-chemical process and conventional biological pathways, reached a high level of maturity that consist of their inability to eliminate many of these contaminants (Ahmad, Zhu e Sun, 2021). In light of it, it calls for the development of innovative clean technologies

and process designs to degrade these complex substances. The new advances have been born to fulfill a gap between maximum treatability and efficiency, greater robustness, and low cost, without generating additional stress to the environment or risk to human health (Dewil *et al.*, 2017; Malato *et al.*, 2009).

Figure 2 – Basic structure of the tetracycline compound.
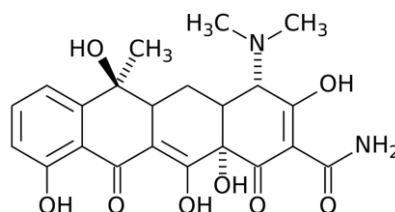
Source: Adapted from (Ahmad, Zhu e Sun, 2021).

3.2. PHOTOCATALYSIS

Advanced oxidation processes (AOPs) have gained attractive interest since they proved to be an efficient technology instead of conventional approaches. AOPs are cost-effective as the process on its own is energy-saving, simple, and possesses high catalytic activity with no selectivity for organic and inorganic pollutant compounds (Oluwole e Olatunj, 2022). The AOP relies on the in situ generations of highly reactive free radicals, known as reactive oxygen species (ROS), which means superoxide ($O_2^{\bullet-}$) and hydroxyl ($OH^{\bullet}$) radicals (Huang, Dong e Tang, 1993). These species demonstrate the ability to degrade biologically toxic materials, pesticides, petroleum components, and mineralize recalcitrant pollutants into harmless compounds or non-toxic final products. Besides, the present oxidative method reveals remarkable biocidal activity, by causing oxidative stress in target microorganisms, that ultimately leads them to a state of irreversible inactivation (Baaloudj *et al.*, 2021; Dewil *et al.*, 2017; Fagan *et al.*, 2016).

In the context of heterogeneous systems of the AOPs, one can cite photocatalysis as an attractive mechanism to be explored. Heterogeneous photocatalysis has been described since 1970, from the development of photoelectrochemical cells to produce fuels through the conversion of solar energy. In 1983, one of the first studies related to decontamination by photocatalytic reactions was reported to degrade the trichloroethylene compound (Fujishima e Honda, 1972; Pruden e Ollis, 1983). Over the last two decades, many pieces of research that accomplish and witnessed the rapid growth of photocatalysis as a single green and safe method to treat water from the two most toxic types of pollutants: antibiotics and microbial biological hazards (Baaloudj *et al.*, 2021; Makropoulou, Panagiotopoulou e Venieri, 2018; Rizzo *et al.*, 2014; Valério *et al.*, 2020).

The phenomena associated with photocatalysis find their theoretical basis in the concepts of band theory in solid semiconductor materials. Semiconductor materials hold an electronic structure built by a valence band (VB) and a conduction band (CB). The space between them is called the band gap energy (E_g) (Marquesa, Stumbob e Canela, 2017). When the material absorbs light photons with energy "hυ" greater than or equal to its band gap, it culminates in an electron (e^-) excited from the valence band to the conduction band, with a simultaneous hole (h^+) left in the CB. Therefore, from this phenomenon, an electron/hole (e^-/h^+) pair is produced. The photogenerated electron/hole pair is the driving force to activate the semiconductor material to establish the highly reactive oxygen species (ROS) (Hoffmann $et\ al.$, 1995).

The electron (e^-) reacts with the oxygen (O_2) adsorbed on the semiconductor surface to promote the $O_2^{\bullet-}$ radicals. While the trapped hole (h^+), when in touch with water and moisture transforms them into hydroxyl radical ($OH^{\bullet}$). These sites are the primary oxidizing agents, which behave as extremely powerful oxidants of organic pollutants. They evolve a chain reaction that can destroy progressively the bonds of stable and unreactive molecules to intermediates and further degrade into CO_2 and H_2O (Baaloudj $et\ al.$, 2021; Fujishima, Rao e Tryk, 2000; Nogueira e Jardim, 1998). Moreover, these specimens damage microorganisms without the aid of chemical oxidants, attacking and disrupting the cell wall membrane. Through them, the pathogens become inactive or dead, with denatured proteins that result in end-products (Pigeot-Rémy $et\ al.$, 2011). Figure 3 illustrates the semiconductor material coupled with the photocatalysis mechanisms based on the above-mentioned system for ROS generation.

More recent studies have ascribed the photocatalytic mechanism not only to hydroxyl and superoxide specimens but also, to other oxygen-derived radical species. The radicals merge with the trapped electrons and produce hydroperoxyl radical ($HO_2^{\bullet}$) and hydrogen peroxide (H_2O_2) (Fan e Yates, 1996; Liu, M. $et\ al.$, 2020). At last, the photocatalysis efficiency depends on the competition between the process in which the electron is removed from the semiconductor surface, called excitation, and when the electron returns to the valence band and releases heat. This is known as recombination, the competitive phenomenon with photocatalysis (Nogueira e Jardim, 1998). The following Equations 1 – 7 describe this entire explanation and reactions of the photocatalysis steps from the electron/hole pair to the effective degradation.

$$\text{Semiconductor} + h\upsilon \rightarrow \text{Semiconductor } (e^-_{BV} + h^+_{BC}) \tag{1}$$

$$O_2 + e^- \rightarrow O_2^{\bullet-} \tag{2}$$

$$H_2O + h^+ \rightarrow OH^{\bullet} \tag{3}$$

$$O_2^{\bullet-} + H^+ \rightarrow HO_2^{\bullet} \tag{4}$$

$$HO_2^{\bullet} + HO_2^{\bullet} \rightarrow H_2O_2 + O_2 \tag{5}$$

$$\text{Organic pollutants} + O_2^{\bullet-} + OH^{\bullet} \rightarrow \text{intermediates} \rightarrow CO_2 + H_2O \tag{6}$$

$$\text{Semiconductor } (e^-_{BV} + h^+_{BC}) \rightarrow \text{Semiconductor} + \text{heat} \tag{7}$$
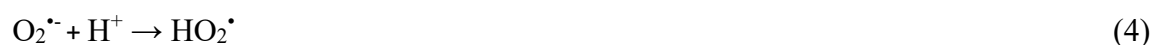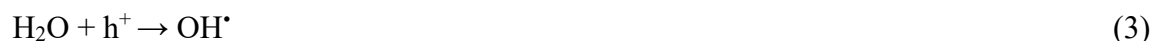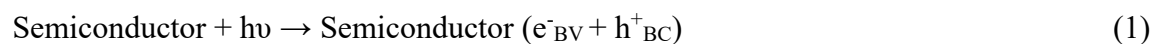
Figure 3 – Mechanisms of the organic and microbial photocatalytic removals through a semiconductor material.
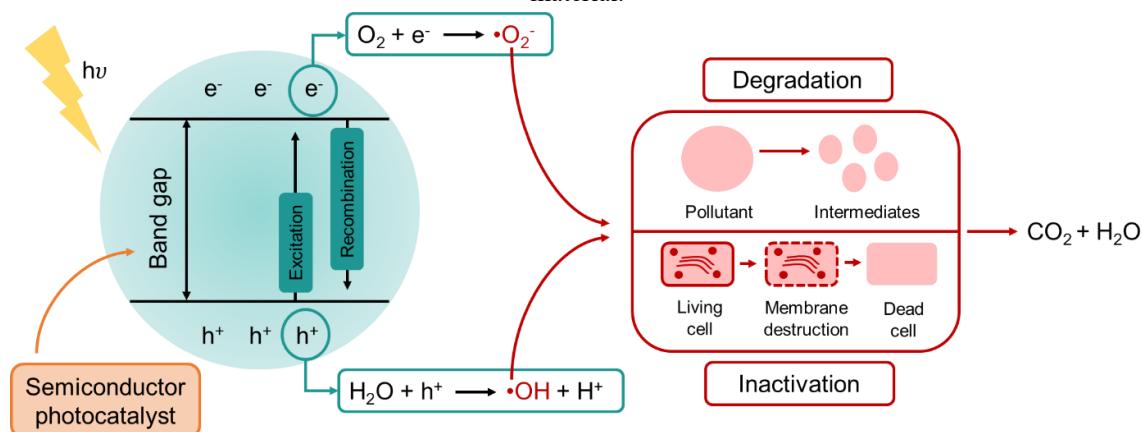
Source: Author (2022), based on (Ateia *et al.*, 2020).

Therefore, the main inherent features of photocatalysis which support the process in the treatment of anthropic effluents to accomplish the world's challenges and the future desires of environmental remediation with less cost and more minor damage dwell on: (I) the reactions run at room temperature and the whole oxygen comes from the atmosphere; (II) the oxidation of the substances may be complete; (III) the semiconductor material is cheap, reusable and embeddable in different types of inert matrices; and (IV) the light source for the photoexcitation of the material may be obtained from sunlight, as a renewable energy source (Malato *et al.*, 2009).

3.3. PHOTOCATALYTIC MATERIALS

According to the International Union of Pure and Applied Chemistry (IUPAC), a photocatalyst is a *"material that absorbs light to bring it to a higher energy level and provides this energy to a reacting substance to make a chemical reaction occur"* (McNaught, Wilkinson e Jenkins, 1997). The applicability of a material as a photocatalyst is intrinsically connected with the character of its properties, such as light absorption range, electronic band structure, surface area, particle size, and morphology. In the field of

Materials Science and Engineering, multidisciplinary research areas have been focusing on the design and development of advanced photocatalytic materials, based on approaches that bring together nanotechnology, surface engineering, and heterostructure between materials to sustain and comply with the concerns of the photocatalytic applications.

With the broad term of a photocatalyst defined, so far more than 190 different materials have been assayed as suitable photocatalysts. These materials may be gathered in standard photocatalytic semiconductors, such as TiO_2, ZnO, SiC, WO_3, CdS e CuO_2, emerging photoelectronic materials, which means nanoscale plasmonic metal particles (e.g. Ag, Au, Al, and Bi), quantum dots, which include carbon-based materials and 2D photocatalytic materials ($g-C_3N_4$ and MoS_2), that when coupled with the first category build photocatalytic composite materials or heterojunctions (Yang e Wang, 2018). Up to now, titanium dioxide (TiO_2) is the most researched photocatalytic material with around four times more published papers than the other ones. Nonetheless, studies devoted to other materials, namely zinc oxide (ZnO) have been growing in attention (Fresno *et al.*, 2014; Majumder *et al.*, 2020).

As an alternative to the gold standard TiO_2 photocatalyst, zinc oxide (ZnO) is in the spotlight of many research efforts with stupendous benefits, such as low cost and high quantum efficiency, as well as the photocatalyzed reactions performed better in neutral pH behavior, which is an added merit over its competitor (Kumar e Koteswara Rao, 2015). Another point of interest to zinc oxide as a photocatalyst is assigned to its potential features compared to other mature solutions in the market, namely silver (Ag). The many dangers around Ag are suppressed by zinc oxide (ZnO) low toxicity levels, biodegradability, friendly-environmentally use, and low-cost synthesis routes for large-scale and proven action of photodegradation of pollutants (Chang *et al.*, 2020; Kołodziejczak-Radzimska e Jesionowski, 2014). Moreover, the activity of zinc oxide can be expanded in the absence of light, known as the dark catalysis phenomenon. In the dark, the ZnO has exhibited high antimicrobial activity, given the presence of surface defects and high surface area that allows a greater attachment and contact of the pollutant in the material (Lakshmi Prasanna e Vijayaraghavan, 2015).

3.3.1. Zinc oxide

In Materials Science, zinc oxide (ZnO) is classified as group II-IV semiconductor oxide, whose covalence is on the border between the ionic and covalent semiconductors. ZnO crystallizes in the hexagonal crystal structure of wurtzite (space group $P6_3mc$,

a = 3.25 Å*, c* = 5.20 Å), as shown in Figure 4. ZnO has an n-type conductivity, which comprises a direct band gap of 3.2 eV and large binding energy of 60 meV (Kołodziejczak-Radzimska e Jesionowski, 2014). The ZnO properties comprehend high mechanical-thermal stability, high photosensitivity, a high driving force to induce redox reactions, non-toxicity, ease of crystallization, and natural abundance (Morkoç e Özgür, 2008). Those specific physicochemical, optoelectronic, and magnetic properties of ZnO stimulate its applications in such fields: light-emitting diodes, solar cells, gas sensors, luminescent materials, pigments, UV shielding materials, surface acoustic wave filters, biomedical materials, antifungals, and piezoelectric generators (Kołodziejczak-Radzimska e Jesionowski, 2014; Özgür *et al.*, 2005; Wang, 2008). Without a doubt, ZnO is a multifunctional material.

Figure 4 – ZnO wurtzite crystal structure: (a) side view and (b) top view.
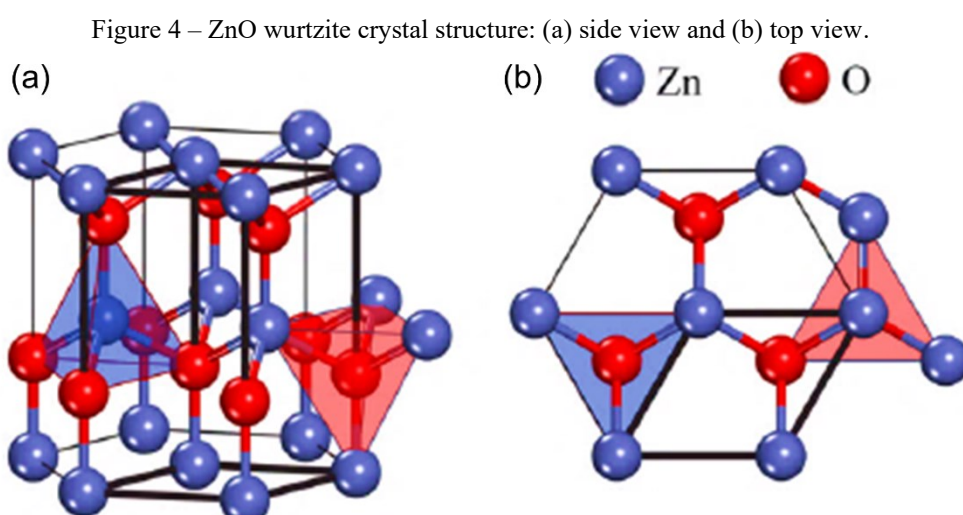
Source: Adapted from (Samadi *et al.*, 2016).

As a photocatalyst, extensive work on the ZnO has been attempted and applied in environmental and renewable energy fields, as illustrated in Figure 5 (a). Based on the Scopus database, from January/2000 to June/2022, around 14.000 scientific papers had been published about zinc oxide performance in photocatalysis (Figure 5 (b)). Those researches are focused to investigate the different synthesis methods, chemical composition, morphology, size, specific surface area, porosity, and crystalline phase on the photocatalytic activity of ZnO. One of the points to explain this exponential growth of ZnO-photocatalyzed processes arises from the technological development anchored in the nanoscale science to achieve high-surface-to-volume semiconductor nanoparticles and other exceptional physicochemical characteristics, making the ZnO a leader against other materials (Ahmed *et al.*, 2014; Bhirud *et al.*, 2012; Lü *et al.*, 2021; Ren *et al.*, 2017; Samadi *et al.*, 2016; Synnott *et al.*, 2013).

Figure 5 – (a) Applications of the ZnO as a photocatalyst material in the environment and energy fields. (b) The number of publications of ZnO as photocatalyst from 2000 to 2022, in the Scopus database for keywords "photocataly*" and "zinc oxide" or "ZnO".
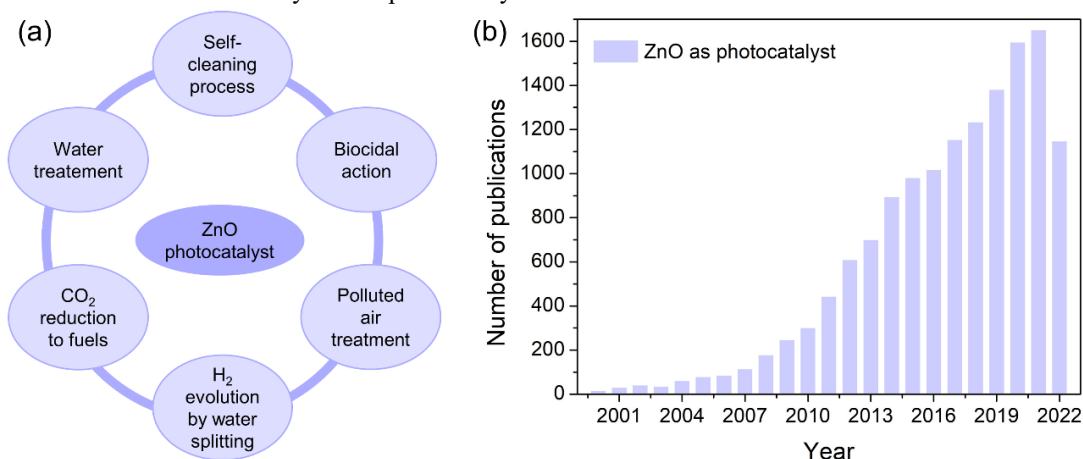
Source: Author (2022).

In recent times, researchers are remarkably interested in the development of green technicalities to synthesize zinc oxide nanoparticles, as compared to conventional ceramic processes, since the photocatalytic activity of ZnO is apt to be initiated when the particles are in the nanoscopic size range (1 – 100 nm) rather than in the macroscopic or bulk size (Islam *et al.*, 2019). Sol-gel, hydro/solvothermal, laser ablation, and microwave-assisted synthesis are some of the commonly employed methods (Kołodziejczak-Radzimska e Jesionowski, 2014; Sudha *et al.*, 2020). However, sometimes these methods require expensive and hazardous substrates, rigorous conditions, and sophisticated techniques. Solution combustion synthesis (SCS), in comparison, is one of the simplest, safest, and most versatile synthesis methods as well is highly energy-efficient, and has strong potential for the large-scale production of nanomaterials in a short time (Wen e Wu, 2014).

The combustion process comprises a self-sustained exothermic reaction among the oxidizing agents, commonly a metal nitrate source, and, the reducing organic molecules, as fuels (Deganello e Tyagi, 2018). SCS comes from propellant chemistry, although it employs a faster procedure at milder temperatures (300 – 500 ºC) than the base techniques (Jain, Adiga e Pai Verneker, 1981). The combustion mixture reacts in a matter of seconds and due to the higher exothermicity, nanocrystalline oxide powders result as the main product. The combustion releases heat and several gases, such as CO_2, N_2, and water vapor, by burning the organic fuels. Thus, the as-combusted powders have foamy and spongy structures, great phase purity, higher surface area, and narrow particle size distribution, whose these features are strictly connected with the chosen synthesis parameters (Li *et al.*, 2015; Novitskaya *et al.*, 2021). Despite the advantages, some disadvantages can be found, such as powder agglomeration, inhomogeneity, and the possible production of hazardous

gases, like NO_x and CO, derived from incomplete combustion of the reactants (Deganello e Tyagi, 2018).

Several works have been devoted to enhancing the photocatalytic degradation efficiency of some pollutants through the ZnO-based nanomaterials produced by solution combustion synthesis, as pointed out in Table 1. The metal precursor to ZnO is mostly a zinc nitrate, single or hexahydrate, incorporated with a wide variety of different fuels, where each one governs unique features. The highly porous structure obtained affords a particular adsorption environment between the pollutant molecules and the catalyst particles, which is crucial for photocatalytic abatement by ZnO (Potti e Srivastava, 2012). Besides, the defective morphological sites (oxygen vacancies) together with the smaller particle size and higher surface area of the ZnO in SCS, produce relatively separable photogenerated charge carriers (electrons/holes), which thereafter gives rise to a higher density of hydroxyl radical, previously described as a ROS and one of the most active oxidative species involved in the photodegradation of environmentally hazardous materials (Section 3.2). These photocatalytic properties in the ZnO catalysts achieved in the SCS emphasize a superior performance over the bulk and commercial ZnO (Essawy *et al.*, 2020; Gowthambabu *et al.*, 2021).

Table 1 – Overview of some reports of the zinc oxide synthesis through the solution combustion method and their photocatalytic application.

Oxidizer/fuel in SCS	Temperature (ºC)	Diameter (nm)	Pollutant	Light source	Time (min)	Photocatalytic efficiency (%)	Reference
$Zn(NO_3)_2.6H_2O$ /sucrose	500	35	Methyl orange	UV-B	30	100	(Islam *et al.*, 2019)
			Methylene blue	UV-B	30	100	
			Methyl orange	Sunlight	30	100	
$Zn(NO_3)_2.6H_2O$/oxalic acid/dextrose	400 – 450	–	Orange G	UV-A	180	70 – 100	(Potti e Srivastava, 2012)
$Zn(NO_3)_2.6H_2O$/urea	500	–	Orange G	UV-B	180	83 – 99%	(Lutukurthi, Dutta e Behara, 2020)
$Zn(NO_3)_2.6H_2O$/citric acid	500	20 – 50	Methyl green	UV-A	40	85 – 100	(Shkir, Hamdy e AlFaify, 2019)
$Zn(NO_3)_2.6H_2O$/pomegranate	425	12 – 17	Flumequine	Sunlight	90	97.6	(Essawy *et al.*, 2020)
$Zn(NO_3)_2.6H_2O$/ lemon juice	500	45	Rhodamine B	UV-B	75	93.2	(Gowthambabu *et al.*, 2021)
			Rhodamine B	Sunlight	75	98.5	
$Zn(NO_3)_2$/CTAB/ glycine	250	–	Methylene blue	UV-B	90	64	(Vahdat Vasei *et al.*, 2019)
$Zn(NO_3)_2$/CTAB/citric acid	250	35 – 50	Methylene blue	UV-B	90	99	(Vahdat Vasei *et al.*, 2019)

Source: Author (2022).

Despite the outstanding performance obtained in the ZnO SCS-produced and even in nanometric size, ZnO-based photocatalysis suffers from some drawbacks: (I) ZnO is excited only in wavelengths below the ultraviolet range (UV) and does not harvest the visible light portion of the solar spectrum; (II) the fast recombination rate of the charge carries (e^-/h^+ pair), consequently, slows down the degradation reaction rate; and (III) the susceptibility to corrosion under the UV light (Samadi *et al.*, 2016). These drawbacks hinder most of the practical applications of ZnO once the solar spectrum is composed only of a small fraction at around 7% of the UV range, while the visible light portion corresponds to a huge amount of 46%, limiting the energy harvesting efficiency (Liu, J. *et al.*, 2020).

The use of visible light to induce the photocatalytic phenomena has been increasing in interest to manage the environmental and energy crisis once this light source is characterized as an abundant, clean, and renewable energy source (Garazhian *et al.*, 2020). So, to overcome the above-mentioned issues, research is growing rapidly to modify the surface-electronic structure of ZnO, largely due to the change in the ZnO defect chemistry to afford and benefit the visible light response and its photocatalysis property under ambient conditions (Kumar e Koteswara Rao, 2015; Qi *et al.*, 2017).

3.4. MODIFICATION STRATEGIES: DOPING

Tailoring the intrinsic defects, surface functionalization with organic compounds, doping with foreign ions (metallic or non-metallic), noble metal deposition, heterostructuring with other semiconductors, and modifications with carbon nanostructures: a wide framework of successful strategies to tune and improve the stability and the photoactivity of ZnO nanostructured photocatalysts under visible light ($400 \leq \lambda \leq 700$ nm), to accelerate the electron transfer process, to promote the electron-hole separation, and to lower the thermodynamic barrier (Kowalska, Wei e Janczarek, 2018; Samadi *et al.*, 2016; Singh, Kumar e Singh, 2019).

The doping phenomenon has been recognized as one of the most feasible strategies. In the sense of the concept, doping is the intentional introduction of a heteroatom in a material, which aims to modulate its properties. The doping in ZnO initially changes the coordination environment of the host ions in the lattice through a turn in the chemical nature of the solid. Further, it modifies the electronic band structure via the introduction of localized electronic energy levels within the band gap states. The former alters the pristine defect structure, and consequently, affects the mobility of the charge carriers. Whereas, the latter effect enables more efficient control of the incident photons and momentarily traps

the photogenerated charge carriers, positively affecting the photocatalytic pathways (Kowalska, Wei e Janczarek, 2018; Kumar e Koteswara Rao, 2015; Samadi *et al.*, 2016). Non-metal doping of ZnO that lies on substitute the oxygen atoms has been intensively investigated. A non-metal may easily replace lattice oxygen sites of ZnO or occupy an interstitial site (Khataee *et al.*, 2014). Carbon, sulfur, boron, and nitrogen are common non-metallic dopants (Yu, Zhang e Peng, 2016).

3.4.1. Nitrogen doping

Nitrogen doping is widely used as a dopant to modify the electronic structure of II – IV semiconductors, such as zinc oxide. Nitrogen has an ionic radius ($r_N{}^{3-}$ = 1.46 Å) close to the oxygen ($r_O{}^{2-}$ = 1.38 Å), higher solubility in the ZnO, lower energy to form oxygen vacancies, and a similar hybridization of N 2p and O 2p states (Kumari, Sahai e Goswami, 2015). According to the literature, this hybridization builds a new valence band state which drives band gap narrowing, due to the elevate of the upper edge of the valence band. (Yu *et al.*, 2013). Hence, Figure 6 exhibits a drawn comparison between the electronic structure of the ZnO undoped and nitrogen-doped.

Some studies suggest that the nitrogen substitutional doping into the ZnO does not behave alone to modify the electronic structure. Nitrogen as a dopant can induce oxygen vacancies at the grain boundaries – triggering the activity in longer wavelengths (Lu, Russo e Feng, 2011). The N-doped in a piece of these vacancies operates to hinder the reoxidation or recombination of the electron/hole pair (Ihara *et al.*, 2003). Carrying with it, the nitrogen can occupy the octahedral or tetrahedral interstitial positions. In the more stable octahedral spaces, nitrogen inserts itself in the crystal lattice between an oxygen atom and two adjacents atoms of zinc, which culminates in an N – O bond with an energy state up to 1.4 eV upper of the ZnO valence band (Gallino *et al.*, 2010).

Figure 6 – Comparativeness of the electronic structure of the ZnO undoped and doped with nitrogen.
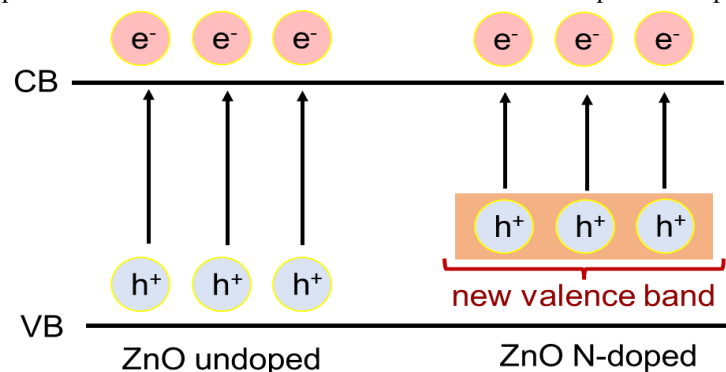
Source: Author (2022), based on (Chen *et al.*, 2010).

Nitrogen source and doping processing play a pivotal role in improving the photocatalytic property of zinc oxide. Depending on them, different degrees of extending the absorption range and properties may be observed in photocatalysis. Macías-Sánchez reported N – ZnO doped with urea by sol-gel method with varying the [N]/[Zn] ratios. For the authors, at 3 wt.% N-ZnO, the photocatalyst has a decrease in its band gap (E_g) by 0.19 eV and provides total photocatalytic mineralization of 2,4-D and picloram herbicides, which means a 3.8 times higher efficiency than pure ZnO (Macías-Sánchez *et al.*, 2015). Contrary, when using direct ammonia gas, a higher temperature is required for N-doping ZnO of high-crystallinity materials, undesirably converting the substitutional nitrogen to molecular nitrogen, which limits the doping effect and reduces the specific surface area, resulting in a negative impact on the photocatalytic degradation (Yu *et al.*, 2013).

Another nitrogen source is nitrogen gas (N_2). At lower pressure plasmas, the molecular nitrogen breaks on atomic nitrogen (N), and this atom is accelerated to be incorporated in the ZnO, having a high nitrogen content. Zinc oxide nanoparticles doped with N_2 in an RF-plasma system revealed 100% of photocatalytic degradation of 2-chlorophenol after 180 minutes under solar light (Salah *et al.*, 2016). Also, nitrogen doping in a DC-plasma of ZnO has antibacterial properties against *E. coli* through ROS generation in visible light (Lin, Liao e Hung, 2005).

3.4.2. Doping by solution combustion synthesis

As underlined in topic 3.3.1, solution combustion synthesis (SCS) has found tremendous success in the literature to produce zinc oxide, in the form of a highly crystalline, thin, porous, and nanoscaled material – crucial features of targeting photocatalytic applications. The attractiveness and advantages of this synthesis route remain in its intrinsic ability to be an in-situ strategy to modify the chemistry of the semiconductor oxide by simply adapting the composition of the metal ion and fuel precursor. In other words, the full power of the material doping occurs simultaneously with the self-sustained combustion solution synthesis reaction (Deganello e Tyagi, 2018; Rajeshwar e Tacconi, De, 2009).

The technical base of the solution combustion arises from the thermodynamic concepts and the chemistry of the propellant theory, as already mentioned. The mechanism of the reaction is complex and still under study. Fuel-to-oxidizer ratio (φ) mainly controls the kinetics of the combustion and the final features of the materials synthesized by SCS. Besides, the influence of different fuels distinguishes them concerning the amount of gases

released during combustion, as well as the temperature of the flame ignition (Deganello e Tyagi, 2018; Novitskaya *et al.*, 2021). However, the temperature to initiate the reaction is enough to allow the doping elements to be incorporated into the crystal lattice (Wen e Wu, 2014). Glycine, citric acid, carbohydrazide, and urea are typical fuels employed in SCS. Adopting these fuels, nitrogen or carbon doping is expected since the aforementioned elements are part of them (Li *et al.*, 2015).

As a fuel, urea (CH_4N_2O) is simultaneously a good nitrogen dopant source. Urea holds on its structure two amino groups ($- NH_2$) located at both ends of the chemical structure. During the combustion process, it decomposes to generate in situ ammonia (NH_3) as a nitrogen origin and assures a reducing atmosphere (Toniolo *et al.*, 2007). Urea easily acts as a complexing agent for metal ions from the metal nitrate (oxidizer), which explains why it is a more reactive fuel to trigger more vigorous combustion reactions (Deshpande, Mukasyan e Varma, 2004). The stoichiometric equilibrium combustion reaction between zinc nitrate and urea to generate the zinc oxide is written in the following Equation 8, where $\varphi = 1$ means a stoichiometric state in which the atmospheric oxygen is not needed for the complete oxidation of the fuel (Wen e Wu, 2014).

$$Zn(NO_3)_2 + \varphi CH_4N_2O + 5(\varphi - 1)O_2 \rightarrow ZnO + \frac{5\varphi+3}{3}N_{2(g)} + \frac{5}{3}\varphi CO_{2(g)} + \frac{10}{3}\varphi H_2O_{(g)} \qquad (8)$$
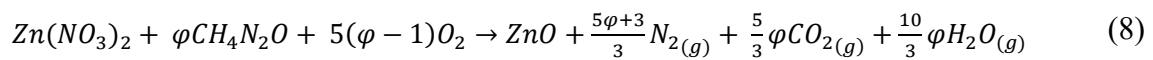
K. Sivaranjani and C.S. Gopinath explained the doping of titanium dioxide towards the use of urea as a part of the first ongoing studies on N-doping in metal oxides by solution combustion methods (Sivaranjani e Gopinath, 2011). Oxo-titanium nanoclusters (Ti_xO_y, $x/y > 1$) grow with the presence of defects under the ammonia atmosphere, from the urea molecule. As an electron donor, NH_3 easily interacts with the defect-rich clusters, which culminates in the incorporation of the N element into the TiO_2 lattice to develop $TiO_{2-x}N_x$ materials. According to the authors, urea-assisted doping in solution combustion builds materials that have aspects like visible light absorption, mesoporosity, smaller particle size with high crystallinity, and high surface area to achieve a faster dye photocatalytic degradation under direct sunlight.

A similar concept has been adopted to obtain $ZnO_{1-x}N_x$ or $N - ZnO$ materials. For M. Mapa and C.S. Gopinath, doped zinc oxide is produced by the solution combustion method at 500 ºC under different degrees of the urea/zinc nitrate molar ratio. Since the material can form oxygen vacancy on the heating induced by the reaction, the large amount of vacancies grants the higher nitrogen loading on the ZnO structure, with bulk concentrations of up to 15 at.%. The authors recognized the visible light absorption

extended up to 650 nm for $ZnO_{1-x}N_x$ that highlighting the employment of the material as a visible-light photocatalyst (Mapa e Gopinath, 2009).

In the work of I.M. Silva and co-authors, they developed a simple, fast, and easy strategy for N:ZnO synthesis by modifying the base precursor of Zn salts and citric acid with urea, as an N-source molecule. The characterizations of the as-prepared N:ZnO nanoparticles proved that doping affects neither the particle morphology nor the crystal structure. Instead, it largely changes the photoactivity mechanism for Rhodamine-B degradation, with an optimum content of 2 wt.% N for visible activity, even though the nanoparticle band gap was not modified. Under visible light illumination, the radical $O_2H^\bullet$ and holes (h^+) participated together in the dye degradation by the doped samples, against only the $OH^\bullet$ radical action on the undoped one. The results enhance the essential comprehension of the photocatalytic activity of the semiconductor doping processes (Silva *et al.*, 2016).

Another example of ZnO-assisted doping with urea lies in the work of H. Sudrajat and S. Babel. They introduced a combustion reaction between zinc acetate dihydrate and urea in a 1:2 molar ratio at 500 ºC for preparing N-doped ZnO (Sudrajat e Babel, 2017). According to the authors, the N dopants do not combine to create N_2 molecules and remain in the N-ZnO structure as substitutional or interstitial sites. The N-doping narrows the band gap from 3.15 eV to 1.7 eV, with a visible light response due to the mid-gap in the electron transition and the presence of oxygen defects, which acts as electron traps. The paper ensures that the improved absorption coupled with a higher surface area of the material extended the carrier lifetime and boosts the long-term application of the catalyst for effective degradation of organic pollutants, such as methylene blue, under visible light photocatalysis.

Although the chemistry of a solution combustion synthesis with urea is well proven to be a good and efficient nitrogen doping source, highlighting the above-cited results of N-doped ZnO, urea changes the thermodynamics of the reaction. When using urea as a fuel, the reaction varies from a mild state with only a smoldering effect to a vigorous burning reaction, which produces an intense flame of higher temperature (Jain, Adiga e Pai Verneker, 1981; Novitskaya *et al.*, 2021). In this case, nitrogen-based fuels could favor materials with larger crystallites and particle size, and a greater tendency to aggregation, due to the large energy to nucleate and grow the primary particles (Lazarov *et al.*, 2017). Therefore, this Master's thesis goes with a clear aim to develop a one-step synthesis and doping through the different fuel ratios of sucrose and urea to find out an equilibrium

between the band gap narrowing and the available surface area, which together grants an optimized photocatalysis of recalcitrant pollutants under visible light.

4. MATERIALS AND METHODS

The present research is divided into three main steps: (I) the development of the ZnO functionalization through a one-step synthesis and doping by solution combustion method; (II) a comprehensive characterization of the ZnO-based materials SCS-produced, and (III) the evaluation of the visible-light-driven photocatalytic activity of the ZnO/N-ZnO materials doping by SCS. In this section, all the materials and methods inside the scope of the work are cited and detailed described. This Master's research has been held in the Materials Laboratory (LabMat), in the Mechanical Engineering Department of the Federal University of Santa Catarina (EMC/UFSC) with support of associated laboratories from the Physics Department (FSC/UFSC) and Department of Chemical Engineering and Food Engineering (EQA/UFSC).

4.1. MATERIALS

All the materials employed to develop this work are shown in Table 2.

Table 2 – Features of the reactants used and their respective role.

Material	Molecular formula	Molecular weight (g/mol)	Reaction role	Manufacturer
Zinc nitrate hexahydrate	$Zn(NO_3)_2 \cdot 6H_2O$	297.49	Oxidizer	Neon Comercial
Sucrose	$C_{12}H_{11}O_{22}$	342.3	Fuel	Neon Comercial
Urea	CH_4N_2O	60.06	Fuel and nitrogen source	Neon Comercial

Source: Author (2022).

Zinc nitrate hexahydrate, sucrose, and urea are the main precursors of the zinc oxide nanoparticles produced by the combustion method in this research. The zinc nitrate hexahydrate comprises the source of the metal cations, namely the Zn ions. The nitrate anions $(NO_3)^{-2}$ in its formula are oxidants and have strong activity in the redox reaction when combustion occurs. Beyond the oxidizing power, this nitrate being hydrated may offer lower decomposition temperature and good solubility in water (Zhang *et al.*, 2012). Sucrose, as the primary fuel, is an eco-friendly and cheap fuel. The sucrose molecule has a noticeably high reducing power and creates an environment around the metal cation, which may govern the oxidation state and modulates the morphology and textural properties (Tummino *et al.*, 2020). Urea is also one of the most common fuels used in SCS, due to its good availability, high exothermicity, as well as its high coordination ability toward

nitrates. But more than fuel, urea is a proper dopant as the nitrogen driving source for the one-step synthesis and doping of the zinc oxide nanoparticles, in this study. Moreover, the choice of urea is highly supported in all that has been mentioned in Section 3.4.

4.2. ONE-STEP SYNTHESIS AND DOPING OF ZINC OXIDE

This study synthesizes zinc oxide-based nanoparticles through solution combustion synthesis (SCS) adapting the method reported by Islam et al. (Islam *et al.*, 2019). The basic steps for the undoped ZnO for a yield of around one gram are as follows. 3.569 g (12 mmol) of zinc nitrate hexahydrate and 1.2 g (3.5 mmol) of sucrose are complexed with 3 ml of distilled water in a ceramic beaker until the complete dissolution of the solid parts. For this amount of oxidizer and fuel, the fuel-to-oxidizer ratio (φ) is calculated by Equation 9. In propellant chemistry, the valency in this ratio is based on each element that composes the reactants. The total oxidizing valence from the metal cation (zinc nitrate hexahydrate, $Zn(NO_3)_2 \cdot 6H_2O$) is equal to 10. While the reducing valences of the fuels are – 48 and – 6 for sucrose ($C_{12}H11O_{22}$) and urea (CH_4N_2O), respectively (Novitskaya *et al.*, 2021). As an example, the reducing valence of urea is calculated from Equation 10 – 14, based on the method reported in the cited reference (Lopez, McKittrick e Shea, 1997). With the molar amounts and the valencies described, in this work, the fuel-to-oxidizer ratio should be equal to 1.4026, corresponding to a fuel-rich mixture ($\varphi > 1$).

$$\varphi = \frac{\sum(moles\ of\ elements\ in\ chemical\ formula\ of\ fuel).(valency)}{\sum(moles\ of\ elements\ in\ chemical\ formula\ of\ oxidizer).(valency)} \quad (9)$$

- The total oxidizing valence of urea

$$C = 1\ x\ (-4) = -4 \quad (10)$$

$$H = 4\ x\ (-1) = -4 \quad (11)$$

$$N = 2\ x\ (0) = 0 \quad (12)$$

$$O = 1\ x\ (2) = 2 \quad (13)$$

$$Total = -6 \quad (14)$$

The mixture of the reactants is placed in a Muffle furnace pre-heated at 500 ºC, which turns into a uniform viscous paste and, starts to decompose and releases a huge amount of gas. The overall reaction of the combustion is very fast and undergoes in seconds. The combustion blows the melted viscous paste and causes it to swell to form a

porous foam. This foam is reached due to the decomposition of zinc nitrate salt to produce the zinc oxide nanoparticles. A standard time for these steps is fixed in 10 minutes. Meanwhile, sucrose is partially carbonized through dehydration and polymerization during the reaction. Due to it, the foam-like material might have residual carbon embedded in the structure. The foam is broken by a spatula to expose this carbon, while kept at 500 ºC in the Muffle furnance. So, the carbon in the powder is combusted away as carbon dioxide (CO_2). Afterward 20 minutes, the nano-ZnO could be cooled down to room temperature and ground in a mortar with a pestle, resulting in a thin white powder of nano-ZnO. The scheme of Figure 7 illustrates the above-mentioned stages to obtain the zinc oxide by SCS.

Figure 7 – Scheme of the solution combustion synthesis steps for zinc oxide nanoparticles.
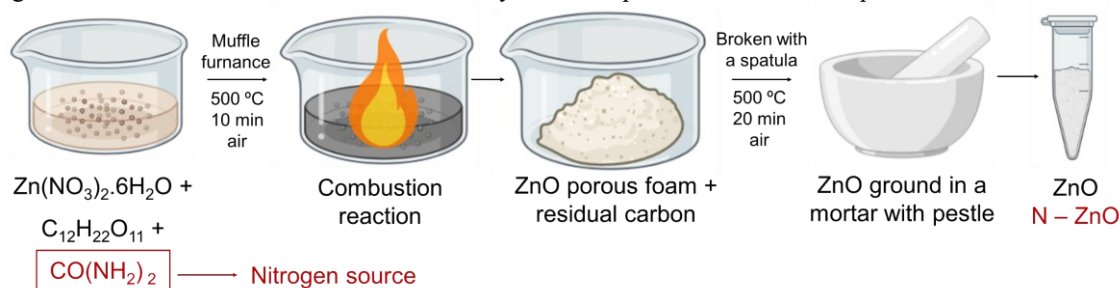
Source: Author (2022).

With the base ZnO synthesis described, the present work starts to explain the proposed doping strategy of ZnO with nitrogen, which relies on the approach of simultaneous synthesis and doping by the solution combustion method. As referred to in the review (Section 3.4.2), the SCS method allows an in situ functionalization of the final product by choosing different fuels in the starting reactants. This one-step approach emphasizes the versatility of the SCS and its advantages, which favors the growth of new SCS variants for advanced technological solutions. The present method comprises the incorporation of urea as a fuel and nitrogen source to the previously mentioned reactants, i.e., Zn-nitrate and sucrose, to functionalize and obtain the nitrogen-doped ZnO (N – ZnO), as highlighted in red in Figure 7.

In this work, to maintain the stoichiometric, the fuel-to-oxidizer ratio is kept constant at 1.4026 (Equation 9), together with the quantity of zinc nitrate hexahydrate. The planned method is anchored in the modification of the molar ratio between sucrose and urea, as the fuels. In this system, sucrose helps to control the particle size, while urea acts as the doping signatory. The changes applied to the amount of sucrose/urea used might influence the concentration of nitrogen doping in ZnO. Consequently, promoting different morphologies, sizes, electronic, textural, and chemical states properties, which ultimately drive the photocatalytic properties of the materials.

The method comprises a scale of five molar percentages of urea, calculated base on the molar amount of sucrose as described in Table 3 and named the urea-to-sucrose molar ratio. This scale starts with 0% of urea, which corresponds to the undoped zinc oxide (ZnO U0). The doping increment with urea follows a step of 25%, so, ranging in 25% (ZnO U25), 50% (ZnO U50), 75% (ZnO U75), and 100% (ZnO U100). At the ZnO U100, urea will be the only fuel in the reaction. To the best of our knowledge, the sucrose-urea-based combustion method has not been reported yet for ZnO nitrogen-doped with visible light photocatalysis of emerging contaminants. The SCS synthesis and doping were done in quadruplicate to assure the reproducibility of the method.

Table 3 – Urea-to-sucrose molar variation to the one-step synthesis and doping of nano-zinc oxide by SCS.

Urea-to-sucrose molar ratio	ZnO U0	ZnO U25	ZnO U50	ZnO U75	ZnO U100
% urea molar	0	25	50	75	100
Sucrose in mmols	3.5	3.4	3.1	2.5	0
Urea in mmols	0	1.1	3.1	7.6	28
Zn-nitrate in mmols	12	12	12	12	12
Fuel-to-oxidizer ratio	1.4026	1.4026	1.4026	1.4026	1.4026

Source: Author (2022).

4.3. CHARACTERIZATION TECHNIQUES

The next subsections will detail and specify the material characterization techniques applied to give a deep understanding of the features and properties accomplished in the ZnO materials by one-step synthesis and doping by solution combustion method.

4.3.1. X-ray diffraction (XRD)

X-ray diffraction (XRD) has been used to ensure the crystalline structure of the zinc oxide after the SCS synthesis. For doping, the technique measures the distortions in the materials, since the lattice parameters could be modified by nitrogen doping (Kumari, Sahai e Goswami, 2015). The X-ray diffractograms were acquired with a Rigaku MiniFlex600 diffractometer (Cu Kα / λ = 1.5406 Å). The angular range is 5º < 2θ < 90º with a step size of 0.1º and a scan rate of 10º.min^{-1}. The data treatment is supplied through the X'Pert HighScore Plus software and supported by the Inorganic Crystal Structure Database (ICSD) database. The lattice parameters and the crystallite size were executed and

calculated by the Rietveld refinement in the Maud software v2.933 (2022) with Crystallography Open Database (COD). The quality of the refinements was quantified by the control parameter χ^2 simultaneously calculated in the refinement, which is a compliance statistical test.

4.3.2. Scanning electron microscopy (SEM)

The morphology and size of the zinc oxide nanoparticles undoped and doped were captured by scanning electron microscopy (SEM), on a VEGA3 LM TESCAN microscope. This equipment has been coupled with it an energy-dispersive X-ray spectroscopy probe (EDX), for qualitative chemical analysis. The micrographs were acquired at 25 kV, 6 of beam intensity, and a work distance of 5 mm, at magnifications ranging from 50.000x to 150.000x. For this technique, the zinc oxide nanopowders were prepared on silicon stubs and covered with gold.

4.3.3. Particle size distribution

The ZnO synthesis and doping reactions may affect the particle size of the materials. To understand it, particle size distributions by hydrodynamic diameter were performed in a Malvern Zetasizer Nanosizer (from 0.3 nm to 10 µm) equipment, based on the dynamic light scattering (DLS) at 173º. The measurements are guided by ISO 22412:2017, related to the particle size analysis. For it, the samples were prepared from the removal of an aliquot of a mother suspension of the solid materials in deionized water with pH-controlled by sodium ammonium hydroxide (NH_4OH).

4.3.4. N_2 adsorption-desorption (BET/BJH)

To get a discernment of the role of the one-step SCS of the ZnO/nitrogenated ZnO on the textural properties, N_2 adsorption-desorption analyses were performed, which are relevant properties for photocatalysis reactions. The analysis is based on the Brunauer-Emmet-Teller (BET) method, where it is possible to determine the surface area of the materials. While, pore volume and pore size distribution are estimated by Barrett−Joyner−Halenda (BJH) method. For it, N_2 isotherms were obtained at 77 K in a Quantachrome Instrument Autosorb. All the samples were tested with pure nitrogen (99.999%) after a degassing step at 80 ºC for 24 hours.

44

4.3.5. X-ray photoelectron spectroscopy (XPS)

X-ray photoelectron spectroscopy (XPS) is employed in this work to identify the elements that exist in the first few nanometers from the surface of the doped materials, as well as their chemical state, highlighting the presence of nitrogen. This detection was carried out on a ThermoScientific K-alpha with a monochromatic Al Kα X-ray source and an energy step size of 0.025 eV. A C1s level of 284.8 eV was used as an internal standard. The software CasaXPS was used to calculate the elementary composition.

4.3.6. CHN (S) elemental analysis

CHN (S) elemental analysis is a technique capable to determine the amounts of carbon (C), hydrogen (H), and nitrogen (N) in a material. The CNH (S) allows a more comprehensive view of the chemical composition given its volume of interaction throughout the bulk of the material. The presence of these elements in the studied samples is intrinsically connected with the single-step synthesis and doping by solution combustion method. In this measurement, a CHNS-O equipment model Fisions – EA1108 was used. Cystine and benzoic acid were employed as the solvents.

4.3.7. Ultraviolet-visible spectroscopy (UV/vis)

The ultraviolet-visible spectroscopy is essential to photocatalytic materials. Here, it is used to measure the optical properties related to the light absorbance phenomenon in the visible range by the studied materials. Absorbance measurements were made in a PerkinElmer Lambda 750 spectrophotometer, in a wavelength range from 190 to 900 nm. Solid-state samples in the form of pellets were made with potassium bromide (KBr), as the substrate and control reference. 100 mg of KBr for 10 mg of each as-synthesized ZnO-based material are blending and pressed at 9 MPa.

4.4. PHOTOCATALYSIS ESSAYS

The photocatalytic activity and performance of the ZnO-based materials under visible light were evaluated by degrading the tetracycline hydrochloride (TC – HCl) pharmaceutical compound ($C_{22}H_{24}N_2O_8$.HCl, 480.9 g/mol, MedQuimica), as the pollutant model. Tetracycline, as well indicate in Section 3.1, is an emerging contaminant that imposes a severe threat to humans and the environment because it severely disturbs the ecological equilibrium due to the poor degradation and development of bacterial resistance

(Ahmad, Zhu e Sun, 2021). Likewise, to support the tetracycline as the model pollutant, many studies on photocatalysis are well-established with organic dye pollutants, especially those devoted to ZnO, as previously exemplified in Table 1. But these molecules have a quite widespread concern around them with the potential to provide biased conclusions. By the dyeing approach, sensitization of the dye is a confounding factor, in the photocatalytic assessment. In the irradiated media, the degradation could be either by photocatalysis – the genuine effect to study and highlight – or by a dye-sensitized, the abatement by photolysis and both (Barbero e Vione, 2016; Yan *et al.*, 2006). To sum up, the photocatalysis of dye pollutants might generate inconclusive data. So, acquiring fundamental knowledge on photocatalysis of promising new materials, designs, and strategies to move forward in the future calls for a reliable methodology, to bring this technology from the laboratory to industry.

The experiments were conducted on a closed photocatalytic box reactor equipped with a visible light source, by means of a fluorescent lamp (15 W, $\lambda > 420$ nm), as illustrated in Figure 8 (a). 10 ppm of TC – HCl and 0.5 g/L of each catalyst were homogeneously dispersed in the aqueous media with the aid of a sonicator (Misonix S4000-010) and without pH adjustment. Before light illumination, the suspension is kept in the dark for 20 minutes with magnetic stirring at 500 rpm to establish the adsorption-desorption equilibrium between the ZnO catalysts and the pollutant.

Figure 8 – (a) Setup of the photocatalytic box reactor for the photocatalysis essays. (b) Absorbance spectra of the tetracycline hydrochloride (TC – HCl) as a model pollutant.
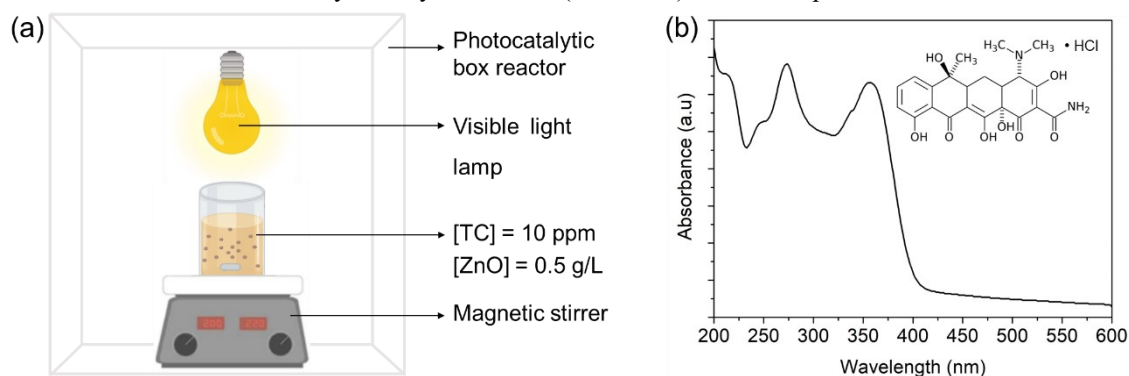
Source: Author (2022), based on (Ahmad, Zhu e Sun, 2021; Zanchettin *et al.*, 2021).

The catalyst is irradiated under the fluorescent lamp in the box reactor while continuing in the suspension with the same magnetic stirrer. At a regular interval of 20 minutes, an aliquot of 5 ml of the samples was withdrawn and filtered through a PTFE 0.45 µm syringe filter Filtrilo® and centrifugated at 4000 rpm (K14-4000 KASVI) for 15 minutes. The abatement of the pollutant was measured using a UV-visible spectrophotometer (HITACHI, U1700). According to the Beer-Lambert law, the relative

concentration (C/C_0) of the tetracycline hydrochloride was determined by the relative absorbance (A/A_0) based on the absorbance spectra at 357 nm, which is the characteristic absorption peak of TC – HCl (Figure 8 (b)). A_0 and A are the absorbances of the tetracycline solution at the starting time (t_0) of the photocatalytic essay and at each time "t", respectively. The essays were made in quadruplicate to assure the reproducibility of the process and its performance.

5. RESULTS AND DISCUSSIONS

In this Section, the results obtained through the experimental protocol described in Section 4 will be reported and discussed. The results are organized in a sequence that first describes the physicochemical features and properties of the ZnO-based materials developed by one-step synthesis and doping by solution combustion method in different urea-to-sucrose molar ratios, and correlates them with the experimental parameters and what is already found in the literature. And next, a line-up that explores the potential of the materials under visible-light photocatalysis and the deployments to understand the behavior of the materials' performance to degrade the tetracycline hydrochloride as a model emerging contaminant.

5.1. CRYSTALLINE STRUCTURE

X-ray diffraction patterns of the as-synthesized ZnO and N-doped ZnO with varying urea-to-sucrose molar ratios in the solution combustion synthesis and doping are depicted in Figure 9 (a). All the diffractograms have sharp peaks at $2\theta = 31.70º$, $34.35º$, $36.19º$, $47.48º$, $56.54º$, $62.80º$, $66.32º$, $67.89º$, and $69.04º$, which are assigned to the (100), (002), (101), (102), (110), (103), (200), (112), and (201) lattice planes of ZnO, respectively. These features correspond to the hexagonal wurtzite structure of zinc oxide, which matches the standard ICSD pattern no. 31052 (crystallographic space group $P6_3mc$). This indicates that the zinc oxide was produced directly from the self-propagating and exothermic combustion reaction. After it, neither secondary phases nor peaks of impurities are observed in any of the patterns, which assures the transformation of the solution into a crystalline material with a degree of compositional homogeneity.

Given the doping phenomenon, it is well established that lattice distortions should be induced in the crystal structure, e.g. vacancies, interstitials, substitutions, and local structure transformations (Kumari, Sahai e Goswami, 2015). As a doping signature, a slight shift toward higher 2θ angles of the XRD peak positions occurs in this work. And to represent it, the prominent (101) peak of the ZnO-based material, located at around $36.19º$, was analyzed by an enlarged view of this peak as brings Figure 9 (b). The shift in this peak position is up to $0.146º$ and is more perceived in higher urea-doped ZnO materials, from ZnO U50 to ZnO U100, as evident through the dashed line.

This displacement can be attributed to the partial replacement of the oxygen by nitrogen into the crystalline structure of the zinc oxide, as an effect of the difference in the

size of the ionic radius of oxygen and nitrogen (r_{O}^{2-} = 1.38 Å and r_{N}^{3-} = 1.46 Å) (Kumari, Sahai e Goswami, 2015). Together with the shift in the (101) peak position, the peak is also broadened and may appear that the nitrogen also affects the crystallite size since this correlates with the observed broadening (Yu *et al.*, 2013). Based on these aforesaid qualitative inferences, these are the first indications of the effect of the urea-to-sucrose molar ratio in the ZnO materials and, consequently, a sign of N-doping into the ZnO lattice.

Figure 9 – (a) XRD patterns of ZnO nitrogen-doped with urea by SCS. (b) Shifts in peak position and broadening through the enlarged view of the (101) peak from ZnO U0 to U100.
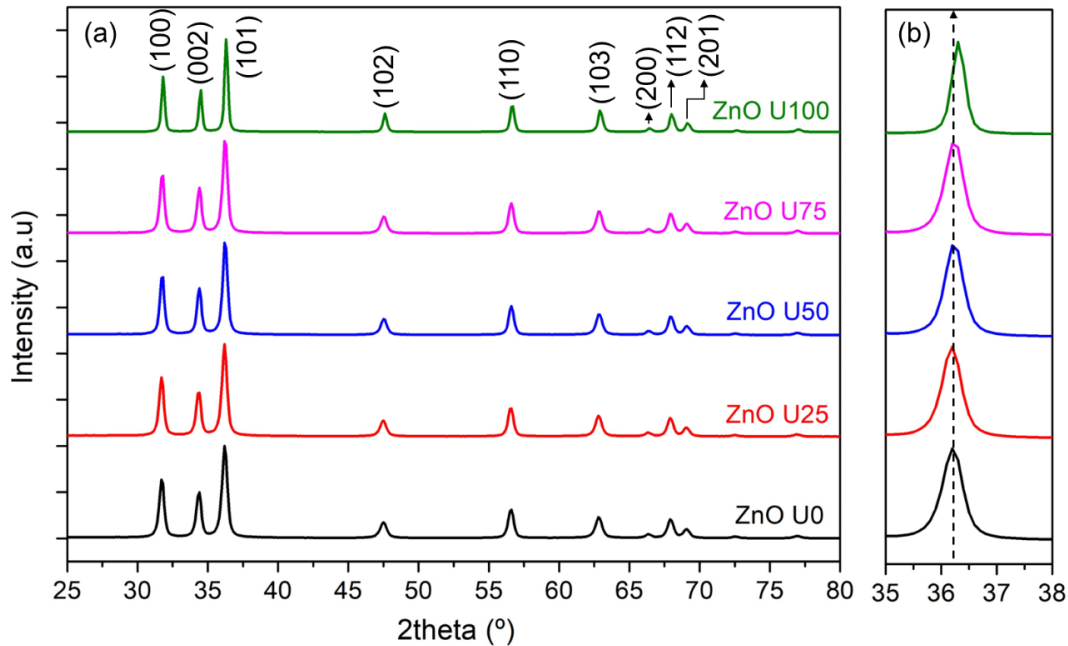
Source: Author (2022).

To get a deep understanding of the effects of nitrogen in the ZnO lattice, quantitative measurements were performed on the lattice constants *a* and *c*, and the crystallite size. The detailed structural studies were carried out by Rietveld refinement in Maud software and the values are shown in Table 4. The refined lattice parameters are found to agree with the reported values in the COD standard (CIF no. 2300112) since low values for χ^2 were found. And, it may be concluded that the crystal parameters obtained in this work are sufficiently close to the real ones.

Through the Rietveld analysis in Table 4, there is a decrease in both lattice parameters *a* and *c*. For *a*, it hands from 3.2531(2) Å to 3.2460(0) Å, while the *c* parameter goes from 5.2141(0) Å to 5.2026(9) Å, which indicates a global contraction of the unit cell of the materials well illustrated in Figure 10 (a). Compared to the undoped one (ZnO U0), in the N-doped samples with urea (ZnO U25 to ZnO U100), the shrinkage enhances as the urea-to-sucrose molar ratio enhances in the SCS solution and reaches the maximum point, for this work, at 100% of urea. In the sense of the ionic size of the oxygen and nitrogen

earlier mentioned, it could be expected that the doping phenomena expands the ZnO lattice instead of contracts since nitrogen is a slightly bigger element than oxygen.

Table 4 – Lattice parameters and crystallite size of the SCS-synthesized and doped ZnO calculated by Rietveld refinement.

Sample code	Lattice parameter (Å)		Crystallite size (nm)	χ^2
	a	*c*		
ZnO U0	3.2531(2) ± 0.00025	5.2141(0) ± 0.00011	36.84 ± 0.40	3.5574
ZnO U25	3.2522(9) ± 0.00029	5.2126(0) ± 0.00037	38.37 ± 0.28	3.5150
ZnO U50	3.2499(6) ± 0.00033	5.2088(9) ± 0.00085	40.65 ± 0.43	3.1453
ZnO U75	3.2495(6) ± 0.00044	5.2076(7) ± 0.00012	48.19 ± 0.45	3.6502
ZnO U100	3.2460(0) ± 0.00049	5.2026(9) ± 0.00049	86.41 ± 0.11	3.3255

Source: Author (2022).

Figure 10 – Graphs of the Rietveld refinement for (a) lattice parameters and (b) crystallite size.
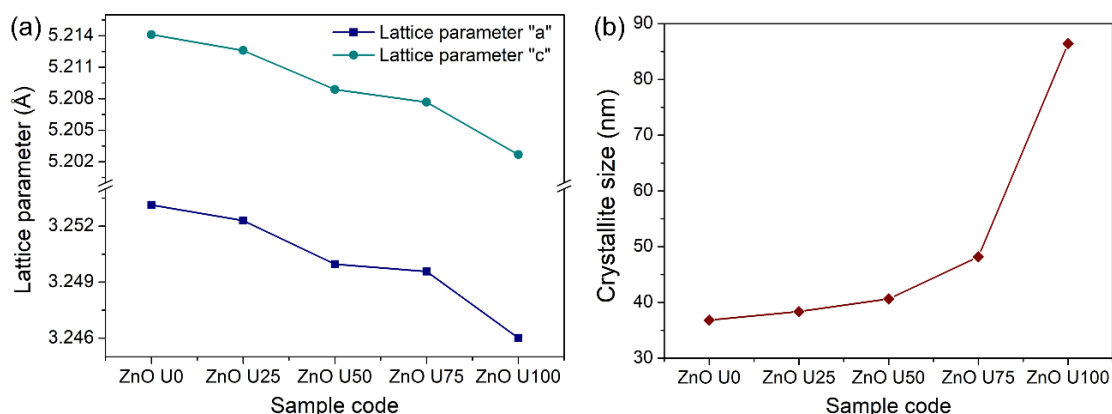
Source: Author (2022).

H. Sutanto et al. when preparing ZnO N-doped using urea in the spray coating technique verified that the N-doping generated a positive strain in the materials and causes the ZnO lattice to become larger (Sutanto *et al.*, 2017). In another example, R. Kumari and co-authors, adopted a chemical precipitation route with ammonium acetate to functionalize ZnO nanoparticles that led to lattice constants up to $a = 3.2795$ Å and $c = 5.240$ Å, attributed to internal tensile strain in a movement of expansion (Kumari, Sahai e Goswami, 2015). However, here, the ZnO lattice contraction explains itself as follows. With more urea in the reaction medium from ZnO U25 to ZnO U100, the reducing power of the fuel and the amount of thermally generate gases along the one-step synthesis and doping by SCS intensifies and gets the reaction to be more vigorous (Rajeshwar e Tacconi, De, 2009). This enables two simultaneous effects: (I) under the combustion conditions, significant oxygen deficiencies are yielded; and (II) more nitrogen atoms are supplied to be dope in

the ZnO (Mapa e Gopinath, 2009; Nair *et al.*, 2017). In this work, it is supposed that the rate of losing oxygen atoms is greater than the insert of the nitrogen atoms. And due to it, the respective lattice is enabled to contract, once the structure does not saturate enough with nitrogen to expand.

Similar behavior in the lattice parameters was reported in works that produce ZnO through solution combustion synthesis by applying urea as the fuel for applications as photocatalysts and photoanodes. In M. Mapa and C.S. Gopinath's research, they achieved a lattice parameter $c = 5.1784$ Å and based the aforementioned result on the well-known mechanism of oxygen vacancies to introduce nitrogen into the ZnO lattice (Mapa e Gopinath, 2009). A. Lucilha et al. in its turn achieved $a = 3.2498$ Å and $c = 5.2051$ Å, values closer to the ZnO U75 sample (Lucilha *et al.*, 2014). The higher contractive strains are often observed in nanocrystalline materials due to the displacement of the unit cells from their normal positions. This underlines the presence of lattice vacancies, which are greatly crucial in exploring the merits of ZnO photocatalysis in which these defects at an appropriate amount on the surface of the material improve its properties (Essawy *et al.*, 2020; Potti e Srivastava, 2012).

Another important feature of Table 4, the crystallite size ranges from around 36 to 86 nm in the samples synthesized and doped by SCS. All the ZnO powders were found to be nanocrystalline powders, however, exponential growth is noticed the higher the urea molar ratio provided (Figure 10 (b)). In the urea-concentrated samples (ZnO U75 and ZnO U100), the solution swells and burns rapidly from room temperature to ignition temperature in the pre-heated Muffle furnace. The higher heating rates improve the rate of decomposition of the precursors and offer a significant release of heat in the system, thereby, speeding up the rate of crystal growth (Lutukurthi, Dutta e Behara, 2020; Novitskaya *et al.*, 2021). So, the final powders, especially ZnO U100 with particles of a primary size of 86 nm are bigger on a scale of twice the size of ZnO U50.

In ZnO U25 and ZnO U50, the higher percentage of sucrose instead of urea in the sucrose-urea fuel mixtures controls the combustion kinetics and promotes slower reactions (Tarragó, Malfatti e Sousa, de, 2015). As it goes, the in situ temperature in the flame ignition is lower than in urea-rich systems, and relatively few crystals grow for a large size. So, compared to ZnO U0 on a pure sucrose fuel, slightly larger crystal sizes in ZnO U25 and U50 are obtained, which means around 36, 38, and 40 nm, respectively. All that has been discussed in this XRD section is essential and gives a primary assessment of the

nitrogen doping from the urea-to-sucrose molar ratio as an optimizable variable in the one-step approach of ZnO synthesis and doping by solution combustion synthesis.

5.2. MORPHOLOGY AND PARTICLE SIZE

In SEM micrographs, the influence on the synthesized and modified ZnO by SCS from various urea-to-sucrose molar ratios is retracted in Figure 11 (a) – (e). Detailed analyses of the morphology, dispersity and further particle size are delivered. Figure 11 (a) belongs to undoped ZnO U0, produced with the fuel of pure sucrose. It is feasible to see that the particles are nanoparticles in the range of 50 nm with a predominantly spherical shape. The SEM images in Figure 11 (b) and (c) are assigned to ZnO U25 and ZnO U50, respectively, where the nanoparticles are kept near a cylindrical shape in nature. In these free and lowest urea ratios in the sucrose-based fuel mixture, the particles assemble dense networks of weak aggregates with poor separation between them. And in most cases, it is hard to establish where the boundary of one particle finishes and starts the other one. In the nanoscale, the ZnO powder-like morphology lies down to aggregate, due to polarity, electrostatic attraction, and higher surface energy of the nanoparticles (Islam *et al.*, 2019).

In Figure 11 (d), related to ZnO U75, it is likely to see a sintering effect from the fusion of the particles. As the flame temperature enhances at a 75%-urea molar ratio, the elementary crystallites coalesced into each other due to the higher heat that drives the particle coarsening (Novitskaya *et al.*, 2021). At the micrograph of ZnO U75, even with the sintering necks and the formed larger particles, the thermodynamic effect is not significant enough to transform the morphology and the particle size from nanometer to micrometer. Oppositely to all the other samples, the morphology of complete urea fuel, namely ZnO U100, is entirely different, with corresponding morphology changes transitioning from spherical to pyramidal or hexagonal structures (Figure 11 (e)). In the SCS phenomenon, the competition between the heat of the reaction with the amount of the released gases is the main reason for the observed morphology change (Cao *et al.*, 2015). The highly aggregated particles from Figure 11 (e) well agree with the previous exponential growth to larger crystallite sizes (Figure 10 (b)). This can be attributed to the upper flame temperature reached in ZnO U100 among the studied samples by solution combustion synthesis. The extra energy from a 100% urea-based fuel benefits from a swift rise in the temperature in a narrow timeframe, which leads to crystal and grain growth through enhanced surface diffusion paths and renders the products to display similar behavior to sintering in a structure of submicrometer particles (Tarragó, Malfatti e Sousa, de, 2015).

In the materials characterization, each technique has its advantages and limitations. In this view to contributing to the SEM analysis, once Figure 11 is quite not able to determine the particle size, the present work chooses the principle of dynamic light scattering (DLS) to measure the studied nanoparticles, from ZnO U0 to ZnO U100. DLS is one of the most reliable methods to quantify the particle sizes of powders materials. Hence, it may provide a more direct measurement that allows a correlation with the real size of the nanoparticles, as represented by Figure 12. But before Figure 12 description, it is worth mentioning that the measured diameter is the hydrodynamic diameter and refers to ZnO-based particles combined with the layer of the water droplets on their surfaces, due to the interactions with the aqueous solvent.

Figure 12 assesses the representative particle size distributions with an average size (d_{50}) in number, coupled with an inset of the SEM micrograph from each sample. The average particle size increases proportionally, in the same way, pointed out by the previous analyses. Overall, during the solution combustion synthesis and doping of the ZnO, the growth process of the nanoparticles has two steps when the content of the molar ratio of the urea in the sucrose-based fuel is changed from 0% to 100%. While the particles slowly raise from about 78 nm to 120 nm with a urea-to-sucrose molar ratio of up to 50%, it suddenly enlarges from 120 to around 820 nm at a urea content of 50 – 100%. This phenomenon may be attributed to the higher local flame temperature reached in the environment between the zinc nitrate and urea than the one of nitrate/sucrose.

When the urea-to-sucrose molar ratio in the fuel is lower than or equal to 50%, most of the thermic energy between the precursors in the reaction will be spent to crystallize the material. And, only a small fraction of the heat is for particles' growth. Upon 50%, an excess of heat is produced and there is a large amount of energy that remains to accelerate the growth of the particles, besides those for the crystallization of the material (Liao *et al.*, 2005). These two steps are entirely following the reported discussion on the topic from XRD and SEM characterizations. And even this work is mainly focused on ZnO materials, the crucial factor of each fuel type and its content on the microstructure and size have been already aimed at the literature for other materials by solution combustion method.

Figure 11 – SEM micrographs of ZnO-based materials produced through the one-step combustion synthesis and doping of ZnO with urea. (a) ZnO U0, (b) ZnO U25, (c) ZnO U50, (d) ZnO U75, and (e) ZnO U100.
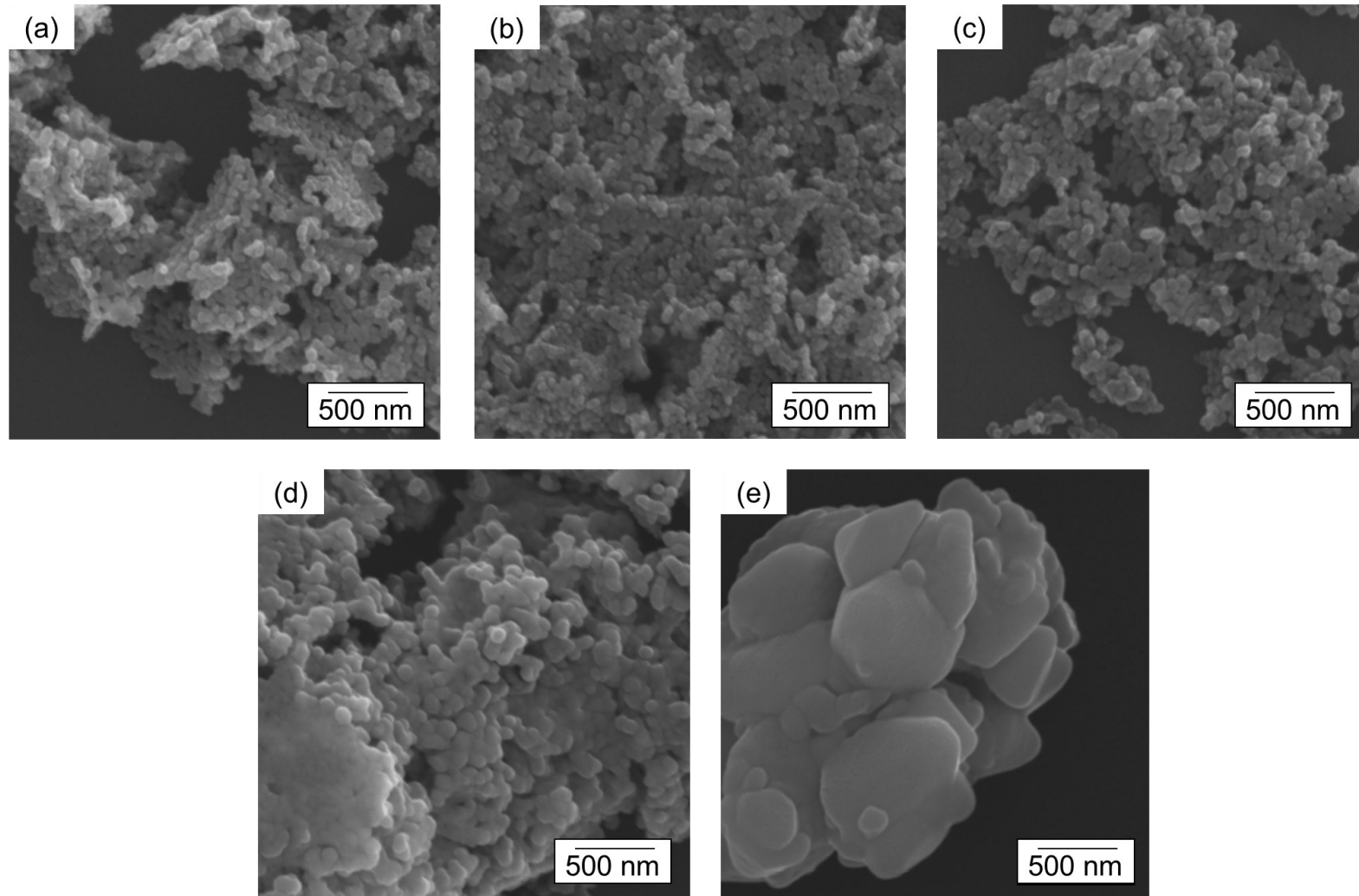
Source: Author (2022).

Figure 12 – Particle size measurement by DLS of the as-synthesized ZnO U0 to ZnO U100 in one-step SCS synthesis and doping with urea.
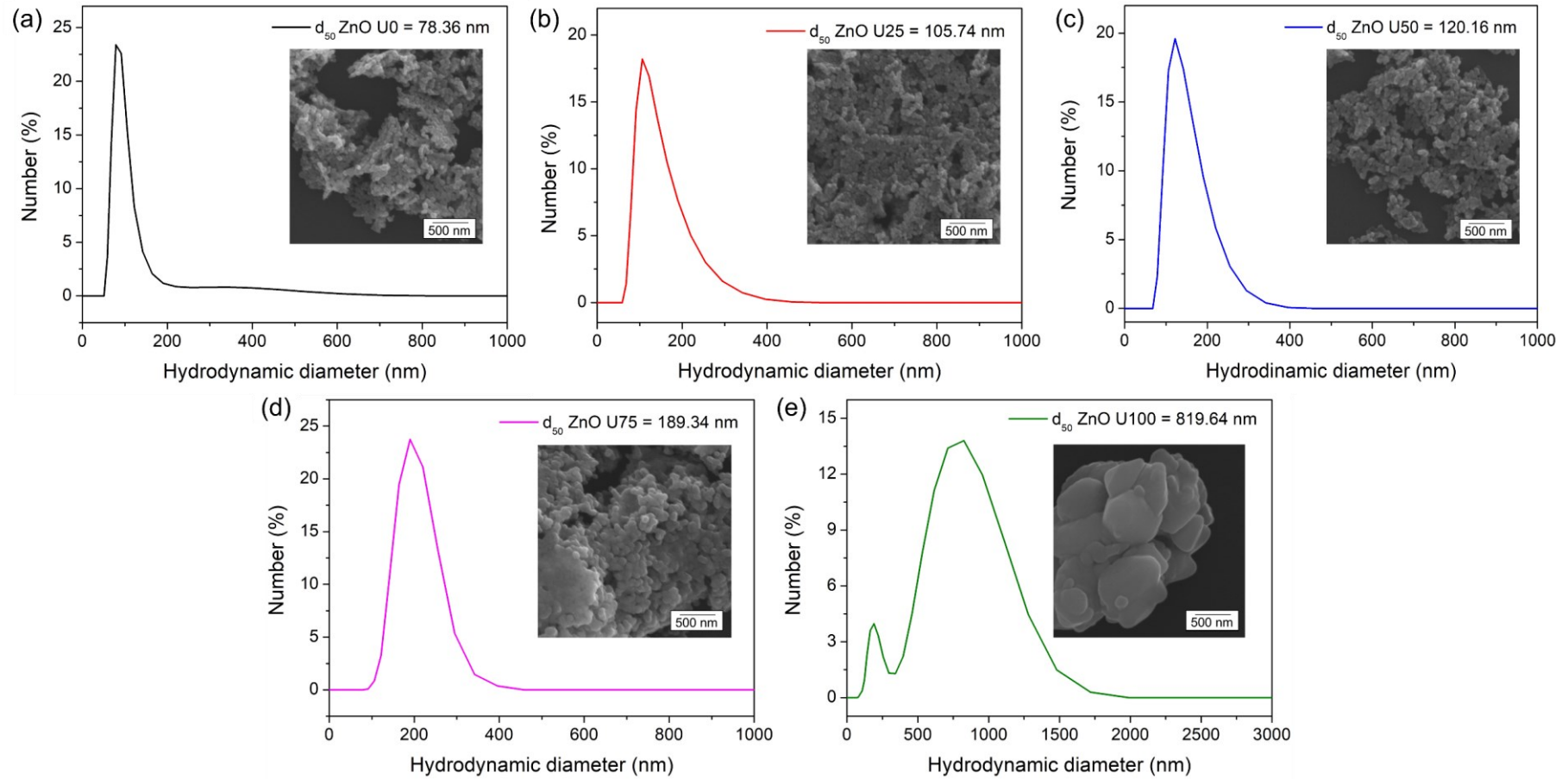
D.P. Tagaró et al. obtained perovskites-based materials in a solution combustion synthesis that used sucrose and urea alone, and a new fuel mixture of sucrose and urea. The different fuels resulted in very distinct sizes, from 18 nm in sucrose to 100 nm or more in urea-based fuel, while mixed-fuel intermediate values and a peculiar spongy morphology were developed. The sucrose alone or mixed with urea promoted higher amounts of exhausted gases during the combustion and a certain amount of the reaction energy is carried away through convective heat losses, which hinders the local sintering (Tarragó, Malfatti e Sousa, de, 2015).

Y. Liao et al. tailored the urea-to-glycine ratio in the fuel to synthesize Tb-doped $Lu_3Al_5O_{12}$ oxide ceramic by SCS and established a well-defined relation of the influence of urea content. For them at an elevated urea molar ratio in the mixed fuel, the particle size becomes significantly larger from $25 – 40$ nm to around 900 nm, deeply matching what has been obtained here for a sucrose-urea mixed fuel (Liao *et al.*, 2005). This particle size behavior can probably affect and reduce the surface area of the as-synthesized materials, which will be the subject of the next section.

5.3. TEXTURAL PROPERTIES

Specific surface area, pore size, and pore volume comprise the array of textural properties. The porous structure and surface area create the environment between the catalysts particles and pollutant molecules, which is essential for the activity and selectivity of the ZnO photocatalyst in pollutant degradation (Lutukurthi, Dutta e Behara, 2020). The N_2 adsorption-desorption isotherms at 77 K of the ZnO products at different urea-to-sucrose molar ratios are displayed in Figure 13. At lower relative pressure (P/P$_0$), the isotherms carry slow nitrogen uptake, followed by a sharp increase in adsorption at higher P/P$_0$ values (P/P$_0$ close to 1). Due to it, the isotherms are type IV with an H3 hysteresis loop, following the IUPAC classification and indicating the presence of mesopores (Thommes *et al.*, 2015). According to the work of W. Wen, J. Wu, and Y. Wang, this behavior may be attributed to the capillary cohesion that occurs from narrow voids among the neighboring flakes on the ZnO structure, when also produced by SCS with zinc nitrate hexahydrate as an oxidizer and glycine as the reductant fuel (Wen, Wu e Wang, 2012).

Through the adsorption isotherms (Figure 13, filled symbols), the specific surface area of the materials is calculated by the Brunauer-Emmet-Teller (BET) method. The surface area varies from values of 4.47 m^2/g to 25.93 m^2/g, depending on the urea-to-sucrose molar ratio. Furthermore, the pore size and volume are performed by the

Barrett−Joyner−Halenda (BJH) method from the desorption branch of the isotherms (Figure 13, open symbols). Table 5 summarizes all these values and the BJH pore diameter confirmed the predominance of mesopores (2 – 50 nm) in all the ZnO samples. The pore size distributions are not actively exhibited here, but they were carefully studied and helped to confirm the last sentence.

Figure 13 – N_2 adsorption-desorption isotherms of the ZnO-based materials by sucrose/urea-assisted SCS. Filled and open symbols are related to adsorption and desorption phenomena, respectively.
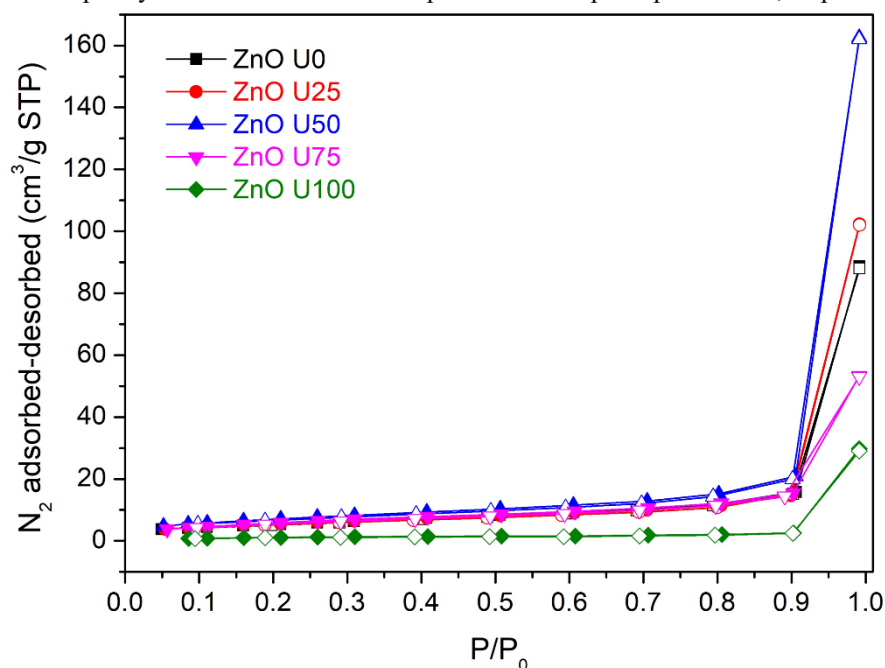
Source: Author (2022).

Table 5 – Textural properties of the ZnO synthesized and doping with urea by SCS.

Sample code	S_{BET} (m^2/g)	BJH pore diameter (nm)	Pore volume (cm^3/g)
ZnO U0	19.82	2.292	0.137
ZnO U25	20.25	2.269	0.158
ZnO U50	25.93	2.439	0.225
ZnO U75	12.54	3.119	0.071
ZnO U100	4.47	4.121	0.046

Source: Author (2022).

In the solution combustion synthesis, the textural properties of the materials are a compromise between the liberated heat and gaseous products. In urea-lean molar ratios, there may exist a synergy between urea and sucrose that promotes an enhancement of the surface area from ZnO U0 to ZnO U50 with a maximum point of 25.93 m^2/g of the ZnO U50. Theoretically speaking, a greater number of moles of gaseous products, such as CO_2, H_2O, and N_2, could be predominant instead of the produced thermal heat in these

combustions (Liao *et al.*, 2005; Lutukurthi, Dutta e Behara, 2020). With more amounts of released gases, the particle size can be better controlled (Figure 12 (b) and (c)) and at the same time raise the surface area. Unlike, in urea-rich molar ratios, the thermal energy for the urea decomposition takes place much more than the liberated gases, which tends to grow the particles, as already observed and, consequently, decrease the surface area to the lowest value of only 4.47 m^2/g in ZnO U100, due to the effect of the high flame temperature on it (Figure 11 (e)).

The above mechanism is also predominantly valid for the pore size and volume. The superior pore volume in the ZnO U50 (0.225 cm^3/g) dwells on the evolved gases during the decomposition of the zinc nitrate-sucrose-urea complex, which is beneficial to developing a mesoporous structure. Since the kinetics of the ZnO U25 and ZnO U50 are governed by sucrose, in general, sucrose and carbohydrates fuels with their large and bulky molecules, tend to leave large voids while burning, benefiting high porosity with reduced pore size and high surface area powders (Lazarov *et al.*, 2017). Instead of it, the aforementioned tiny surface area of the ZnO U100 is now corroborated by its short pore volume (0.046 cm^3/g), holding up a bulk nature rather than a porous structure when the reaction is managed by the urea. According to, A. Andriani et al., a large amount of urea leads to lower specific surface area, larger pore diameter, and smaller pore volume when using urea as the hydrolyzing agent in a solvothermal method to produce ZnO nanosheets as photocatalysts (Andriani *et al.*, 2022). Works from the combustion method support it when using urea as the fuel for the ZnO synthesis, whose barely 7 and 3.6 m^2/g of surface area were developed, for example (Lutukurthi, Dutta e Behara, 2020; Potti e Srivastava, 2012).

So far, this research has addressed the crystalline structure, morphology/size, and textural properties of the ZnO materials and brought deep attention to the interaction between sucrose and urea to determine the features of the one-step synthesis and doping by solution combustion method on ZnO photocatalysts, by tailoring the urea-to-sucrose molar ratio. Before starting the next section, it is worth mentioning an emerging concept called "nanoarchitectonics", based on the work to prepare functional materials systems from nanoscale components, where understanding the surface and porosity is a key to discerning their quality and utility (Ariga, 2021). All the above and the previous sections' results indicate that the developed materials with a mesoporous nanocrystalline structure may be attractive in photocatalytic applications due to the advantages to improve the

number of available active sites since the adsorption is the early stage for photocatalysis (Cao *et al.*, 2015).

5.4. CHEMICAL COMPOSITION

When doping is the phenomenon to modify the zinc oxide in photocatalysis, the chemical behavior of the material is as essential as the previous characterization (Sections 5.1, 5.2, and 5.3). Once photocatalysis is a surface-mediated reaction, hence, X-ray photoelectron spectroscopy (XPS) has been widely applied to verify whether nitrogen is successfully doped in the ZnO. The XPS technique has been done only for the samples ZnO U0 and ZnO U100. The analyses of ZnO U25, U50, and ZnO U75 have been in progress when, unfortunately, the equipment broke down, and there is no new forecast for the delivery of these results until now. Once this issue is out of control and to does not harm the work, the results of ZnO U0 and ZnO U100, as the extreme points of the studied samples, will be demonstrated and discussed qualitatively. The XPS spectra of these samples produced by the one-step synthesis and doping by solution combustion method with urea as the nitrogen source are viewed in Figure 14.

The spectra of ZnO U0 and ZnO U100 over a wide energy range are examined in Figure 14 (a), where the main elements are zinc (Zn), oxygen (O), and carbon (C). Based on the XPS data, the chemical composition of the samples was found to be stochiometric for zinc and oxygen with an atomic content of $11 - 14$ at.% of carbon. Carbon in both of the samples could be some unburnt carbonaceous residues from the SCS synthesis and impurities, such as carbon dioxide adsorbed on the material's surface. The signal related to nitrogen is too weak to be observed in Figure 14 (a). Therefore, for a better analysis of the elements, high-resolution core levels of Zn 2p, O 1s, and N1s spectra were scanned.

Figure 14 (b) represents the energy peak characteristics of Zn 2p core level spectra in the ZnO structure, at 1022 eV (Zn $2p_{3/2}$) and 1045.1 eV (Zn $2p_{1/2}$) for ZnO U0. These absolute positions reflect the charge and the chemical environments around the Zn atom, which is supposed to change after the nitrogen functionalization as the symmetry of the crystal lattice has been modified (Cao *et al.*, 2008). After the doping with urea on ZnO U100, a slight shift of 0.16 eV toward higher binding energy is observed on this sample, as highlighted by the inset of Zn $2p_{3/2}$ core level in Figure 14 (b). The doping or incorporation of nitrogen interferes in the Zn – O bonding and leads to a possible formation of the Zn – N bond in the powders (Silva *et al.*, 2016).

Figure 14 – XPS spectra of (a) complete survey of ZnO U0 and ZnO U100; (b) Zn 2p high-resolution spectra of both samples; (c) – (d) O 1s high-resolution spectra and the Gaussian deconvolution of ZnO U0 and ZnO U100, respectively; and (e) N 1s high-resolution spectra of the ZnO U100 SCS-doped with urea.
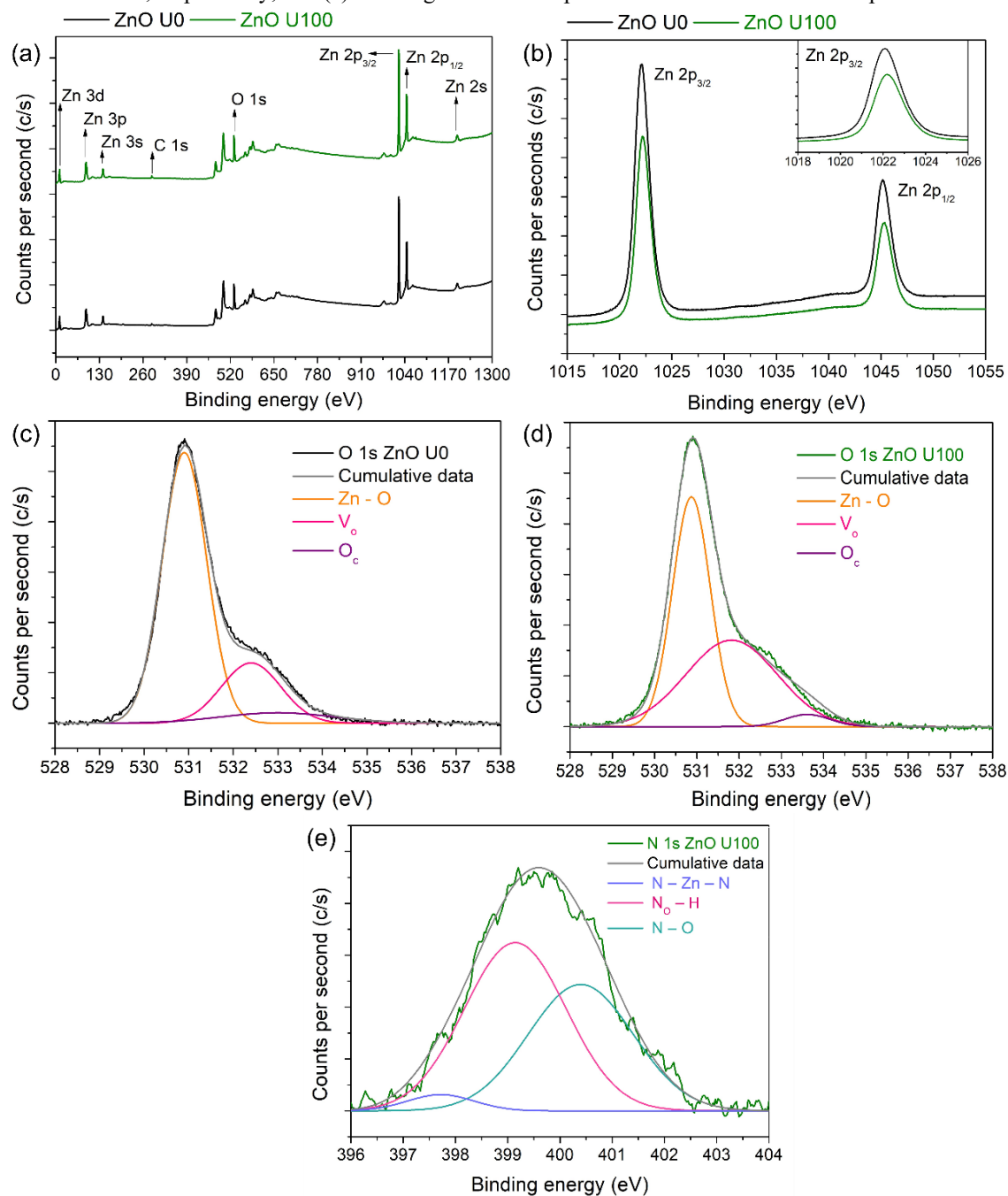
Source: Author (2022).

Figure 14 (c) – (d) assigns to the O 1s core level spectra for the ZnO U0 and ZnO U100, respectively. The curves were fitted by Gaussian deconvolution to specify the chemical states of the oxygen on the samples' surface and three energy peaks are achieved. The peak deconvolved at 530.8 – 531 eV correlates with the O^{2-} ions coordinated with Zn atoms (Zn – O) in the hexagonal wurtzite ZnO structure. The peak at 531.8 – 532.4 eV indicates oxygen deficient sites due to losing of O^{2-}, in the form of oxygen vacancies (Vo). And the last one, on 533 – 533.6 eV refers to chemisorbed oxygen (O_c) from the carbon

dioxide in the air (C=O) or irreversibly oxygen adsorbed from the atmosphere (Reis *et al.*, 2020; Shifu *et al.*, 2009). Comparing the ZnO U0 and ZnO U100, the displacements in the binding energies and intensities of the O 1s spectra signify a change in the ZnO network after the doping, corroborating what was seen in Figure 14 (b), for the Zn 2p spectra. After doping with urea by combustion synthesis, the process intensifies the number of oxygen vacancies in the ZnO U100, since the peak related to them (V_O) is larger than on ZnO U0, while simultaneously, the Zn – O peak decrease. In photocatalysis, these vacancies become captives of photo-generated electron-hole pairs directly or indirectly, improving the quantum efficiency of the photocatalysts materials (Shifu *et al.*, 2009).

Figure 14 (e) is an enlarged XPS high-resolution scanning of the N 1s spectra of ZnO U100. Despite the weak intensity, there are some nitrogen signals deconvoluted by Gaussian fitting in three distinct forms of nitrogen, related to about 0.64 at.% N in the ZnO U100. In the literature, a wide range of values for the nitrogen-doped in the ZnO are found measured by XPS, which means 0.01 to 0.08 at.% for I.M. Silva, 6.8 at.% in the work of H. Sudrajat and S. Babel, and up to 15.1 at.% for M. Mapa and C.S. Gopinath, all of them using urea as the nitrogen source (Mapa e Gopinath, 2009; Silva *et al.*, 2016; Sudrajat e Babel, 2017). The presence of nitrogen reported in ZnO U100 proves the doping of the powder synthesized and simultaneously doped by SCS, which corroborates the observed XRD displacement for this sample in Figure 9 (b).

The first peak of the spectra is centered at 397.71 eV and dwells on N^{3-} in metallic nitrites (N – Zn – N bondings), which assures the substitutional lattice oxygen for nitrogen in the ZnO structure (Silva *et al.*, 2016). Some controversy is found in the literature regarding the exact assignment of the N – Zn binding energy position. Ma et al. reported the binding energy at 396.2 eV in N-doped ZnO by radio frequency reactive magnetron sputtering. Whereas, C. Shifu and co-authors, proposed a center at 398.8 eV to nitrogen substitution on the oxygen sublattice (N_O) (Ma e Liu, 2004; Shifu *et al.*, 2009). And most of the authors usually give the N 1s core level of N – Zn bonds at around 397 eV (Yu *et al.*, 2013). These differences should be attributed to the different nitrogen sources and the doping processing adopted by the researchers.

The signal at 399.14 eV uncovers itself from the surface adsorbed NH_3 amines that derive from the partial urea decomposed along the one-step synthesis and doping by combustion. Here, the binding energy at 399.14 eV (N – H) is much stronger than the standard N – Zn (397.71 eV), which means a lower electron density on nitrogen and a more covalent character of the N – Zn bond in the N-doped ZnO U100 (Mapa e Gopinath, 2009).

J. Gao et al. proposed that this signal relies on the neutral configuration of $N_O - H$ by combining of substitutional nitrogen (N_O) atom and an interstitial hydrogen atom, as long as the nitrogen source in the current work is from amino groups in urea. The configuration of $N_O - H$ frequently gets when hydrogen exits in the reactants (Gao *et al.*, 2010; Wang *et al.*, 2007). This mechanism was also reported by W. Wen and co-authors when they fabricated nitrogen-doped ZnO with zinc nitrate hexahydrate and urea under solution combustion synthesis to develop gas-sensing applications, which feasible help to understand the present work (Wen, Wu e Wang, 2013).

Nitrogen in ZnO could form different complexes and sometimes is not an easy task to distinguish the XPS emission peak, which explains the concomitant presence of N species with similar binding energies but of different chemical nature (Quesada-Cabrera *et al.*, 2014). The energy side at 400.39 eV is likely accredited to different forms of nitrogen. The first one belongs to the $N - O$ bond for the $Zn - O - N$ state for oxygen-rich compounds (Cao *et al.*, 2008). Although, it is not the current case, once the system is abundant in oxygen vacancies (V_O). This energy bound also indicates that the N dopants combine to form N_2 complexes because of the thermodynamic instability and do not remain in the $N - ZnO$ structure as substitutional or interstitial (Quesada-Cabrera *et al.*, 2014). Ultimately, it is associated with chemisorbed species, such as NO^- or NO_2, on the material after the urea decomposition in the combustion reaction (Sudrajat e Babel, 2017).

Since ZnO U100 is the upper limit among the studied samples and while this research does not have the XPS results of the samples ZnO U25, ZnO 50, and ZnO U75, it is assumed that these may follow the ZnO U100 tendency of the chemical composition and the chemical states nature, varying in degree, intensity, position, and area, respectively, to help in justifying the next results. In this view, XPS is a surface measurement technique that responds to the first atomic layers of the materials, and given that carbon, nitrogen, and hydrogen are light and hard to be quantified, this research carried out an elemental analysis to identify these elements in the specimens. Since the solution combustion synthesis is an in-situ technique to dope a material, it is expected that the dopants may be distributed in the entire bulk, not only at the materials' surface. But, instead of it, here, the nitrogen and hydrogen are under the detection limit of the equipment (0.2 at.%), not allowing their quantification. If it is thought that in doping processes only 0.01% of N atoms substitutes the oxygen in ZnO, it is appropriate to cite that the nitrogen is more predicted to be qualitatively analyzed than with an exact number amount (Cao *et al.*, 2008).

For the carbon case, it has been obtained in a range from 0.28 to 0.37 at.% in the entire volume of the samples (ZnO U0 to ZnO U100) against more than 10 at.% in XPS of ZnO U0 and ZnO U100 samples. Consequently, it is supposed that the carbon remains concentrated on the surface after the synthesis and doping by SCS. The method established in this work considers a calcination step at 500 ºC for 20 minutes after the combustion reaction (Section 4.2), since a greater amount of carbon residues in fuel-rich compositions ($\varphi > 1.4026$) may be left in the as-synthesized powders due to incomplete burning of the fuel – a typical effect of sucrose on the microstructure (Deganello e Tyagi, 2018). This further heating of the partially carbonized materials should cause the oxidation of the carbon to CO_2. But, as it has been seen, there is an intrinsic fraction of carbon embedded in the materials even after applying the heat treatment step. The author is aware that with this step a fraction of the doped nitrogen may be suppressed from the doped materials due to nitrogen desorption at the set temperature. And, a larger amount of nitrogen and its effects would be obtained if this step would be not applied. The carbon residues might be responsible to have a synergistic effect with nitrogen, favoring the surface charge of the ZnO when irradiated by a light source in the photocatalysis process. However, the overall influence of this process and all the deployments are out of the scope of this work and should be subject of future works.

5.5. ABSORBANCE AND BAND GAP

UV – vis absorbance spectra are pivotal to determining the absorption ability of a semiconductor material toward light. The effect of urea SCS-doping to create visible-light responsive ZnO N-doped is discussed in Figure 15 (a), based on the representative curves of the materials' absorbance. The absorbance curve of ZnO U0 has a sharp absorption edge at 372 nm, an intrinsic characteristic of the ZnO for the electron transition from the valence band to the conduction band (O 2p → Zn 3d), in a band gap of 3.2 eV (Islam *et al.*, 2019).

With the adding on of the urea-to-sucrose molar ratio, the N-containing ZnO powders modify their absorption edges and intensities. The spectral response was greatly extended from ZnO U25 to ZnO U100, not only to the visible-light region but also to the near-infrared spectra, as in the ZnO U100. For ZnO U25, ZnO U50, and ZnO U75, the absorption intensifies in the range of 380 – 550 nm. Generally, the visible light activity depends on the concentration of doped nitrogen and the absorption is more extended as higher this amount is (Shifu *et al.*, 2009). But here, is not clear and does not have enough data to assure why the absorption of ZnO U50 is higher than ZnO U75.

Figure 15 – (a) UV – vis absorbance spectra and (b) Tauc plot for the band gap energy of the SCS-doped samples with urea.
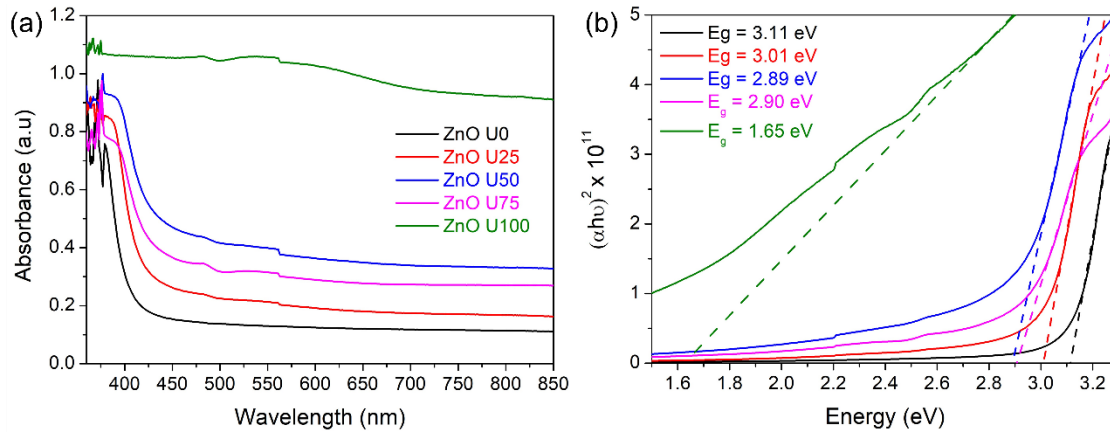
Source: Author (2022).

In photocatalytic pollutant abatement, where the semiconductor material is employed as a catalyst, its band gap (E_g) is a vital role to help in the choosing of the light to activate the material and to tailor its practical applications. By using the optical absorption spectra of each ZnO-based sample in Figure 15 (a), the respective band gap is estimated through the Tauc method described in the paper from P. Makula, M. Pacia, and M. Macik (Makuła, Pacia e Macyk, 2018). On the Tauc method, the absorption coefficient assumes a dependence on the energy behavior as expressed in Equation 15

$$(\alpha * h\nu)^{1/\gamma} = B * (h\nu - E_g) \tag{15}$$

in which, h is Planck's constant, α is the absorption coefficient, ν is the frequency of the phonon, E_g is the band gap energy, B is a constant, and the exponent "γ" is dependent on the nature of the electronic transition. Here, γ is equal to 0.5 due to the direct electron transitions in ZnO (Kumar e Koteswara Rao, 2015). The band gap energy (E_g) values from ZnO U0 to ZnO U100 are calculated from $(\alpha h\nu)^2$ versus the $h\nu$ graph. The linear portion of each curve is extrapolated to the *x*-axis and where intersects it, E_g is extracted, as pointed out in Figure 15 (b). The band gap at ZnO U0, ZnO U25, ZnO U50, ZnO U75, and ZnO U100 is 3.11 eV, 3.01 eV, 2.89 eV, 2.90 eV, and 1.65 eV, respectively.

The band gap of the ZnO U0 was found to be 3.11 eV, unpretentiously lower than the bulk value of 3.2 eV. This shift of around 0.09 eV does not undergo a doping phenomenon, but a possible development of the structural defects during the solution combustion synthesis time, which can give rise to states near the conduction band in the energy band gap (Rajeshwar e Tacconi, De, 2009). Some papers that report the solution combustion synthesis of ZnO have been achieving the same profile, with band gap values of 3.13 and 3.07 eV. The narrowed band gap is characterized based on nanoporous oxygen vacancies in defective morphological sites, as described by the authors (Essawy *et al.*,

2020; Gowthambabu *et al.*, 2021).

The energy difference between the aforementioned samples, now in the doped samples with varying urea-to-sucrose molar ratio, demonstrates that the nitrogen doping in the crystalline lattice of the ZnO enables the creation of midgap states to narrow the band gap up to a 0.22 eV, in the case of ZnO U50 (2.89 eV). These new states bring a structural rearrangement to the semiconductor and should be located above the ZnO U0 valence band, following the illustrative scheme of Figure 6. The lower band gaps raise the probability of the samples harvesting light of higher wavelengths, which means photons of the visible portion. The above-achieved values for the electronic structure of the studied samples well agree with the literature values. Salah et al. noticed a red shift in band edge from 0.05 eV to 0.29 eV, building up an appreciable visible-light photocatalyst of a 2.86 eV when doped ZnO films under a flow-controlled nitrogen plasma (Salah *et al.*, 2016). Other authors reported an extension in the absorption edge and a band gap narrowing of 0.19 eV with urea to synthesize N-ZnO photocatalysts (Macías-Sánchez *et al.*, 2015).

The distinct pattern on both the absorbance threshold and band gap of ZnO U100 has relied on the nitrogen not performing alone in the mid-gap, rather than it, also correlates to the dopant-induced formation of oxygen vacancies in the crystal matrix of the material, the same but less intense observed in ZnO U0. These vacancies, previously cited by XPS results in Figure 14 (d), enable a level below the conduction band, which acts as electron traps. These coupled features have been reported to be responsible for the appearance of the visible light activity for both TiO_2 and ZnO photocatalysts, with a reduced band gap of 2.01 eV and 1.7 eV, respectively (Makropoulou, Panagiotopoulou e Venieri, 2018; Sudrajat e Babel, 2017).

Some authors published that as the nitrogen amount in the doping phenomenon becomes higher, whereas, the intermediated energy levels between the bands do not significantly modify the band gap values as predicted in this work. For R. Reis et al., the interstitial and substitutional N-doped ZnO developed contradictory effects in the ZnO band gap energy (Reis *et al.*, 2020). In Z. Yu et al. work's, the nitrogen doping of ZnO under an ammonia atmosphere established an additional shoulder-like absorption band ranging from 400 – 800 nm. However, the absorption edge and the band gap remained unchanged and they attributed the photocatalytic response under visible light only to some localized states from nitrogen dopants, at the level of the electronic structure and in the surface layers of the ZnO (Yu *et al.*, 2013).

What therefore comes from is a rather straightforward point trusted in the

significant and stable introduction of nitrogen in the ZnO lattice. The author uses this space to emphasize that detailed knowledge about the above-mentioned point contributes to a better understanding of the doping effects and the solution combustion method as a reliable synthesis toward N-doped ZnO. Homogeneous distribution of the suitable anion dopant throughout the whole particle is indispensable either to narrow the band gap or to tailor the other properties, which ultimately affect the catalytic properties of such material.

5.6. PHOTOCATALYSIS PERFORMANCE

Environmental issues around emerging contaminants have become increasingly prominent and threaten the safety of water ecosystems and human health. It has caused widespread concern, and the search to discover and develop green and sustainable technicalities to overcome it remains a significant challenge (Dewil *et al.*, 2017; Polianciuc *et al.*, 2020). Efficient photocatalysts to fight against the environmental fate of tetracycline as a potential emerging contaminant are still growing and not widely explored with a response under visible light (Ahmad, Zhu e Sun, 2021). Hence, the photocatalytic process now is applied to the tetracycline hydrochloride's (TC – HCl) removal with the one-step synthesized and doped ZnO, once these materials have suitable features to be applied as potential photocatalysts materials. The as-synthesized particles at 0, 25, 50, 75, and 100% of the urea-to-sucrose molar ratio in the solution combustion method are evaluated on the system described in Section 4.4 to assess their photocatalytic performance under visible-light irradiation and concerning the previously discussed results.

Previous reports using solution combustion synthesis for ZnO as photocatalysts on dye degradation have already been published (Table 1) and other researchers report this technique to dope the ZnO and extend its activity to a broad-spectrum range (Section 3.4.2). To the best of our knowledge, however, no study has reported N-doped ZnO catalysts fabricated by SCS and applied under visible-light-driven photocatalysis of tetracycline hydrochloride as a pollutant model coupled with a deep understanding of their structural, morphological and size, textural, compositional, and optical properties on the respective application. Thus, the results achieved in this research are as follows.

Figure 16 (a) brings the photodegradation efficiency of the 10 ppm TC – HCl solution by the catalysts (0.5 g//L) irradiated for 60 minutes under a fluorescent lamp ($\lambda > 420$ nm). The curves in Figure 16 are an average of the points from the photocatalytic essays in quadruplicate from each sample. The photocatalytic efficiency of the materials was calculated through the end-points of Figure 16 (a) at 60 minutes and reported in Table

6. All the photocatalytic data are kept up with their average and respective confidence interval extracted from the statistical analysis at a 95% confidence level. Before any result, the impressive decay of the relative C_t/C_0 while the systems are in the dark (Lamp OFF) to reach the adsorption-desorption equilibrium is a subject matter of further discussion. This work is initially focused on the performance of the materials in the visible light part (Lamp ON). Besides, it is worth mentioning that some dyes are photosensitive and will self-degrade under light, which is not the case with tetracycline. The photolysis of tetracycline is feasible to be negligible with a removal rate of barely 0.57%. Besides, the thermostability of the TC – HCl and the influence of the sonicator on the pharmaceutical compound were evaluated. No effects were found, which assures all the adsorption and photodegradation effects on the TC – HCl to the ZnO-based photocatalysts.

Figure 16 – (a) Photocatalytic efficiency of TC – HCl on ZnO U0 to ZnO U100 (0.5 mg/L of catalysts, [TC – HCl] = 10 ppm, λ > 420 nm, room temperature); (b) Pseudo-first-order kinetic model fitting curve of ZnO U0 to ZnO U100.
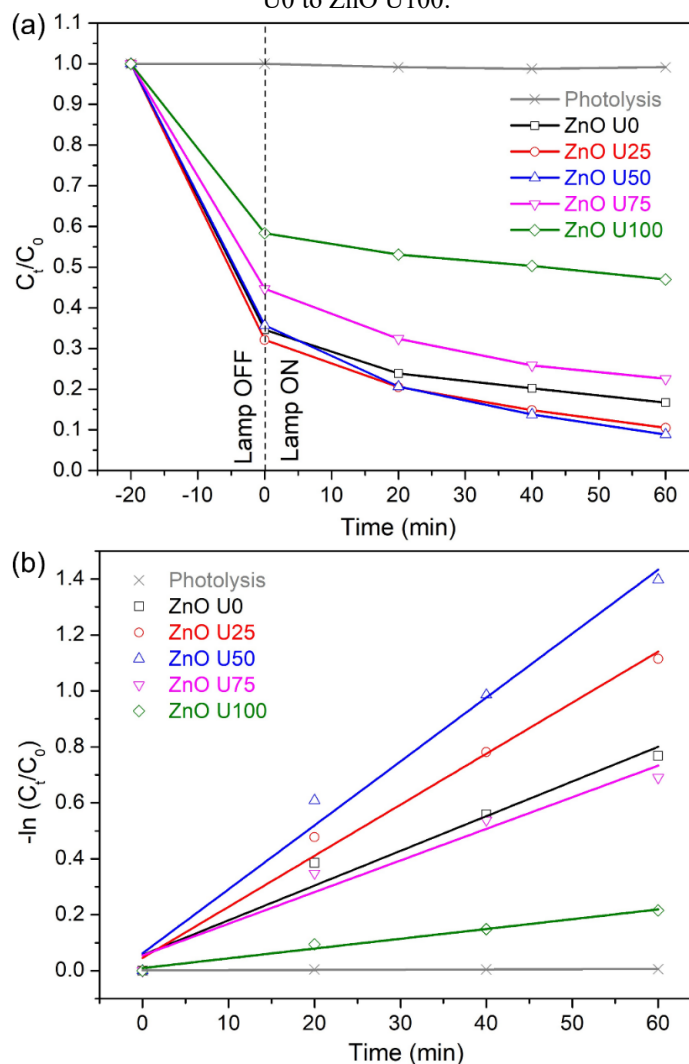
Source: Author (2022).

The approach based on the urea-to-sucrose molar ratio grants a valuable result in photocatalytic activity. Through the curves of Figure 16 (a), the improvement of the photocatalytic degradation does not behave linearly with the nitrogen input, thus, it is possible to notice an optimum percentage of urea-to-sucrose molar ratio for N-doping to promote the best photocatalytic performance. Moreover, the photocatalytic activity is compared using the degradation kinetics of each sample by assessing the constant rate (k), which assumes a pseudo-first-order kinetic model on the tetracycline hydrochloride abatement. The values of this rate were acquired from the slope of the graph $-\ln (C_t/C_0)$ versus irradiation time (Figure 16 (b)) and reported together with the efficiency values (Table 6). The R-squared (R^2) ensures that the samples follow the adopted kinetic model.

ZnO U0 solely has a TC – HCl degradation efficiency of 53.62%. ZnO U50 outperforms the first-rate photocatalytic performance with a TC – HCl abatement of around 75% within 60 minutes on a rate of 22.68 x 10^{-3} min^{-1}, which means an improvement of 39.33% in the degradation efficiency and a reaction 1.86 times faster than the pristine ZnO U0. Shortly thereafter, ZnO U25 also reveals an excellent removal efficiency of around 25% with a constant rate of 1.51 times over the ZnO. Increasing the urea-to-sucrose molar ratio further hinders the photocatalytic activity to effectiveness below the standard ZnO U0. For ZnO U75, the loss in efficiency is 7.5% compared to the ZnO U0. The ZnO U100 photoactivity goes through the worst degradation of only 19.17%, which implies a lower performance of 64.24% and 3.15 times slower than ZnO U0. Statistically speaking by an ANOVA Games-Howell analysis, all the samples behave differently, except for the ZnO U0 and ZnO U75 samples which have equal behaviors.

Table 6 – Photocatalytic efficiency and the constant rate of the reaction for the ZnO U0 to ZnO U100 photocatalysts after 60 minutes of visible-light irradiation.

Sample code	Photocatalytic efficiency (%)	Constant rate k (x10^{-3} min^{-1})	R-square (R^2)
Photolysis	0.57 ± 0.37	0.54 ± 0.88	0.98947
ZnO U0	53.62 ± 2.14	12.17 ± 0.77	0.97497
ZnO U25	67.17 ± 2.36	18.42 ± 1.17	0.98113
ZnO U50	74.71 ± 2.15	22.68 ± 1.25	0.96357
ZnO U75	49.56 ± 3.37	11.07 ± 1.02	0.91130
ZnO U100	19.17 ± 10.04	3.86 ± 1.75	0.92589

Source: Author (2022).

Understanding the above results involves having a whole view of the photocatalysts and to shed a light on the different ways in which the one-step synthesis and doping may alter the photocatalytic profile of the developed materials. If the ZnO U100 has the narrowest band gap with absorbance in the visible region (400 – 700 nm, Figure 15 (a)) to overlap the major drawback of the ZnO to absorb light, why this sample does not have the best photocatalytic performance? The answer is that photocatalysis relies upon a systemic background where many properties ensure the specific contributions to accurately achieve the best performance.

The poor TC – HCl photodegradation rate for ZnO U100 corresponds to its reduced specific surface area (4.47 m^2/g) and lower porosity (0.046 cm^3/g) developed in almost micrometric particles (Figure 12 (e)). The compact nature of this sample slows down the surface adsorption sites for the TC – HCl molecules. Simultaneously, the band gap of this sample was hugely narrowed to 1.65 eV, which in turn would generate more electron-hole pairs to create the reactive oxygen species. Although, it will be suppressed once the distance between the valence and conduction band is too short that the electron that arrives in the conduction band, fastly returns to its valence position, and so, the recombination process is stronger than the photocatalysis toward the TC – HCl degradation (Kumar e Koteswara Rao, 2015; Rangel *et al.*, 2017).

If we get an overview of Table 5 on the textural properties, it is easy to recognize that by increasing the urea-to-sucrose molar ratio from 0% to 50%, there is a raising in the specific surface and pore volume. And it is known that surface area is essential for achieving higher degradation efficiency. This is where it starts to clarify why ZnO U50 has a great advantage in the photocatalytic removal of tetracycline. Contrariwise to ZnO U100, the surface area of 25.93 m^2/g and a pore volume of 0.225 cm^3/g on ZnO U50 infer that the nanoporous structure of this sample plays a vital role in the enhancement of the photocatalytic activity of TC – HCl. It enables a short-range contact between the catalysts and the pollutant through spatially arranged active sites, which facilities mass diffusion, not only to TC – HCL get adsorbed in the ZnO U50 surface but also permits more adsorption of water and hydroxyl molecules and improved light transmittance (Zhang *et al.*, 2022).

The band structure of the photocatalysts directly affects the catalytic performance and mechanism. The suitable narrowed band gap of the ZnO U50 may significantly promote photoexcitation in the visible light region. When the catalyst-pollutant system of ZnO U50/TC – HCl is irradiated, the exposed faces and active sites of the material coupled

with the N – doped band gap of 2.89 eV allow a greater number of photons to reach the catalysts' surface. The synergy between the surface area, porosity, and band gap structure developed in ZnO U50 can first avoid the undesired surface recombination of the charge carriers (e^-/h^+) toward the trapping sites in the valence and conduction band. And thus, targeting the pair e^-/h^+ to react with the adsorbed water and oxygen from the medium, which leads to a larger amount of free reactive oxygen species (ROS) as the front-runners in the photocatalytic degradation of TC – HCl (Lu, Russo e Feng, 2011; Qi *et al.*, 2017). This mechanism is based on what has been explained in Section 3.2, illustrated in Figure 3, and based on what the literature reports after nitrogen doping (Salah *et al.*, 2016; Silva *et al.*, 2016; Yu, Zhang e Peng, 2016). Aside from these findings and explanations, this work claims that the intermediates samples in the name of ZnO U25 and ZnO U75 will follow the behavior of ZnO U0 to ZnO U50, and ZnO U50 to ZnO U100, respectively.

This work also predicts a theory in which a balance of the physicochemical properties of a photocatalyst for a higher photocatalytic abatement of a pollutant may be widely accepted. For the papers related to ZnO, the photocatalytic activity toward a complete degradation of azo dyes attempts to a consistency between good crystallinity and small crystallite size, higher surface area, and good optical properties, i.e, narrow band gap (Andriani *et al.*, 2022; Potti e Srivastava, 2012; Silva *et al.*, 2016).

For the doping strategy adopted in this research, the improvements in the photocatalytic activity are non-linear with the nitrogen content, which translates itself to the urea-to-sucrose molar ratio. As ZnO N-doped with a moderated urea ratio is a photocatalyst significantly better than a ZnO undoped (ZnO U0) or doped in a rich urea ratio (ZnO U100), a mathematical model is hypothesized to identify an optimum urea-to-sucrose molar ratio in a one-path SCS synthesis and doping. The graph from Figure 17 depicts the fitting model derived from the experimental data from the photocatalysis essays executed in this work (Figure 16 (a)), at the light part (Lamp ON)). Through the modeling, the optimal content of the urea-to-sucrose molar ratio is 37.59% with $R^2 = 0.9552$ at a 95% confidence level. For this value, it is presumable that a good arrangement between the physiochemical properties would result in a photocatalytic efficiency of around 75.68% – a little above the 74.71% of the ZnO U50 – with a prediction interval that allows varying from a lower limit of 62.56% to an upper limit of 82.4% of photocatalytic efficiency.

Afterward, many questions and points of this work could be explored and more developed, from materials processing to photocatalysis applications. To date, the aim of this work is, therefore, to assess whether and how the ZnO modified with nitrogen is able

and improve the removal of tetracycline hydrochloride by photocatalysis under visible light irradiation. The relationship between the material's properties and their catalytic activity was well correlated and achieved. But now, the question that should be answered is about what happens during the dark side (Lamp OFF) of the photocatalysis essays reported in Figure 16 (a). So, to further evaluate the above-mentioned phenomenon, the ZnO U50 was chosen as a model to carry out the next series of experimental results, due to its better photocatalytic activity among the studied samples.

Figure 17 – Modeling of the urea-to-sucrose molar ratio for the photocatalytic efficiency on the one-step synthesis and doping of ZnO-based photocatalysts.
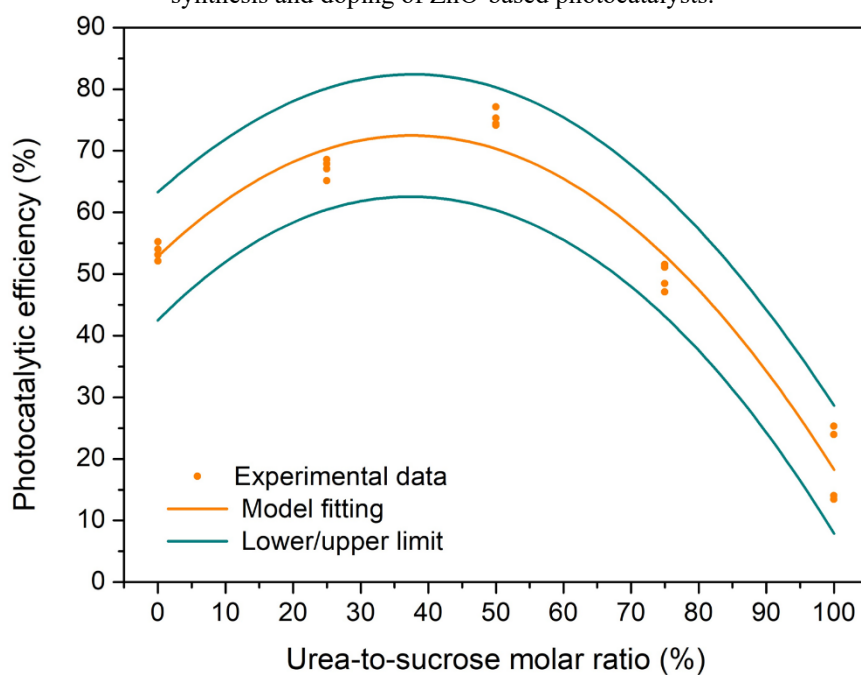
Source: Author (2022).

The first 20 minutes of a photocatalysis essay are applied to the catalyst and the pollutant to reach the equilibrium of adsorption-desorption, in absence of light. At this step, it would expect a few reactions to switching the whole environment. Nevertheless, a decrease near 65% has been observed in this step, based on the blue curve of Figure 16 (a), for ZnO U50. The primary hypothesis of this decay relies on heterogenous dark catalysis. Dark catalysis is based on an advanced oxidation process (AOPs) that dismisses the need for light. This is a new feasible and unexplored treatment for recalcitrant pollutants abatement, directly related to the surface contact pollutant-catalyst, where the catalyst has surface defects and high surface area (Besegatto *et al.*, 2021; Lakshmi Prasanna e Vijayaraghavan, 2015).

As a way to clarify it, an essay following the entire photocatalytic protocol described in Section 4.4 was employed under total dark conditions for 120 minutes to have an overview of the system. For comparison, the same was done for 120 minutes under the

fluorescent light. From Figure 18 (a) two main issues are deduced when the pollutant concentration is 10 ppm. Except for the decline of the first 20 minutes, the ZnO U50 has a worthless catalytic activity under the simulated dark condition. If potential dark catalysis had occurred in the system, the light blue curve might keep on a behavior similar to the blue one after 120 minutes, due to the degradation of the tetracycline. And secondly, the pollutant has an outstanding removal as the irradiated reaction approaches 120 minutes, which recalls the efficiency of ZnO U50 as a visible-light photocatalyst. Besides, with the inexistence of the dark phenomena, it is feasible to argue that the adsorption equilibrium is reached in 20 minutes.

The same set of experiments was done for 100 ppm of tetracycline hydrochloride, labeled on light pink and pink curves in Figure 18 (a). This step aimed to saturate the surrounding of the catalyst and analysis its absorption capacity. On this tremendous initial concentration, the step on the dark adsorption exhibits the same profile of adsorption capacity on 10 ppm of TC – HCl, which agrees with the porous structure of the ZnO U50 with a high adsorbent capacity. Whereas the photodegradation efficiency has decreased because the higher pollutant content delays the arrival of light at the catalyst surface and the absorption of photons through the material is hindered. Other works already stated that the higher the concentration of the pollutants, the slower the degradation is (Chen *et al.*, 2022; Zanchettin *et al.*, 2021; Zhang *et al.*, 2022). The photocatalytic efficiency reduces from 81.13% when the TC – HCl is at 10 ppm to almost a twice lower value of 45.93% at 100 ppm.

With the dark catalysis hypothesis excluded and the high TC – HCl concentrations experiments performed, thereafter, a photocatalytic essay was directly carried out without the prior adsorption step in the dark, which means direct light in the catalyst-pollutant system (green curve, Figure 18 (b)). The impressive decay noted in both Figure 16 (a) and Figure 18 (a) is observed again. And so, this behavior is independent of the light or dark, and it is addressed to the intrinsic spongy structure of the ZnO U50, developed during the solution combustion synthesis and doping (Section 5.3, Textural properties). Which becomes here, therefore, could be regarded as a synergy of both adsorption and photocatalysis, illustrated by the green curve in Figure 18 (b). In a dual treatment process, a catalyst reaches adsorption-desorption equilibrium and pollutant removal is then achieved by photocatalysis (blue curve, Figure 18 (a)). Simultaneously, adsorption enhances the mineralization efficiency of photocatalysis due to the rapid

reactions that take place between photoactive species and the pollutant molecules adsorbed on the surface of the photocatalyst material (Kant *et al.*, 2014).

Figure 18 – Comparative data of (a) the ZnO U50 catalyst activity under dark and photocatalysis at TC – HCl pollutant concentrations of 10 and 100 ppm; (b) photocatalytic efficiency of pure photocatalysis and adsorption-photocatalysis synergy (direct irradiation without dark adsorption step), and the inset of the pseudo-first-order kinetic fitting of both behaviors.
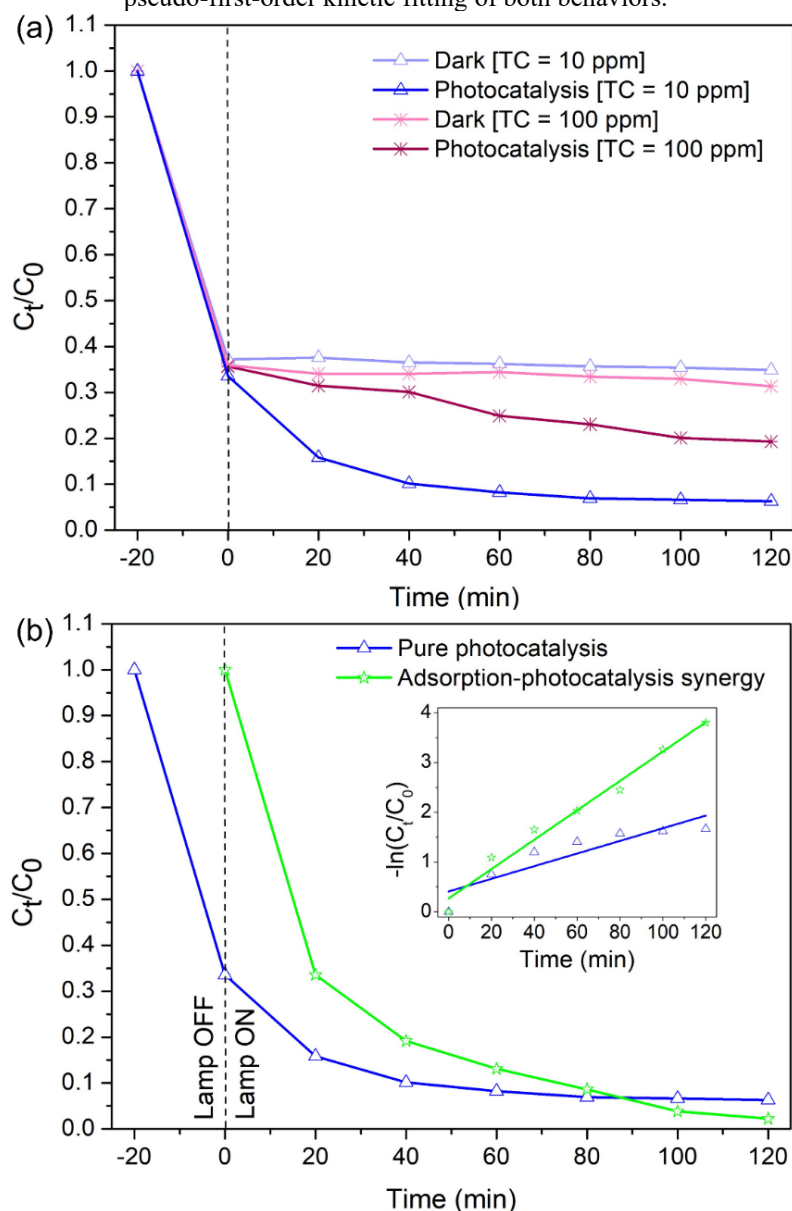
Source: Author (2022).

The graphic curves in Figure 18 (b) display that although pure photocatalysis already has an outstanding photocatalytic performance, when combined with the adsorption, they further improved the mineralization of TC – HCl. The synergy of adsorption-photocatalysis has a photocatalytic performance of 97.76%, while pure photocatalysis has 81.13% on the mineralization of TC – HCl. The pseudo-first-order kinetic constants rate of 29.53×10^{-3} min^{-1} against 18.17×10^{-3} min^{-1} is 1.62 times better for the synergistic than the pure behavior. The remarked mechanism would be promising

as follows. Firstly, according to the literature by zeta potential analysis, it is observed that ZnO has a positive potential in the aqueous solution at around pH 7 – the pH of the photocatalytic essay here – which mainly contributed to the diffusion of negatively charged tetracycline hydrochloride to the surface of the photocatalyst particles (Zhang *et al.*, 2022). Besides, the N_2 sorption isotherm proved the highly porous characteristics of ZnO U50 (Figure 13 and Table 5). The accessible pore diameter of 2.439 nm at a volume of 0.225 cm^3/g offers enough space for the TC – HCl molecule (6 × 7 × 14 Å) to be adsorbed on the active sites (Xia, Gao e Yu, 2021). The amount of these sites is great too due to the surface area of 25.93 m^2/g. As soon the pollutant is adsorbed onto the ZnO U50 surface, simultaneously, the N-doped broads the light absorption from the ultraviolet to the visible region, allowing a great transfer of photogenerated carries that accelerate the reactions to generate the free oxygen radicals, responsible for the photocatalysis of the pollutant (Chen *et al.*, 2022).

Through this perspective, the synergic phenomenon of higher adsorption capacity and great photocatalytic properties favors the efficient and fast removal of tetracycline hydrochloride, as a model emerging contaminant. To date, however, there are few reports about adsorption-photocatalytic degradation of TC-based pollutants and despite the difficulty of rigorous comparisons between the different photocatalysts systems developed today, removal efficiency data found in the literature is given in Table 7 sorted by surface area. In our case for the ZnO U50 as a model example from this study, competitive performances were found compared to the first-rate state-of-the-art photocatalysts. If it is supposed a comparison based on the same amount of catalyst (1 g/L) when comparing the ZnO U50 (25.93 m^2/g) with the nitrogen-doped N – TiO_2 (54.1 m^2/g) from Wu et al. work (Wu *et al.*, 2020), the free surface area available for the photocatalytic reaction is about twice as large for N – TiO_2 as for ZnO U50, but results in similar photocatalytic performances between both materials. Another example of the 40%MIL-53(Fe, Al) (Chen *et al.*, 2022), a metal-organic framework, even with its highest surface area of 1397.27 m^2/g, the developed photocatalytic removal of TC – HCl is almost equal to the ZnO U50 with a surface area of 25.93 m^2/g, which is about two orders of magnitude smaller than the 40%MIL-53(Fe, Al).

Table 7 – Photocatalytic data about different systems on the removal of tetracycline pollutant.

Material	Surface area (m²/g)	Light source	Catalyst dose (g/L)	TC dose (ppm)	Degradation time (min)	Photocatalytic efficiency (%)	Reference
40%MIL-53(Fe, Al)	1397.27	500 W mercury lamp*	0.2	20	50	81.82%[1] 93.53%[1]	(Chen *et al.*, 2022)
ZIF-8@ TiO₂	556.8	300 W Xenon lamp*	0.6	100	90	90.0[2]	(Li, R. *et al.*, 2020)
ZnO@ZIF-8	331	300 W Xenon lamp*	0.5	20	50	91.0[2]	(Zhang *et al.*, 2022)
Cu@Cu₂O@ CuO	138	White LED (1.6 W)	0.5	40	80	76.5[2]	(Serrà *et al.*, 2021)
3% Nd₂O₃ /ZnO	126	300 W Xenon lamp*	2.4	20	120	100.0[2]	(Mohamed *et al.*, 2021)
Ag₂O-ZnO	117	300 W Xenon lamp*	1.8	20	120	40.0[2]	(Mohamed *et al.*, 2020)
N – TiO₂	54.1	300 W Xenon lamp*	0.2	10	120	87.0[2]	(Wu *et al.*, 2020)
ZnO U50	25.93	15 W fluorescent lamp	0.5	10	120	81.83%[2] 97.56%[1]	This work

[1] Pure photocatalysis
* λ > 420 nm
[2] Synergy adsorption-photocatalysis

Table 7 – Photocatalytic data about different systems on the removal of tetracycline pollutant (continue).

Material	Surface area (m²/g)	Light source	Catalyst dose (g/L)	TC dose (ppm)	Degradation time (min)	Photocatalytic efficiency (%)	Reference
Nb_2O_5/g-C_3N_4	17.18	250 W Xenon lamp	1	20	150	76.2[2]	(Hong *et al.*, 2016)
2% Ca – ZnO	14.10	1.6 W white LED	0.5	10	90	73.52[2]	(Bembibre *et al.*, 2022)
Nb_2O_5/Nb_2CT_x	14.07	500 W Xe lamp*	1	10	180	91.2[2]	(Cui *et al.*, 2021)

Source: Author (2022).

Given these observations, we highlight the feasibility of the ZnO U50 as a photocatalyst. For example, in the case of TiO_2 due to its higher level of maturity, a great variety of entirely novel photoactive semiconductors have been developed and considered as possible substitutes for titanium dioxide, which includes ZnO. The recent advances in nanotechnology enable the ZnO to decontaminate heavily polluted effluents from low to higher irradiance without the saturation of the system does not drop the energetic efficiency of the process, and at relatively cheaper costs than TiO_2 (Hernández-Alonso *et al.*, 2009). On the other side, for MOF-based materials, the major challenges include issues associated with stability, pore modulation, complexity, durability, and high production costs that restrict their practical use (Vikrant *et al.*, 2017). Whereas the ZnO by solution combustion method is suitable for an easy and simple design that overcomes the challenges of those materials. Therefore, it opens a door to put the ZnO-based catalysts in the spotlight of research with new properties and novel applications in the fields of photocatalysis, adsorption, or the joint process called photocatalytic-adsorbents materials.

Overall, this work supports a potential method for developing zinc oxide (ZnO) materials at the nanoscale and modified by nitrogen doping through a one-step synthesis and doping by solution combustion method. Appropriate surface modifications employed by simply adapting the urea-to-sucrose molar ratio as fuels, in a mixture with zinc nitrate hexahydrate as the zinc precursor play a crucial role in the physical and chemical characteristics of the nanostructured ZnO-based materials and their photocatalytic applications. In this framework, the promising aspects of the SCS route adopt here accomplish the sucrose as a fuel to control the thermodynamics of the combustion reaction, resulting in well-controlled size and surface parameters, such as area and porosity. And simultaneously, supplying suitable nitrogen from urea to behave as a dopant and modulate the semiconducting material to make it more visible light responsive without the assistance of other templates, decreasing the overall processing costs and time. This one-step SCS approach would pave the way for developing advanced nanomaterials whilst meeting the standards of quality, greenness, circularity, and social wellness for a sustainable future.

6. CONCLUSIONS

The summarized results obtained and discussed in this work are below.

- The synthesis and doping of zinc oxide through the solution combustion method produced around one gram of each urea-to-sucrose molar ratio formulation (ZnO U0, ZnO U25, ZnO U50, ZnO U75, and ZnO U100);

- The hexagonal wurtzite crystal structure is obtained in all the samples and no other phases or impurities are observed after the nitrogen doping;

- The ZnO-based particles are almost spherical with a base size of around 50 nm in ZnO U0, by SEM analysis. For the higher N-doped samples, the particles become larger and sintered;

- The ZnO N-doped materials by the SCS method are mesoporous with surface area, pore volume, and pore diameter which vary according to each urea-to-sucrose molar ratio;

- Through the XPS spectra, the main chemical elements are achieved, highlighting the zinc (Zn), oxygen (O), nitrogen (N), and carbon (C) elements; the nitrogen is at a concentration of 0.64 at.% on the ZnO U100 sample;

- The absorbance spectra of the N-doped ZnO are well extended to the visible light spectrum, which means wavelengths higher than 400 nm;

- The best photocatalytic performance in the visible light abatement of the tetracycline hydrochloride is assigned to ZnO U50 with a degradation efficiency of 75% after 60 minutes on a rate of 22.68×10^{-3} min^{-1}, which means 39.33% and 1.86 times better than the ZnO U0;

- The photocatalytic performance is driven by a combination of the available surface area, particle size, and a suitable band gap, which improves the catalytic sites and the absorption of the visible light photon to degrade the TC – HCl.

- The phenomena that happen during the dark step of the photocatalysis essays are attributed to the adsorption capacity of the materials, due to the mesoporous structure;

- The synergy of adsorption-photocatalysis enables the removal of 97.16%, after 120 minutes. In terms of the constant rate, this mechanism provides a reaction 1.62 times faster than pure photocatalysis.

6.1. FUTURE WORKS

After the conclusions, this Master's thesis provides the opportunity to explore and develop further studies on:

- To evaluate the synthesis and doping by solution combustion synthesis without the calcination step to remove the residual carbon. This can have some deployments, such as the synergy of carbon and nitrogen;

- To apply experimentally the optimal urea-to-sucrose molar ratio to verify the influence on the physicochemical properties and photocatalytic performance;

- To study the stability of the nitrogen doping by the proposed method over time and its influence on the properties and applications;

- To synthesize and characterize nanocomposites of two or more semiconductors produced simultaneously by solution combustion synthesis to take advantage of the heterojunction phenomena to improve the photocatalytic activity;

- To investigate the effect of an SCS with a controlled atmosphere on the doping level of the semiconductor and its dependent characteristics;

- To evaluate the possibility of microwave-assisted SCS as a method to enable fast and controlled cooling of the resultant material and to analyze the impact of this modification of the heating method on the nanoparticles' properties of interest;

- To control the kinect of the combustion reaction under real operational time and temperature to control and understand the SCS parameters over the morphology, crystallinity, and size of the materials;

- To develop a plasma-assisted process as a doping route of the undoped ZnO U0 nanoparticles by SCS, as is described in the Appendix;

- To evaluate the effect of different nitrogen-hydrogen atmosphere and plasma parameters on the properties and photocatalytic performance of the materials;

- To perform the experimental evaluation by radical scavengers to elucidate the photocatalytic mechanism and the generation of reactive oxygen species (ROS) during the pollutant abatement;

- To quantify the photocurrent of the photocatalytic samples to have a response about the number of electrons that can be excited under visible light and the free charge carried and transferred at their interface;

- To study deeply the coupled adsorption-photocatalytic mechanism in the samples, realizing thermogravimetric analysis (TGA), for example.

REFERENCES

AHMAD, F.; ZHU, D.; SUN, J. Environmental fate of tetracycline antibiotics: degradation pathway mechanisms, challenges, and perspectives. **Environmental Sciences Europe**, v. 33, n. 64, p. 1–17, 2021.

AHMED, F.; ARSHI, N.; ANWAR, M. S.; DANISH, R.; KOO, B. H. Morphological evolution of ZnO nanostructures and their aspect ratio-induced enhancement in photocatalytic properties. **RSC Advances**, v. 4, n. 55, p. 29249–29263, 2014.

ALRUMMAN, S. A.; EL-KOTT, A. F.; KESHK, S. M. A. S. Water Pollution: Source & Treatment. **American Journal of Environmental Engineering**, v. 6, n. 3, p. 88–98, 2016.

ANDRIANI, A.; BENU, D. P.; MEGANTARI, V.; YULIARTO, B.; MUKTI, R. R.; IDE, Y.; CHOWDHURY, S.; AMIN, M. A.; KANETI, Y. V.; SUENDO, V. Role of urea on the structural, textural, and optical properties of macroemulsion-assisted synthesized holey ZnO nanosheets for photocatalytic applications. **New Journal of Chemistry**, v. 46, p. 9897, 2022.

ARIGA, K. Nanoarchitectonics with porphyrins and related molecules. **Journal of Porphyrins and Phthalocyanines**, v. 25, n. 10, p. 897–916, 2021.

ARIGA, K.; JI, Q.; NAKANISHI, W.; HILL, J. P.; AONO, M. Nanoarchitectonics: a new materials horizon for nanotechnology. **Materials Horizons**, v. 2, p. 406–413, 2015.

ARIGA, K.; MINAMI, K.; EBARA, M.; NAKANISHI, J. What are the emerging concepts and challenges in NANO? Nanoarchitectonics, hand-operating nanotechnology and mechanobiology. **Polymer Journal 2016 48:4**, v. 48, n. 4, p. 371–389, 2016.

ATEIA, M.; ALALM, M. G.; AWFA, D.; S.JOHNSON, M.; YOSHIMURA, C. Modeling the degradation and disinfection of water pollutants by photocatalysts and composites: A critical review. **Science of The Total Environment**, v. 698, n. 1, p. 134197, 2020.

BAALOUDJ, O.; ASSADI, I.; NASRALLAH, N.; JERY, A. EL; KHEZAMI, L.; ASSADI, A. A. Simultaneous removal of antibiotics and inactivation of antibiotic-resistant bacteria by photocatalysis: A review. **Journal of Water Process Engineering**, v. 42, p. 102089, 2021.

BARBERO, N.; VIONE, D. Why Dyes Should Not Be Used to Test the Photocatalytic Activity of Semiconductor Oxides. **Environmental Science & Technology**, v. 50, n. 5, p. 2130–2131, 2016.

BEMBIBRE, A.; BENAMARA, M.; HJIRI, M.; GÓMEZ, E.; ALAMRI, H. R.; DHAHRI, R.; SERRÀ, A. Visible-light driven sonophotocatalytic removal of tetracycline using Ca-doped ZnO nanoparticles. **Chemical Engineering Journal**, v. 427, p. 132006, 2022.

BESEGATTO, S. V.; SILVA, A. DA; CAMPOS, C. E. M.; SOUZA, S. M. A. G. U. DE; SOUZA, A. A. U. DE; GONZÁLEZ, S. Y. G. Perovskite-based Ca-Ni-Fe oxides for azo pollutants fast abatement through dark catalysis. **Applied Catalysis B: Environmental**, v. 284, p. 119747, 2021.

BHARTI; JANGWAN, J. S.; KUMAR, S. S.; KUMAR, V.; KUMAR, A.; KUMAR, D. A review on the

capability of zinc oxide and iron oxides nanomaterials, as a water decontaminating agent: adsorption and photocatalysis. **Applied Water Science**, v. 12, n. 3, p. 1–14, 2022.

BHIRUD, A. P.; SATHAYE, S. D.; WAICHAL, R. P.; NIKAM, L. K.; KALE, B. B. An eco-friendly, highly stable and efficient nanostructured p-type N-doped ZnO photocatalyst for environmentally benign solar hydrogen production. **Green Chemistry**, v. 14, n. 10, p. 2790–2798, 2012.

BORGHI, A. A.; PALMA, M. S. A. Tetracycline: production, waste treatment and environmental impact assessment. **Brazilian Journal of Pharmaceutical Sciences**, v. 50, n. 1, p. 25–40, 2014.

BOYD, C. E. Water Quality Protection. *In*: **Water Quality: An Introduction**. Switzerland: Springer Cham, 2019. p. 379–409.

CAO, P.; ZHAO, D. X.; ZHANG, J. Y.; SHEN, D. Z.; LU, Y. M.; YAO, B.; LI, B. H.; BAI, Y.; FAN, X. W. Optical and electrical properties of p-type ZnO fabricated by NH 3 plasma post-treated ZnO thin films. **Applied Surface Science**, v. 254, n. 9, p. 2900–2904, 2008.

CAO, Z.; QIN, M.; JIA, B.; GU, Y.; CHEN, P.; A.VOLINSKY, A.; QU, X. One pot solution combustion synthesis of highly mesoporous hematite for photocatalysis. **Ceramics International**, v. 41, n. 2, p. 2806–2812, 2015.

CHANG, J. SEN; STRUNK, J.; CHONG, M. N.; POH, P. E.; OCON, J. D. Multi-dimensional zinc oxide (ZnO) nanoarchitectures as efficient photocatalysts: What is the fundamental factor that determines photoactivity in ZnO? **Journal of Hazardous Materials**, v. 381, p. 120958, 2020.

CHEN, X.; LIU, X.; ZHU, L.; TAO, X.; WANG, X. One-step fabrication of novel MIL-53(Fe, Al) for synergistic adsorption-photocatalytic degradation of tetracycline. **Chemosphere**, v. 291, p. 133032, 2022.

CHEN, X.; SHEN, S.; GUO, L.; MAO, S. S. Semiconductor-based photocatalytic hydrogen generation. **Chemical Reviews**, v. 110, n. 11, p. 6503–6570, 2010.

CUI, C.; GUO, R.; REN, E.; XIAO, H.; LAI, X.; QIN, Q.; JIANG, S.; SHEN, H.; ZHOU, M.; QIN, W. Facile hydrothermal synthesis of rod-like Nb2O5/Nb2CTx composites for visible-light driven photocatalytic degradation of organic pollutants. **Environmental Research**, v. 193, p. 110587, 2021.

DADGOSTAR, P. Antimicrobial Resistance: Implications and Costs. **Infection and Drug Resistance**, v. 12, p. 3903–3910, 2019.

DEGANELLO, F.; TYAGI, A. K. Solution combustion synthesis, energy and environment: Best parameters for better materials. **Progress in Crystal Growth and Characterization of Materials**, v. 64, n. 2, p. 23–61, 2018.

DESHPANDE, K.; MUKASYAN, A.; VARMA, A. Direct synthesis of iron oxide nanopowders by combustion approach: reaction mechanism and properties. **Chemistry of Materials**, v. 16, p. 4896–4904, 2004.

DEWIL, R.; MANTZAVINOS, D.; POULIOS, I.; RODRIGO, M. A. New perspectives for Advanced

Oxidation Processes. **Journal of Environmental Management**, v. 195, p. 93–99, 2017.

ESSAWY, A. A.; ALSOHAIMI, I. H.; ALHUMAIMESS, M. S.; HASSAN, H. M. A.; KAMEL, M. M. Green synthesis of spongy Nano-ZnO productive of hydroxyl radicals for unconventional solar-driven photocatalytic remediation of antibiotic enriched wastewater. **Journal of Environmental Management**, v. 271, p. 110961, 2020.

FAGAN, R.; MCCORMACK, D. E.; DIONYSIOU, D. D.; PILLAI, S. C. A review of solar and visible light active TiO2 photocatalysis for treating bacteria, cyanotoxins and contaminants of emerging concern. **Materials Science in Semiconductor Processing**, v. 42, p. 2–14, 2016.

FAN, J.; YATES, J. T. Mechanism of photooxidation of trichloroethylene on TiO2: Detection of intermediates by infrared spectroscopy. **Journal of the American Chemical Society**, v. 118, n. 19, p. 4686–4692, 1996.

FRESNO, F.; PORTELA, R.; SUÁREZ, S.; CORONADO, J. M.; SÚ AREZ, S.; CORONADO, J. M. Photocatalytic materials: recent achievements and near future trends. **Journal of Materials Chemistry A**, v. 2, n. 9, p. 2863–2884, 2014.

FUJISHIMA, A.; HONDA, K. Electrochemical photolysis of water at a semiconductor electrode. **Nature**, v. 238, p. 37–38, 1972.

FUJISHIMA, A.; RAO, T. N.; TRYK, D. A. Titanium dioxide photocatalysis. **Journal of Photochemistry and Photobiology C: Photochemistry Review**, v. 1, p. 1–21, 2000.

GALLINO, F.; VALENTIN, C. DI; PACCHIONI, G.; CHIESA, M.; GIAMELLO, E. Nitrogen impurity states in polycrystalline ZnO. A combined EPR and theoretical study. **Journal of Materials Chemistry**, v. 20, n. 4, p. 689–697, 2010.

GAO, J.; ZHANG, X.; SUN, Y.; ZHAO, Q.; YU, D. Compensation mechanism in N-doped ZnO nanowires. **Nanotechnology**, v. 21, n. 24, 2010.

GARAZHIAN, Z.; REZAEIFARD, A.; JAFARPOUR, M.; FARROKHI, A. {Mo72Fe30} Nanoclusters for the Visible-Light-Driven Photocatalytic Degradation of Organic Dyes. **ACS Applied Nano Materials**, v. 3, n. 1, p. 648–657, 2020.

GHAZALI, S.; SHAIKH, R.; AHAMMAD, Z. COVID-19 and antimicrobial resistance: A cross-study. **Science of The Total Environment**, v. 807, n. 10, p. 150873, 2022.

GOMES, R. P.; OLIVEIRA, T. R.; GAMA, A. R.; VIEIRA, J. D. G.; ROCHA, T. L.; CARNEIR, L. C. Gene resistance profile and multidrug-resistant bacteria isolated from a stream in midwestern Brazil. **Environmental Nanotechnology, Monitoring & Management**, v. 18, p. 100688, 2022.

GONZALEZ-CORTES, S.; ZHANG, X. Solution combustion synthesis: the relevant metrics for producing advanced and nanostructured photocatalysts. **Nanoscale**, v. 14, p. 11806, 2022.

GOWTHAMBABU, V.; BALAMURUGAN, A.; DHIVYA BHARATHY, R.; SATHEESHKUMAR, S.;

KANMANI, S. S. ZnO nanoparticles as efficient sunlight driven photocatalyst prepared by solution combustion method involved lime juice as biofuel. **Spectrochimica Acta - Part A: Molecular and Biomolecular Spectroscopy**, v. 258, p. 119857, 2021.

HERNÁNDEZ-ALONSO, M. D.; FRESNO, F.; SUÁREZ, S.; CORONADO, J. M. Development of alternative photocatalysts to TiO2: Challenges and opportunities. **Energy and Environmental Science**, v. 2, n. 12, p. 1231–1257, 2009.

HOFFMANN, M. R.; MARTIN, S. T.; CHOI, W.; BAHNEMANN, D. W. Environmental applications of semiconductor photocatalysis. **Chemical Reviews**, v. 95, n. 1, p. 69–96, 1995.

HONG, Y.; LI, C.; ZHANG, G.; MENG, Y.; YIN, B.; ZHAO, Y.; SHI, W. Efficient and stable Nb2O5 modified g-C3N4 photocatalyst for removal of antibiotic pollutant. **Chemical Engineering Journal**, v. 299, p. 74–84, 2016.

HUANG, C. P.; DONG, C.; TANG, Z. Advanced chemical oxidation: Its present role and potential future in hazardous waste treatment. **Waste Management**, v. 13, n. 5–7, p. 361–377, 1993.

IHARA, T.; MIYOSHI, M.; TRIYAMA, Y.; MARSUMATO, O.; SUGIHARA, S. Visible-light-active titanium oxide photocatalyst realized by an oxygen-deficient structure and by nitrogen doping. **Applied Catalysis B**, v. 403, p. 403–409, 2003.

ISLAM, M. T.; DOMINGUEZ, A.; ALVARADO-TENORIO, B.; BERNAL, R. A.; MONTES, M. O.; NOVERON, J. C. Sucrose-Mediated Fast Synthesis of Zinc Oxide Nanoparticles for the Photocatalytic Degradation of Organic Pollutants in Water. **ACS Omega**, v. 4, n. 4, p. 6560–6572, 2019.

JAIN, S. R.; ADIGA, K. C.; PAI VERNEKER, V. R. A new approach to thermochemical calculations of condensed fuel-oxidizer mixtures. **Combustion and Flame**, v. 40, n. C, p. 71–79, 1981.

JUFER, H.; REILLY, L.; MOJICA, E.-R. Antibiotics Pollution in Soil and Water: Potential Ecological and Human Health Issues. **Encyclopedia of Environmental Health (Second Edition)**, p. 118–131, 2019.

JUNIOR, A. G. *et al.* Black TiO2 thin films production using hollow cathode hydrogen plasma treatment: Synthesis, material characteristics and photocatalytic activity. **Catalysts**, v. 10, n. 3, 2020.

KANT, S.; PATHANIA, D.; SINGH, P.; DHIMAN, P.; KUMAR, A. Removal of malachite green and methylene blue by Fe0.01Ni0.01Zn0.98O/polyacrylamide nanocomposite using coupled adsorption and photocatalysis. **Applied Catalysis B: Environmental**, v. 147, p. 340–352, 2014.

KHATAEE, A.; SOLTANI, R. D. C.; HANIFEHPOUR, Y.; SAFARPOUR, M.; RANJBAR, H. G.; JOO, S. W. Synthesis and characterization of dysprosium-doped ZnO nanoparticles for photocatalysis of a textile dye under visible light irradiation. **Industrial and Engineering Chemistry Research**, v. 53, n. 5, p. 1924–1932, 2014.

KLEIN, A. N.; CARDOSO, R. P.; PAVANATI, H. C.; BINDER, C.; MALISKA, A. M.; HAMMES, G.; FUSAO, D.; SEEBER, A.; BRUNATTO, S. F.; MUZART, J. L. R. DC plasma technology applied to powder metallurgy: an overview. **Plasma Science and Technology**, v. 15, n. 1, p. 70, 2013.

KOŁODZIEJCZAK-RADZIMSKA, A.; JESIONOWSKI, T. Zinc oxide - from synthesis to application: a review. **Materials**, v. 7, p. 2833–2881, 2014.

KOWALSKA, E.; WEI, Z.; JANCZAREK, M. Band-gap Engineering of Photocatalysts: Surface Modification versus Doping. **Visible Light-Active Photocatalysis**, p. 447–484, 10 abr. 2018.

KUMAR, S. G.; KOTESWARA RAO, K. S. R. Zinc oxide based photocatalysis: tailoring surface-bulk structure and related interfacial charge carrier dynamics for better environmental applications. **RSC Advances**, v. 5, n. 5, p. 3306, 2015.

KUMARI, R.; SAHAI, A.; GOSWAMI, N. Effect of nitrogen doping on structural and optical properties of ZnO nanoparticles. **Progress in Natural Science: Materials International**, v. 25, n. 4, p. 300–309, 2015.

LAKSHMI PRASANNA, V.; VIJAYARAGHAVAN, R. Insight into the mechanism of antibacterial activity of ZnO: surface defects mediated reactive oxygen species even in the dark. **Langmuir**, v. 31, n. 33, p. 9155–9162, 2015.

LAZAROV, T.; GEORGIEVA, M.; TZANKOV, D.; KOVACHEVA, DIMITRINKA; VOYKOV, L.; CHERKEZOVA-ZHELEVA, Z.; KOVACHEVA, DANIELA. Influence of the type of fuel used for the solution combustion synthesis on the structure, morphology and magnetic properties of nanosized NiFe2O4. **Journal of Alloys and Compounds**, v. 700, p. 272–283, 2017.

LI, F.-T.; RAN, J.; JARONIEC, M.; ZHANG QIAO, S. Solution combustion synthesis of metal oxide nanomaterials for energy storage and conversion. **Nanoscale**, v. 7, p. 17590, 2015.

LI, M.; SONG, W.; ZENG, L.; ZENG, D.; XIE, C.; YANG, Q. Mechanistic study of N-H- A nd H-N-codoping of a TiO2 photocatalyst for efficient degradation of benzene under visible light. **RSC Advances**, v. 10, n. 5, p. 2757–2766, 2020.

LI, R.; LI, W.; JIN, C.; HE, Q.; WANG, Y. Fabrication of ZIF-8@TiO2 micron composite via hydrothermal method with enhanced absorption and photocatalytic activities in tetracycline degradation. **Journal of Alloys and Compounds**, v. 825, p. 154008, 2020.

LIAO, Y.; JIANG, D.; FENG, T.; SHI, J. Fabrication, structural, and spectroscopic investigation of Tb-doped Lu3Al5O12 phosphor. **Journal of Materials Research**, v. 20, p. 2934–2939, 2005.

LIEBERMAN, M. A. **Principles of plasma discharges and materials processing**. New Jersey: J. Wiley & Sons, 2005.

LIN, H. F.; LIAO, S. C.; HUNG, S. W. The dc thermal plasma synthesis of ZnO nanoparticles for visible-light photocatalyst. **Journal of Photochemistry and Photobiology A: Chemistry**, v. 174, n. 1, p. 82–87, 2005.

LIU, J.; MA, N.; WU, W.; HE, Q. Recent progress on photocatalytic heterostructures with full solar spectral responses. **Chemical Engineering Journal**, v. 393, p. 124719, 2020.

LIU, M.; ZHANG, D.; HAN, J.; LIU, C.; DING, Y.; WANG, Z.; WANG, A. Adsorption enhanced

photocatalytic degradation sulfadiazine antibiotic using porous carbon nitride nanosheets with carbon vacancies. **Chemical Engineering Journal**, v. 382, p. 123017, 2020.

LOPEZ, O. A.; MCKITTRICK, J.; SHEA, L. E. Fluorescence properties of polycrystalline Tm3+-activated Y3Al5O12 and Tm3+-Li+ co-activated Y3Al5O12 in the visible and near IR ranges. **Journal of Luminescence**, v. 71, n. 1, p. 1–11, 1997.

LÜ, F.; BAO, H.; HE, F.; QI, G.; SUN, J.; ZHANG, S.; ZHUO, L.; YANG, H.; HU, G.; LUO, J.; LIU, X. Nitrogen dopant induced highly selective CO 2 reduction over lotus-leaf shaped ZnO nanorods . **Materials Chemistry Frontiers**, p. 4225–4230, 2021.

LU, Y. H.; RUSSO, S. P.; FENG, Y. P. Effect of nitrogen and intrinsic defect complexes on conversion efficiency of ZnO for hydrogen generation from water. **Physical Chemistry Chemical Physics**, v. 13, n. 35, p. 15973–15976, 2011.

LUCILHA, A. C.; AFONSO, R.; SILVA, P. R. C.; LEPRE, L. F.; ANDO, R. A.; DALL'ANTONIA, L. H. ZnO prepared by solution combustion synthesis: Characterization and application as photoanode. **Journal of the Brazilian Chemical Society**, v. 25, n. 6, p. 1091–1100, 2014.

LUTUKURTHI, D. N. V. V. K.; DUTTA, S.; BEHARA, D. K. Effect of ignition temperature and fuel amount on photocatalytic activity of solution combustion synthesized ZnO. **Ceramics International**, v. 46, n. 14, p. 22419–22428, 2020.

MA, J. G.; LIU, Y. C. Method of control of nitrogen content in ZnO films: Structural and photoluminescence properties. **Journal of Vacuum Science & Technology B: Microelectronics and Nanometer Structures Processing, Measurement, and Phenomena**, v. 22, n. 94, p. 93–98, 2004.

MACÍAS-SÁNCHEZ, J. J.; HINOJOSA-REYES, L.; CABALLERO-QUINTERO, A.; CRUZ, W. DE LA; RUIZ-RUIZ, E.; HERNÁNDEZ-RAMÍREZ, A.; GUZMÁN-MAR, J. L. Synthesis of nitrogen-doped ZnO by sol-gel method: Characterization and its application on visible photocatalytic degradation of 2,4D and picloram herbicides. **Photochemical and Photobiological Sciences**, v. 14, n. 3, p. 536–542, 2015.

MAJUMDER, S.; CHATTERJEE, S.; BASNET, P.; MUKHERJEE, J. ZnO based nanomaterials for photocatalytic degradation of aqueous pharmaceutical waste solutions – A contemporary review. **Environmental Nanotechnology, Monitoring & Management**, v. 14, p. 100386, 2020.

MAKROPOULOU, T.; PANAGIOTOPOULOU, P.; VENIERI, D. N-doped TiO2 photocatalysts for bacterial inactivation in water. **Journal of Chemical Technology & Biotechnology**, v. 93, n. 9, p. 2518–2526, 2018.

MAKUŁA, P.; PACIA, M.; MACYK, W. How To Correctly Determine the Band Gap Energy of Modified Semiconductor Photocatalysts Based on UV-Vis Spectra. **Journal of Physical Chemistry Letters**, v. 9, n. 23, p. 6814–6817, 2018.

MALATO, S.; FERNÁNDEZ-IBÁÑEZ, P.; MALDONADO, M. I.; BLANCO, J.; GERNJAK, W. Decontamination and disinfection of water by solar photocatalysis: Recent overview and trends. **Catalysis**

Today, v. 147, n. 1, p. 1–59, 2009.

MAPA, M.; GOPINATH, C. S. Combustion Synthesis of Triangular and Multifunctional ZnO1-xNx (x ≤ 0,15) materials.pdf. **Chemistry of Materials**, v. 21, p. 351–359, 2009.

MARQUESA, F. C.; STUMBOB, A. M.; CANELA, M. C. Estratégias e materiais utilizados em fotocatálise heterogênea para geração de hidrogênio através da fotólise da água. **Química Nova**, v. XV, p. 1–11, 2017.

MARSON, E. O.; PANIAGUA, C. E. S.; GOMES JÚNIOR, O.; GONÇALVES, B. R.; SILVA, V. M.; RICARDO, I. A.; MARIA, M. C.; AMORIM, C. C.; TROVÓ, A. G. A review toward contaminants of emerging concern in Brazil: Occurrence, impact and their degradation by advanced oxidation process in aquatic matrices. **Science of the Total Environment**, v. 836, n. April, p. 155605, 2022.

MBENGA, Y.; MTHIYANE, · M N; BOTHA, T. L.; HORN, S.; PIETERS, R.; WEPENER, · VICTOR; ONWUDIWE, D. C. Nanoarchitectonics of ZnO Nanoparticles Mediated by Extract of Tulbaghia violacea and Their Cytotoxicity Evaluation. **Journal of Inorganic and Organometallic Polymers and Materials**, v. 1, p. 3, 2022.

MCNAUGHT, A. D.; WILKINSON, A.; JENKINS, A. D. **IUPAC Compendium of Chemical Terminology: The Gold Book**. United States: Wiley–Blackwell, 1997.

MOHAMED, R. M.; ISMAIL, A. A.; KADI, M. W.; ALRESHEEDI, A. S.; MKHALID, I. A. Facile Synthesis of Mesoporous Ag2O-ZnO Heterojunctions for Efficient Promotion of Visible Light Photodegradation of Tetracycline. **ACS Omega**, v. 5, n. 51, p. 33269–33279, 2020.

___. Photocatalytic performance mesoporous Nd2O3 modified ZnO nanoparticles with enhanced degradation of tetracycline. **Catalysis Today**, v. 380, p. 259–267, 2021.

MORKOÇ, H.; ÖZGÜR, Ü. **Zinc Oxide: Fundamentals, Materials and Devices Technology**. New York: Wiley, 2008.

NAIR, R. G.; MAZUMDAR, S.; MODAK, B.; BAPAT, R.; AYYUB, P.; BHATTACHARYYA, K. The role of surface O-vacancies in the photocatalytic oxidation of Methylene Blue by Zn-doped TiO2: A mechanistic approach. **Journal of Photochemistry and Photobiology A: Chemistry**, v. 345, p. 36–53, 2017.

NAM, S. H.; BOO, J. H. Enhancement of photocatalytic activity of synthesized ZnO nanoparticles with oxygen plasma treatment. **Catalysis Today**, v. 265, p. 84–89, 2016.

NATIONS, U. **70/1. Transforming our world: the 2030 Agenda for Sustainable Development**New York, 2015.

NOGUEIRA, R. F. P.; JARDIM, W. F. A fotocatálise heterogênea e sua aplicação ambiental. **Química Nova**, v. 21, n. 1, p. 69–72, 1998.

NOVITSKAYA, E.; KELLY, J. P.; BHADURI, S.; GRAEVE, O. A. A review of solution combustion synthesis: an analysis of parameters controlling powder characteristics. **International Materials Reviews**, v. 66, n. 3, p. 188–214, 2021.

OLUWOLE, A. O.; OLATUNJ, O. S. Photocatalytic degradation of tetracycline in aqueous systems under visible light irridiation using needle-like SnO2 nanoparticles anchored on exfoliated g-C3N4. **Environmental Sciences Europe**, v. 34, n. 5, 2022.

ÖZGÜR, Ü.; ALIVOV, Y. I.; LIU, C.; TEKE, A.; RESHCHIKOV, M. A.; DOĞAN, S.; AVRUTIN, V.; CHO, S.-J.; MORKOÇ, H. A comprehensive review of ZnO materials and devices. **Journal of Applied Physics**, v. 98, n. 4, p. 041301, 2005.

PHO, Q. H.; LOSIC, D.; OSTRIKOV, K.; TRAN, N. N.; HESSEL, V. Perspectives on plasma-assisted synthesis of N-doped nanoparticles as nanopesticides for pest control in crops. **Reaction Chemistry and Engineering**, v. 5, n. 8, p. 1374–1396, 2020.

PIGEOT-RÉMY, S.; SIMONET, F.; ERRAZURIZ-CERDA, E.; LAZZARONI, J. C.; ATLAN, D.; GUILLARD, C. Photocatalysis and disinfection of water: Identification of potential bacterial targets. **Applied Catalysis B: Environmental**, v. 104, n. 3–4, p. 390–398, 2011.

POLIANCIUC, S. I.; GURZĂU, A. E.; KISS, B.; GEORGIA ȘTEFAN, M.; LOGHIN, F. Antibiotics in the environment: causes and consequences. **Medicine and Pharmacy Reports**, v. 93, n. 3, p. 231–240, 2020.

POTTI, P. R.; SRIVASTAVA, V. C. Comparative studies on structural, optical, and textural properties of combustion derived ZnO prepared using various fuels and their photocatalytic activity. **Industrial and Engineering Chemistry Research**, v. 51, n. 23, p. 7948–7956, 2012.

PRUDEN, A. L.; OLLIS, D. F. Photoassisted heterogeneous catalysis: The degradation of trichloroethylene in water. **Journal of Catalysis**, v. 82, n. 2, p. 404–417, 1983.

QI, K.; CHENG, B.; YU, J.; HO, W. Review on the improvement of the photocatalytic and antibacterial activities of ZnO. **Journal of Alloys and Compounds**, v. 727, p. 792–820, 2017.

QUESADA-CABRERA, R.; SOTELO-VAZQUEZ, C.; DARR, J. A.; PARKIN, I. P. Critical influence of surface nitrogen species on the activity of N-doped TiO2 thin-films during photodegradation of stearic acid under UV light irradiation. **Applied Catalysis B: Environmental**, v. 160–161, n. 1, p. 582–588, 2014.

RAJESHWAR, K.; TACCONI, N. R. DE. Solution combustion synthesis of oxide semiconductors for solar energy conversion and environmental remediation. **Chemical Society Reviews**, v. 38, p. 1984–1998, 2009.

RANGEL, R.; CEDEÑO, V.; RAMOS-CORONA, A.; GUTIÉRREZ, R.; ALVARADO-GIL, J. J.; ARES, O.; BARTOLO-PÉREZ, P.; QUINTANA, P. Tailoring surface and photocatalytic properties of ZnO and nitrogen-doped ZnO nanostructures using microwave-assisted facile hydrothermal synthesis. **Applied Physics A: Materials Science and Processing**, v. 123, n. 8, p. 552, 2017.

REIS, R. Y. N.; LIMA, A. E. B.; COSTA, M. J. S.; CRUZ-FILHO, J. F.; MOURA, J. P. C.; SANTOS, R. S.; LUZ, G. E. Enhanced photoelectrocatalytic performance of ZnO films doped with N2 by a facile electrochemical method. **Surfaces and Interfaces**, v. 21, p. 100675, 2020.

REN, H.; KOSHY, P.; CHEN, W. F.; QI, S.; SORRELL, C. C. Photocatalytic materials and technologies for air purification. **Journal of Hazardous Materials**, v. 325, p. 340–366, 2017.

RIZZO, L.; SALA, A. DELLA; FIORENTINO, A.; LI PUMA, G. Disinfection of urban wastewater by solar driven and UV lamp – TiO2 photocatalysis: Effect on a multi drug resistant Escherichia coli strain. **Water Research**, v. 53, p. 145–152, 2014.

SALAH, N.; HAMEED, A.; ASLAM, M.; ABDEL-WAHAB, M. S.; BABKAIR, S. S.; BAHABRI, F. S. Flow controlled fabrication of N doped ZnO thin films and estimation of their performance for sunlight photocatalytic decontamination of water. **Chemical Engineering Journal**, v. 291, p. 115–127, 2016.

SAMADI, M.; ZIRAK, M.; NASERI, A.; KHORASHADIZADE, E.; MOSHFEGH, A. Z. Recent progress on doped ZnO nanostructures for visible-light photocatalysis. **Thin Solid Films**, v. 605, p. 2–19, 2016.

SANGANYADO, E.; GWENZI, W. Antibiotic resistance in drinking water systems: Occurrence, removal, and human health risks. **Science of The Total Environment**, v. 669, p. 785–797, 15 jun. 2019.

SERRÀ, A.; GÓMEZ, E.; MICHLER, J.; PHILIPPE, L. Facile cost-effective fabrication of Cu@Cu2O@CuO–microalgae photocatalyst with enhanced visible light degradation of tetracycline. **Chemical Engineering Journal**, v. 413, p. 127477, 2021.

SHELDON, R. A. The: E factor 25 years on: The rise of green chemistry and sustainability. **Green Chemistry**, v. 19, n. 1, p. 18–43, 2017.

SHIFU, C.; WEI, Z.; SUJUAN, Z.; WEI, L. Preparation, characterization and photocatalytic activity of N-containing ZnO powder. **Chemical Engineering Journal**, v. 148, n. 2–3, p. 263–269, 2009.

SHKIR, M.; HAMDY, M. S.; ALFAIFY, S. A facile one pot flash combustion synthesis of ZnO nanoparticles and their characterizations for photocatalytic applications. **Journal of Molecular Structure**, v. 1197, p. 610–616, 2019.

SILVA, I. M. P.; BYZYNSKI, G.; RIBEIRO, C.; LONGO, E. Different dye degradation mechanisms for ZnO and ZnO doped with N (ZnO:N). **Journal of Molecular Catalysis A: Chemical**, v. 417, p. 89–100, 2016.

SINGH, P.; KUMAR, R.; SINGH, R. K. Progress on transition metal-doped ZnO nanoparticles and its application. **Industrial & Engineering Chemistry Research**, v. 58, n. 37, p. 17130–17163, 2019.

SIVARANJANI, K.; GOPINATH, C. S. Porosity driven photocatalytic activity of wormhole mesoporous TiO 2-x N x in direct sunlight. **Journal of Materials Chemistry**, v. 21, p. 2639, 2011.

STARLING, M. C.; AMORIM, C.; LEÃO, M. M. Occurrence, control and fate of contaminants of emerging concern in environmental compartments in Brazil. **Journal of Hazardous Materials**, v. 372, p. 17–36, 2019.

SUDHA, M.; SYED KHADAR, Y. A.; SURENDHIRAN, S.; MANOJ KUMAR, P.; SURESH, K. C.; BALAMURUGAN, A. Influence of synthesis methods on various properties of Zinc oxide nanostructures. **The International Journal of Analytical and Experimental Modal Analysis**, v. 12, n. 1, p. 1326–1338, 2020.

SUDRAJAT, H.; BABEL, S. A novel visible light active N-doped ZnO for photocatalytic degradation of

dyes. **Journal of Water Process Engineering**, v. 16, p. 309–318, 2017.

SUTANTO, H.; HIDAYANTO, E.; IRWANTO, M.; MUKHOLIT; WIBOWO, S.; HADIYANTO. The influence of nitrogen doping concentration on the strain and band gap energy of n-doped zinc oxide prepared using spray coating technique. **Solid State Phenomena**, v. 266, p. 141–147, 2017.

SYNNOTT, D. W.; SEERY, M. K.; HINDER, S. J.; MICHLITS, G.; PILLAI, S. C. Anti-bacterial activity of indoor-light activated photocatalysts. **Applied Catalysis B: Environmental**, v. 130–131, p. 106–111, 2013.

TARRAGÓ, D. P.; MALFATTI, C. DE F.; SOUSA, V. C. DE. Influence of fuel on morphology of LSM powders obtained by solution combustion synthesis. **Powder Technology**, v. 269, p. 481–487, 2015.

THOMMES, M.; KANEKO, K.; NEIMARK, A. V.; OLIVIER, J. P.; RODRIGUEZ-REINOSO, F.; ROUQUEROL, J.; SING, K. S. W. Physisorption of gases, with special reference to the evaluation of surface area and pore size distribution (IUPAC Technical Report). **Pure and Applied Chemistry**, v. 87, n. 9, p. 1051–1069, 2015.

TONIOLO, J.; TAKIMI, A. S.; ANDRADE, M. J.; BONADIMAN, R.; BERGMANN, C. P. Synthesis by the solution combustion process and magnetic properties of iron oxide (Fe3O4 and α-Fe2O3) particles. **Journal of Materials Science**, v. 42, n. 13, p. 4785–4791, 2007.

TUMMINO, M. L.; LIOTTA, L. F.; MAGNACCA, G.; FARO, M. LO; TROCINO, S.; ZIGNANI, S. C.; ARICÒ, A. S.; DEGANELLO, F. Sucrose-assisted solution combustion synthesis of doped strontium ferrate perovskite-type electrocatalysts: Primary role of the secondary fuel. **Catalysts**, v. 10, n. 1, 2020.

VAHDAT VASEI, H.; MASOUDPANAH, S. M.; ADELI, M.; ABOUTALEBI, M. R. Photocatalytic properties of solution combustion synthesized ZnO powders using mixture of CTAB and glycine and citric acid fuels. **Advanced Powder Technology**, v. 30, n. 2, p. 284–291, 2019.

VALÉRIO, A.; WANG, J.; TONG, S.; ULSON DE SOUZA, A. A.; HOTZA, D.; GÓMEZ GONZÁLEZ, S. Y. Synergetic effect of photocatalysis and ozonation for enhanced tetracycline degradation using highly macroporous photocatalytic supports. **Chemical Engineering and Processing - Process Intensification**, v. 149, p. 107838, 2020.

VIKRANT, K.; KUMAR, V.; KIM, K. H.; KUKKAR, D. Metal-organic frameworks (MOFs): Potential and challenges for capture and abatement of ammonia. **Journal of Materials Chemistry A**, v. 5, n. 44, p. 22877–22896, 2017.

WANG, H.; HO, H. P.; LO, K. C.; CHEAH, K. W. Growth of p-type ZnO thin films by (N, Ga) co-doping using DMHy dopant. **Journal of Physics D: Applied Physics**, v. 40, n. 15, p. 4682–4685, 2007.

WANG, Z. L. Splendid one-dimensional nanostructures of zinc oxide: A new nanomaterial family for nanotechnology. **ACS Nano**, v. 2, p. 1987–1992, 2008.

WEN, W.; WU, J. M. Nanomaterials via solution combustion synthesis: A step nearer to controllability. **RSC Advances**, v. 4, n. 101, p. 58090–58100, 2014.

WEN, W.; WU, J. M.; WANG, Y. DE. Large-size porous ZnO flakes with superior gas-sensing performance. **Applied Physics Letters**, v. 100, n. 26, p. 1–6, 2012.

___. Gas-sensing property of a nitrogen-doped zinc oxide fabricated by combustion synthesis. **Sensors and Actuators, B: Chemical**, v. 184, p. 78–84, 2013.

WILKINSON, J. L.; BOXALL, A. B. A.; KOLPIN, D. W. A novel method to characterize levels of pharmaceutical pollution in large-scale aquatic monitoring campaigns. **Applied Sciences**, v. 9, n. 7, p. 1–14, 2019.

WU, S.; HU, H.; LIN, Y.; ZHANG, J.; HU, Y. H. Visible light photocatalytic degradation of tetracycline over TiO2. **Chemical Engineering Journal**, v. 382, p. 122842, 2020.

XIA, J.; GAO, Y.; YU, G. Tetracycline removal from aqueous solution using zirconium-based metal-organic frameworks (Zr-MOFs) with different pore size and topology: Adsorption isotherm, kinetic and mechanism studies. **Journal of Colloid and Interface Science**, v. 590, p. 495–505, 2021.

XIA, T.; WALLENMEYER, P.; ANDERSON, A.; MUROWCHICK, J.; LIU, L.; CHEN, X. Hydrogenated black ZnO nanoparticles with enhanced photocatalytic performance. **RSC Advances**, v. 40, n. 78, p. 41654–41658, 2014.

XUE, X.; WANG, L.; XING, H.; ZHAO, Y.; LI, X.; WANG, G.; WANG, Z. Characteristics of phytoplankton-zooplankton communities and the roles in the transmission of antibiotic resistance genes under the pressure of river contamination. **Science of The Total Environment**, v. 780, n. 1, p. 146452, 2021.

YAN, X.; OHNO, T.; NISHIJIMA, K.; ABE, R.; OHTANI, B. Is methylene blue an appropriate substrate for a photocatalytic activity test? A study with visible-light responsive titania. **Chemical Physics Letters**, v. 429, n. 4–6, p. 606–610, 2006.

YANG, X.; WANG, D. Photocatalysis: From Fundamental Principles to Materials and Applications. **ACS Applied Energy Materials**, v. 1, n. 12, p. 6657–6693, 2018.

YU, W.; ZHANG, J.; PENG, T. New insight into the enhanced photocatalytic activity of N-, C- and S-doped ZnO photocatalysts. **Applied Catalysis B: Environmental**, v. 181, p. 220–227, 2016.

YU, Z.; YIN, L. C. L. C.; XIE, Y.; LIU, G.; MA, X.; CHENG, H. M. H. M. Crystallinity-dependent substitutional nitrogen doping in ZnO and its improved visible light photocatalytic activity. **Journal of Colloid and Interface Science**, v. 400, p. 18–23, 2013.

ZANCHETTIN, G.; FALK, G. DA S.; GONZÁLEZ, S. Y. G.; HOTZA, D. High performance magnetically recoverable Fe3O4 nanocatalysts: fast microwave synthesis and photo-fenton catalysis under visible-light. **Chemical Engineering and Processing - Process Intensification**, v. 166, p. 108438, 2021.

ZHANG, J.; GUO, Q.; LIU, Y.; CHENG, Y. Preparation and characterization of Fe2O3/Al2O3 using the solution combustion approach for chemical looping combustion. **Industrial & Engineering Chemistry Research**, v. 51, n. 39, p. 12773–12781, 2012.

ZHANG, X. *et al.* Template-directed synthesis of pomegranate-shaped zinc oxide@zeolitic imidazolate framework for visible light photocatalytic degradation of tetracycline. **Chemosphere**, v. 294, p. 133782, 2022.

APPENDIX

As written in Section 2.1, the main subject of this work is "*to develop zinc oxide (ZnO) nanoparticles functionalized through nitrogen doping and apply them in the photocatalysis processes of emerging contaminants under visible light irradiation.*" And to execute nitrogen doping, a wide cluster of techniques has been assigned and well-developed. In this research, the main one is the one-step synthesis and doping by the solution combustion method. But, this Appendix is devoted to describing another doping route that has been explored during this Master's work, namely plasma-assisted doping.

Compared to conventional methods, plasma technology has become an enthusiastic point for research and development in Materials Science and Engineering. The advantages of plasma are given due to the higher density of reactive chemical species and particles that allows a fast process without multiple steps, the absence of toxic reagents, by-products, and the prospect to modify and functionalize the material only at their surface level, without tailoring the bulk properties (Pho *et al.*, 2020). The physics of the plasma phenomenon occurs with a potential difference between two electrodes in a gaseous environment at low pressures. Due to the electric field, the electrons have enough energy to provoke a series of collisions between the atoms and molecules of the gas. From this mechanism, a glow discharge is generated, known as plasma (Lieberman, 2005). And this discharge has the potential to create reactive radicals of doping elements and dope them on the lattice of the target material, especially semiconductor materials such as zinc oxide (Junior *et al.*, 2020; Lin, Liao e Hung, 2005; Nam e Boo, 2016; Salah *et al.*, 2016).

The idea around plasma-assisted doping in this work is based on a hollow cathode system, where the geometry exponentially multiplies the ionization/dissociation rates of the dopants radicals and improves the efficiency of doping (Klein *et al.*, 2013). The glow discharge is created from different mixtures of gaseous nitrogen (N_2) and hydrogen (H_2). At low pressure, nitrogen is decomposed and this atom can be quickly incorporated into the crystal structure, providing a high nitrogen dopant content (Salah *et al.*, 2016). While the hydrogen behaves as a reducing agent and may create a layer of defects and oxygen vacancies on the material's surface (Xia *et al.*, 2014). The synergy between these two elements changes the chemical potential of the environment which influences and leads to a better optical absorbance of the material in visible light and, ultimately, improves the photocatalytic activity in this spectrum range (Li, M. *et al.*, 2020).

In this study, a bunch of preliminary and official experiments has been revealing

the effect of nitrogen-hydrogen plasma-assisted doping on the undoped zinc oxide nanoparticles produced by solution combustion synthesis. However, in this design system, two main interconnected drawbacks were found: (I) inside the hollow cathode, only the uppermost layer of the ZnO nanoparticles are exposed to the plasma and being doped, which leads to low yields (around 0.1 grams per cycle) and a non-homogeneous doping process since it is impossible to separate the undoped and doped nanoparticles; and (II) the system is static and the particles are not in movement, so, the thermal heating induced by the plasma enables the sintering of the particles, which is the driving force to grow the particle size and decrease of the surface area – two negative points for the photocatalysis performance.

One of the solutions to overcome these issues is to build a plasma system where the particles should stay in movement during the doping cycles with plasma. In this framework, the entire material is exposed to the plasma, assuring a homogeneous treatment and allowing more material content to be doped. Also in movement, the particles are not close enough to the ones in their surroundings to coalesce, which is thought to maintain their nanoscale size. This kind of apparatus may improve the solid know-how that the Materials Laboratory (LabMat) has on plasma technology. But here, we are aware that to build it complex challenges would be found since the plasma source is in the direct current mode and need electrical insulation, the vacuum system should be accurate enough to support materials in the nano range, the equipment could be expensive and financial support is needed. And most of the challenges, the time to execute all of this is out of the scope.

Altough all these restrains does not enable an entire thesis about plasma doping and thinking that in the future this research line would be occur, as a way to highlight what has been discovered and made on this innovative doping route, the work has been submitted to be presented in the oral form at the XX Brazil MRS Meeting, promoted by SBPMat – Brazilian Materials Research Society at Foz do Iguaçu – PR on September/2022. The work will be held in the Surface Processing field at Symposium U – Surface Science and Engineering and the accepted extended abstract is shown in the next pages.

Plasma-assisted N-doping of zinc oxide nanoparticles for photocatalysis of emerging contaminants

Tainá Pigosso[1], Byron Andrade Amorim Melo[1], Leandro Lima Evangelista[1], Sergio Yesid Gómez González[2], Cristiano Binder[1]

[1] *Federal University of Santa Catarina, Department of Mechanical Engineering, SC, Brazil*

[2] *Federal University of Santa Catarina, Department of Chemical Engineering, SC, Brazil*

e-mail: *taina.pigosso@labmat.ufsc.br*

ABSTRACT: Photocatalysis is an assertive and feasible approach to degrading and inactivating chemical and biohazard pollutants. Zinc oxide (ZnO) is a robust semiconductor and a promising photocatalyst material. Strategies such as doping are assigned to modify the ZnO structure and surface, enhancing its photocatalytic response. This work describes a novel nitrogen-doping route of ZnO nanoparticles through a plasma-assisted process. The undoped zinc oxide nanoparticles were submitted to a DC N_2-H_2 glow discharge on a hollow cathode system at two different gas mixtures (25% N_2/75% H_2 and 75% N_2/25% H_2) for 30 minutes. Doped and undoped ZnO were tested under visible light, assessing their performance using tetracycline as a pollutant model. The results display the excellent potential of plasma processing to develop doping reactions in the material. The samples change from white color to gray and yellow, which is indicative of the doping occurrence. The X-ray diffraction confirms the wurtzite structure of ZnO and no new phases by plasma doping. By UV-vis spectroscopy, we observed the bandgap narrowing from 3.15 eV to values around 2.7 eV, confirming that the nanoparticles turn active in the visible light range due to the higher density of doping species and the surface defects induced through the plasma. The nitrogen-hydrogenated ZnO exhibits a photocatalytic improvement of 42% compared to the undoped material**.** Further developments to enhance the performance of the herein technique should target hindering catalysts sintering and the homogenization of the plasma process.

Keywords: *N-doped zinc oxide; plasma functionalization; nanocatalysts; visible light active.*

INTRODUCTION

Earth's water has been polluted continuously with different persistent pollutants - such as antibiotics- untreated by conventional wastewater treatment plants, which are not designed to eliminate them at trace concentrations. Even in trace amounts, their presence can be potentially hazardous to human health and the environment (Sanganyado e Gwenzi, 2019; Valério *et al.*, 2020). Photocatalysis is a growing technology based on the advanced oxidation process applied for environmental remediation and water decontamination, being a green and safe method that profiles as promising to eliminate those persistent organic pollutants. Zinc oxide is one of the most studied photocatalysts for water treatment due to its stability, catalytic activity, effective antimicrobial, anticancer activity, and UV absorbance quality (Bharti *et al.*, 2022). However, its inability to harvest a significant visible-light fraction hinders its application for solar and visible-driven processes under room conditions (Samadi *et al.*, 2016).

The photocatalyst activity can be extended to visible light by tailoring the surface and structural properties. As a non-metal, nitrogen doping into the surface of the photocatalyst material has been determined to be one of the most effective doped elements (Kumari, Sahai e Goswami, 2015). Based on the nitrogen source and the doping process, different properties of N-doped ZnO can be achieved. Compared to the traditional methods, the plasma-assisted doping processing of materials allows a fast and environmentally friendly process by reducing starting reactants and eliminating multiple steps. Most importantly, the high energy of the plasma species develops the bombardment and incorporation of impurities only at the surface level of the materials, without changing their volume properties (Pho *et al.*, 2020).

EXPERIMENTAL PROCEDURE

The undoped zinc oxide nanoparticles were produced through the solution combustion synthesis (SCS) with zinc nitrate hexahydrate and sucrose as reagents, at 500 ºC in a Muffle furnace. The doping reactions were performed in a direct current (DC) plasma reactor in a hollow cathode setup fed by nitrogen and hydrogen gaseous atmosphere at 250 sccm. The design and the plasma parameters are presented below in Figure 1. The materials were tested in photocatalytic essays to degrade the tetracycline organic compound under a 15 W fluorescent lamp ($\lambda > 420$ nm) that simulates the visible light for

60 minutes. Materials characterization techniques were used to support the study, such as SEM, XRD, and UV/vis spectral analysis.

Plasma-assisted doping parameters

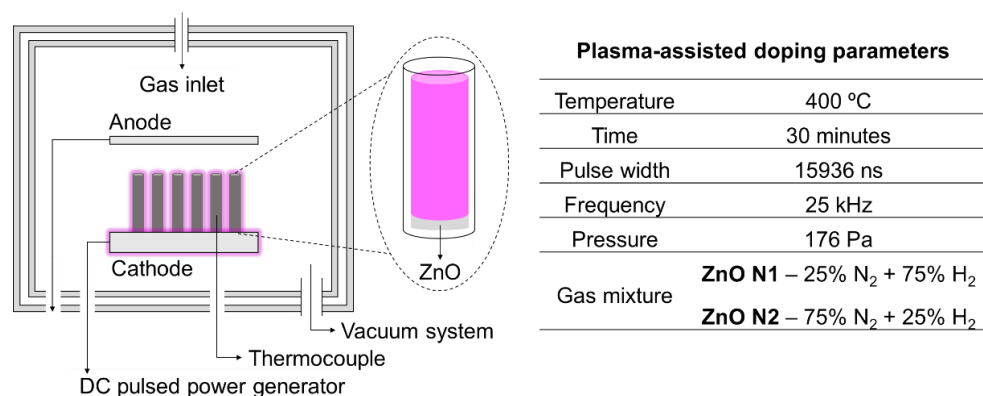| Temperature	400 ºC
Time	30 minutes
Pulse width	15936 ns
Frequency	25 kHz
Pressure	176 Pa
Gas mixture	**ZnO N1** – 25% N_2 + 75% H_2 **ZnO N2** – 75% N_2 + 25% H_2

Figure 1 – Plasma-assisted doping setup and parameters.

RESULTS AND DISCUSSION

The ZnO nanoparticles synthesized through the solution combustion route are presented in Figure 2 (a). This is a fast, straightforward, and cost-effective method to obtain nanomaterials. The nanoparticles have a spherical shape with a size near 50 nm. The XRD analysis reveals the hexagonal wurtzite structure of the ZnO (Figure 2 (b)), and no other phases were identified after the plasma doping with a nitrogen-hydrogen atmosphere. The optical bandgap is reduced from 3.15 eV (ZnO) to values of 2.75 eV (ZnO N1) and 2.83 eV (ZnO N2), corroborating the expanded absorption in the visible-light range ($\lambda > 400$ nm) by the doped samples, as shown in Figure 2 (c). From these results, plasma-assisted doping enables nitrogen incorporation in the ZnO lattice during the doping reactions. Furthermore, the hydrogen seems to induce surface defects, such as losing oxygen to create vacancies. The photocatalytic activity was compared using the degradation kinetics, assessing the rate constants adopting a pseudo-first-order kinetic model on the tetracycline abatement, calculated as 13.08, 18.59, and 12.59 x 10^{-3}.min^{-1} for ZnO undoped, ZnO N1, and ZnO N2, respectively (Figure 2 (d)). The nitrogen-hydrogenated ZnO N1 has a higher and faster photocatalytic response comparatively, improving 42% the reaction rate compared to the undoped ZnO.

CONCLUSIONS

The work demonstrated the potential of plasma-assisted doping of ZnO nanoparticles to improve photocatalytic activity. The achievements may be attributed to the synergistic effect between the nitrogen and hydrogen atoms to introduce a higher

optical absorption due to the benefits of ZnO's defective and doped structure after the plasma processing. The composition of the plasma atmosphere highly impacts the photocatalysis rate. Besides, future improvements in the plasma setup should be made to have a more homogeneous process and avoid the nanoparticles' sintering.
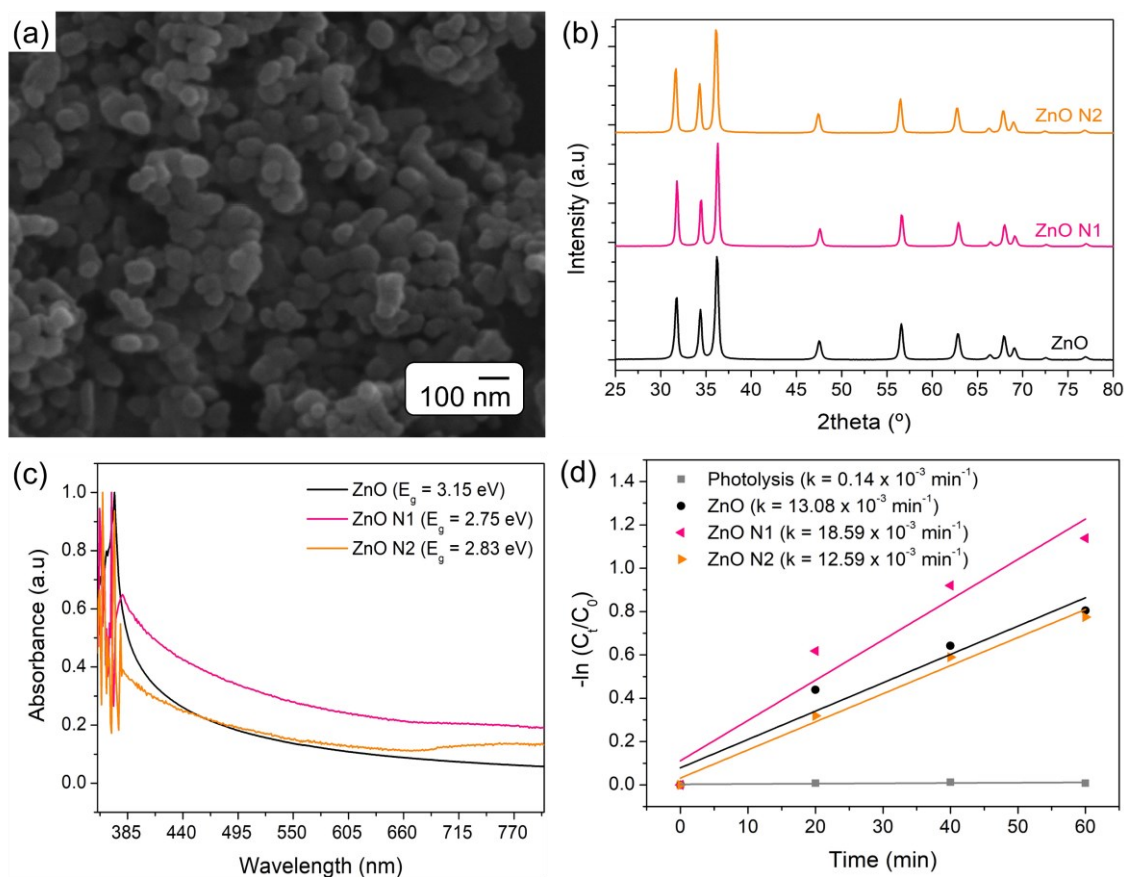

Figure 2 – (a) SEM of ZnO undoped nanoparticles synthesized through the SCS route; (b) XRD patterns of the ZnO undoped and the doped samples by the plasma; (c) UV/vis absorbance spectra and bandgap energy of the raw and modified ZnO; (d) the constant degradation rate (k) of the samples in the photocatalysis essays of the tetracycline as an emergent contaminant.

ACKNOWLEDGES

REFERENCES

The references cited in the Appendix can be found in the References section.